MITIGATION OF MUTUAL COUPLING IN DUAL POLARIZED MIMO ANTENNAS WITH WAVE PROPAGATION MODELS FOR 5G BASE STATION APPLICATIONS

Thesis

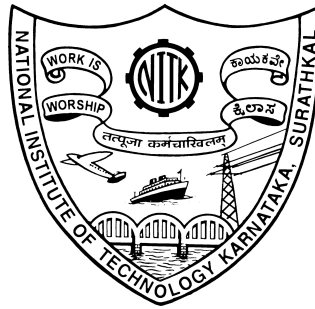Submitted in partial fulfillment of the requirements for the degree

of

DOCTOR OF PHILOSOPHY

by

ANUDEEP B

DEPARTMENT OF ELECTRONICS AND COMMUNICATION

ENGINEERING

NATIONAL INSTITUTE OF TECHNOLOGY

KARNATAKA,SURATHKAL

MANGALORE - 575025, INDIA

SEPTEMBER 2022

DECLARATION

I hereby *declare* that the Research Thesis entitled **MITIGATION OF MUTUAL COUPLING IN DUAL POLARIZED MIMO ANTENNAS WITH WAVE PROPAGATION MODELS FOR 5G BASE STATION APPLICATIONS** which is being submitted to the **National Institute of Technology Karnataka, Surathkal** in partial fulfillment of the requirements for the award of the Degree of **Doctor of Philosophy** in **Department of Electronics and Communication** is a *bonafide report of the research work carried out by me*. The material contained in this thesis has not been submitted to any University or Institution for the award of any degree.

Anudeep B.
Register No.: 177099EC001
Department of Electronics and Communication Engineering

Place: NITK Surathkal
Date: 29-09-2022

CERTIFICATE

This is to *certify* that the Research Thesis entitled **MITIGATION OF MUTUAL COUPLING IN DUAL POLARIZED MIMO ANTENNAS WITH WAVE PROPAGATION MODELS FOR 5G BASE STATION APPLICATIONS**, submitted by **Anudeep B.** (Reg. No.: 177099EC001) as the record of the research work carried out by him, is *accepted as a Research Thesis submission* in partial fulfillment of the requirements for the award of degree of **Doctor of Philosophy**.

Dr. Krishnamoorthy K.
Research Guide
Assistant Professor
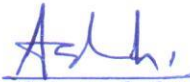Department Electronics and Communication Engg.
NITK Surathkal - 575025

Dr. P.H.Rao
Co-Research Guide
Director General
SAMEER - Centre For Electromagnetics
IIT Mumbai Campus - 400076

29-9-2022
Chairman - DRPC
(Signature with Date and Seal)

प्राद्योगिक एवं विभागाध्यक्ष / PROF & HEAD
ई एवं सी विभाग / E & C Department
एन आई टी के, सुरतकल/NITK Surathkal
मंगलूर / MANGALORE - 575 025

This thesis is dedicated to my beloved parents

ACKNOWLEDGEMENTS

them for their invaluable friendship, care, concern and timely interventions.

Throughout the different phases of my Ph.D., the love and support provided by my family know no bounds, I thank them for always having worked behind the scenes for me. Their silent prayers and gentle chiding have molded me into the person I am today. A special word of thanks to my brother for his benevolence and guidance at every juncture of my course. I especially wish to thank my parents, who have provided me, for the sacrifices they have made, and for always believing in me.

ABSTRACT

Fifth Generation or 5G, is the contemporary new release of cellular generation, engineered to drastically increase the speed and approachability of wireless networks. 5G performance objectives high data rate, increased capacity, low latency and large device connectivity. 5G enables massive increase in amount of data handling capacity due to its broad spectrum allocation covering both sub 6GHz range and mm-wave frequency bands. Massive MIMO (additionally referred to as huge-Scale Antenna structures, Very large MIMO, and Hyper MIMO) is an electrifying concept in wireless communications studies that promises to deal with the huge capacity requirement demanded by means of 5G systems. Massive multiple-input multiple-output (MIMO) technology, where a base station is installed with huge number of antennas serves large number of users by utilizing time-frequency resource will meet the requirements for 5G. Hence, MIMO is selected as promising candidate technology for upcoming generations of wireless systems. The selection of antenna and building the MIMO base stations which address both spatial and polarization diversity is one of the major task.

The thesis focuses on design and implementation of dual polarized MIMO antennas with both spatial and polarization diversity. The designed dual polarized MIMO antennas are implemented with different MIMO configurations to address the high data rate with massive connectivity for 5G requirements. Novel dual polarized MIMO antenna element with complete planar printed balun feed network is designed, fabricated and tested. In extension, a compact 2×2 dual slant 45^0 polarized MIMO antenna for 4G LTE band 40 is designed. The stringent parameter

while developing MIMO antennas is mutual coupling associated with the adjacent antenna elements in both azimuth and elevation planes. By considering array of split ring resonators(SRRs) embedded with transmission line low mutual coupling and high isolation are achieved for 2×2 MIMO antenna. The selected configuration is also extended for massive 8×8 MIMO antenna by addressing both spatial and polarization diversity for C-RAN applications. Here, mutual coupling mitigation is carried out by inserting U shaped aluminium strips in both azimuth and elevation planes.

As there is also need for wide band antennas with low profile for quick installation in compact base stations. So here, a wide band, low profile dual polarized bow-tie antennas for band 42 covering sub 6 GHz range for 5G communication is implemented. Wide band dual polarized bow-tie antenna is designed with both polarization and spatial diversity. Low profile miniaturized dual polarized 1×2 MIMO antenna backed with chessboard configured artificial magnetic conductor (AMC) surface is designed for compact base station applications. To mitigate the mutual coupling between two low profile dual polarized antennas a novel approach with frequency selective surface (FSS) wall is constructed. The FSS cell is properly designed for wideband operation which indirectly suppress the near fields for entire band of operation. The other parameters like isolation, impact on with and without FSS wall, radiation patterns, front to back ratio, co-cross polarization levels are also discussed. MIMO performance related parameters like envelope correlation coefficient, diversity gain and total active reflection coefficient are also discussed.

The thesis also focuses of practical deployment of base station antennas with various wave propagation models and network planning. For practical deployment, dual polarized antenna covering the sub 6 GHz range is considered along

with 2×2, 4×4 and 8×8 MIMO configurations. The study of propagation models, modulation schemes, data rates and throughput over the selected geographical terrain that is NITK campus are reported. The maximum data rate with 8×8 massive MIMO antenna configuration is achieved to meet the 5G requirements. Also, the radome analysis with dual band microstrip patch antenna operating at both 4G and 5G frequencies also discussed. Metamaterial based radome is considered to enhance the gain for the designed dual band patch antenna.

Proposed designs are fabricated using LPKF protomat machine S103 and experimentally verified using far field and anechoic chamber radiation pattern measurement set-up. Impedance bandwidth, peak gain, isolation, mutual coupling, front to back ratio, cross-polarization level, envelope correlation coefficient, diversity gain and total active reflection coefficient are various metrics considered for the performance measures of the proposed MIMO antenna.

Keywords: Dual polarized antenna, Patch antenna, MIMO, Metamaterials, Artificial magnetic conductor, Split ring resonator, Frequency selective surface, Wave propagation models, Radio network planning.

TABLE OF CONTENTS

LIST OF FIGURES

LIST OF TABLES

ABBREVIATIONS

5G   Fifth Generation

3GPP   3rd Generation Partnership Project

4G   Fourth Generation

LTE   Long Term Evolution

MIMO   Multiple Input Multiple Output

DPA   Dual Polarized Antenna

DSPA   Dual Slant Polarized Antenna

AMC   Artificial Magnetic Conductor

FSS   Frequency Selective Surface

SRR   Split Ring Resonator

LP   Linear Polarization

MTM   Metamaterial

WPM   Wave Propagation Models

IRS   Intelligent Reflecting Surface

CHAPTER 1

INTRODUCTION

Antenna plays a very predominant role in mobile communication. An antenna is usually a metallic device which is used for radiating or receiving radio waves. As per IEEE definition of an antenna is "a means of radiating or receiving electromagnetic waves". For any mobile communication to exist an antenna is the first device at both transmitter and receiver end. Therefore, proper selection of antenna is needed to acquire the desired performance in the communication systems. This chapter briefly elaborates the history of mobile communication and their antenna systems. Various types of antennas are designed to meet their specific requirements in communication systems. There are certain research gaps need to be filled in the upcoming future wireless communication that requires antennas with compact structures exhibiting polarization and spatial diversity. The work motivation, problem definition, problem statement and objectives, work methodology and organization of thesis also reflects in this chapter.

1.1   History of Mobile Communication and its Evolution

Radio waves have nearly magical homes that capture the imagination and lead to a diffusion of various uses. When the radio waves starts traveling through our atmosphere or the universe, they join points that could be related in no other way.

Travelling at a acknowledged speed, they make us to locate flying objects, finding our own location, or even chart the entire universe. Possibly no other technology would call their capacity to fill this space. It carries the information by connecting all over the universe and making the radio communication possible. It allows a specific person each time, everywhere and as antenna can move by sending or receiving the signals that makes the "**mobile communication**" viable.

When we go back to history initially Marconi initiated his wireless telegraph in 1895. It was the first commercial telephone system launched at BELL labs. Early mobile communication started with analog frequency modulation techniques that would cover over the range of 50 miles and only limited users were addressed due to shortage in bandwidth. To overcome the scarcity of bandwidth and to cover the larger areas, BELL lab proposed the concept of cellular communication. Frequency reuse technology has been utilized for better coverage and more usage of frequency spectrum by reducing the power at the transmitter side.

Mobile wireless industry evolved in early 1970 and from mid 1990's the cellular communication took over and witnessed explosive growth. Wireless communication networks have come to be an awful lot extra pervasive than each person could have imagined while the cell concept turned into first deployed in 1960's and 1970's. Mobile cellular subscribers are drastically increasing when compared with fixed telephone lines. The wide unfold fulfilment of cellular and its requirements has led to the improvement of new wireless standards for different types of telecommunication traffic. As the new standards and requirements emerges there is a new cellular technology or generation leading by the corresponding modulation technique.

The range of radio waves and allocated frequency spectrum is 3KHz to 300GHz as shown in Figure 1.1
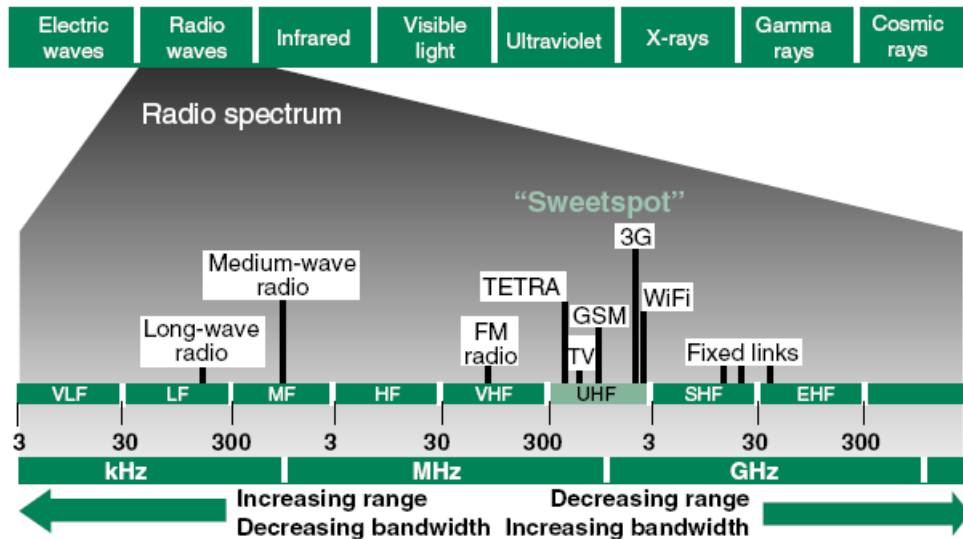
Figure 1.1: Radio Wave Frequency Spectrum

Cellular Mobile communication has different generations a brief description of every generation is given below.

1G First generation: The cellular mobile communication started with first generation with analog standards which was introduced in 1980s. The voice communication typically used frequency modulation and FDMA techniques. The 1G cellular phones came into existence in 1982 for purely voice services and was based on Advanced Mobile Phone System (AMPS). The AMPS is based on analog with poor voice quality, limited capacity and battery life. Mohammad Meraj ud in Mir (2015).

2G Second generation: This refers to the second form of cellular communication system. The systems were digital supporting voice with low data speed services. Systems utilized GSM with a mixture of TDMA and FDMA techniques.

It was developed in 1980 referring to personal communication services which mainly focused on digital signals. It also supported the users with service to deliver message with images at a very low speed (in Kbps).

2.5G - GPRS(General Packet Radio Service): 2.5G is extension of the previous 2G network with GPRS technology in which data are sent with packet based services. Second half generation have implemented packet switched domain along with circuit switched domain. GPRS supports the data rates from 56 Kbps to 384 Kbps. It also provides Wireless Application Protocol (WAP) and Multimedia Messaging Service (MMS) for internet services. 2.5G network supports WAP, MMS, mobile games and SMS services and well internet services.

2.75G - EDGE(Enhanced Data Rates for GSM Evolution): GPRS networks modified to EDGE networks by utilizing 8PSK modulation scheme. It is also called as Enhanced GPRS (EGPRS). This allows with improved data transmission rates over to the extension of GSM. EDGE is considered by 3GPP as a part of GSM family which achieves higher data rates with more additional methods of coding (8PSK) within existing GSM techniques. It transfers data in fewer seconds when compared to GPRS technology. EDGE is a part of radio technology which comes under third generation technologies. EDGE is selected over GSM due to its flexibility to carry data packets and switch data and circuit. Mohammad Meraj ud in Mir (2015).

3G Third Generation: Third generation evolution is based on Code Division Multiple Access (CDMA) technology. As per 3GPP standards the 3G technologies service provides offer greater network capacity addressing to a wide number of users with advanced services. The services include voice calls, video calls,

broadband wireless data, mobile television, video conferencing, GPS. CDMA 2000 and wideband CDMA also called as Universal Mobile Telecommunication Service (UTMS) are part of 3G technology. Arun Agarwal (2019).

3.5G HSDPA (High-Speed Downlink Packet Access):   3.5G supports High-Speed Downlink Packet Access (HSDPA) which provides easy path for UMTS-based 3G networks with higher data speeds. H-SDPA is also a packet based data service like GPRS with data transmission of 8-10 Mbit/s and 20 Mbit/s for MIMO systems. HSDPA technology includes Multiple Input Multiple Output (MIMO), Hybrid Automatic Request (HARQ) and advanced receiver design. Arun Agarwal (2019).

4G Fourth Generation: Fourth generation is the next generation wireless networks which replace the 3G networks. In present generation we are able to access the internet through all cellular/mobile devices which supports various technologies like, Wi-Fi, Wi-Max, GPRS, EDGE and WAP. 4G provides a download data rate of 100Mbps and less mobility of 1GBps. Compared to 3G which utilizes the combination of both CDMA and IS-95 4G introduces new technology OFDMA. Arun Agarwal (2019).

OFDMA is a concept of neither time like TDMA nor code divided CDMA but it is frequency domain process symbolizes as OFDMA. Long Term Evolution (LTE) is incorporated with 4G mobiles. Difference between WiMAX and LTE is that LTE is based on IP address. A restricted IP address will be provided for additional security with high data transferability to avoid latency and also to adjust the available bandwidth. 3GPP organization has introduced two major wireless standards for 4G that is LTE and IEEE 802.16.

Table 1.1: Summary on Evolution of Mobile Communication

Generation	Features	Applications
1G	Uses Analog technology	Voice communication
2G	Primary technologies used	Slow data rate
3G	144Kb/s for mobile	Advacned applications
4G	Require ability of 40Mhz	More data rate

5G Fifth Generation: 5G is the fifth generation mobile network. It is a new emerging wireless standard after 1G, 2G, 3G and 4G networks. It enables world wide wireless web which connects virtually everyone and everything all together with different objects and devices. It is meant to deliver multi-Gbps peak data speeds, more reliability, ultra low latency, massive network capacity and more uniform user to experience increased availability. Different types of advanced features are enabled in upcoming 5G. It is more effective and more attractive when compared with other generations.

For 5G technology IMT 2020 vision has prescribed the limit of peak data rate of 10 Gbps within a minimum latency of 1ms. Figure 1.2 shows 5G spectrum comparing the existing mobile spectrum with new mobile spectrum based on coverage and capacity. Figure 1.3 shows the difference between 4G and 5G and how users are addressed from the base station antennas. When compared with all previous wireless technologies which are of telephone and data sharing but when it comes to 5G it brings a new touch enabling the life real mobile life. Arun Agarwal (2019).

Table 1.2: Expected performance parameters for 5G

Important parameters	Values
Data rate	100 Mbps to 1 Gbps
Peak data rate	20 Gbps
Mobility	500 km/h
Spectral efficiency	3 times more than 4G
Latency	1 ms
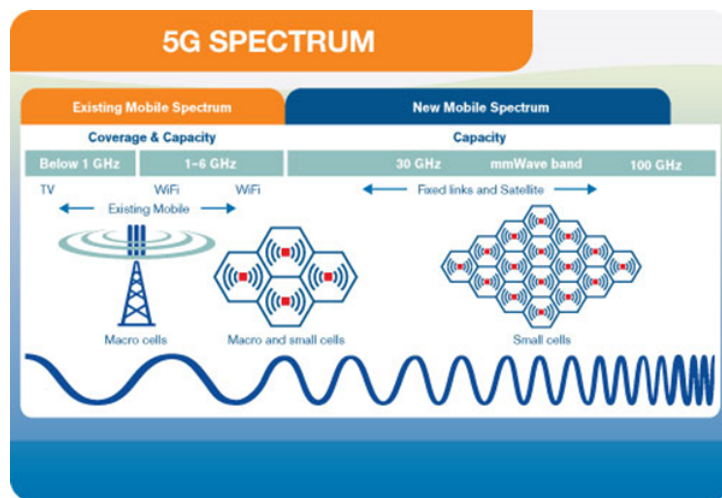
Figure 1.2: 5G Spectrum
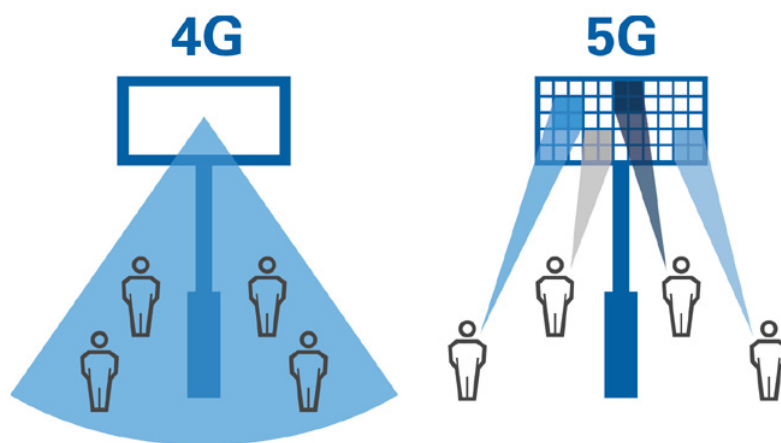
Figure 1.3: Difference between 4G and 5G

1.2 Motivation

The 5th generation (5G) of mobile communication is expected to have a very large impact on both society and industry that will go far beyond the information and communications technology (ICT) field. The 5G developments as per 3rd generation partnership project (3GPP) requirements stresses the exact objective of

the 5G system design. Due to the increasing demand for high data rates in mobile communication, it is required to design antennas with polarization and spatial diversity. The antennas need to be deployed practically to achieve maximum data rates overcoming the propagation path losses. Wide applications need a compact, low profile, wideband and high gain antennas, which can be easily integrated into the base stations.

To obtain the desired functionalities of designed antennas with polarization and spatial diversity some of the stringent parameters are to be considered which degrades the entire performance of the MIMO system. Mutual coupling is one such parameter which has to be reduced in MIMO antenna system. Dual polarized antennas are considered for polarization diversity but when two such antennas are placed closed enough it affects the system performance. Mitigation of mutual coupling with different techniques are studied but by implementing metamaterials (MTMs) desired characteristics are obtained. The integration of designed MTMs to the antenna structures led to changes in S-parameters of the antenna. The proper and effective design of these walls in between antenna elements should maintain the antenna characteristics and reduce the surface waves and current distribution among the existing antennas.

In practical scenario, the deployment of base station antennas is considered with effective coverage providing the maximum data rates. To achieve the maximum data rates and to meet the 5G requirements the designed base station antennas have to deployed. The wave propagation models suitable for rural, sub-urban and urban areas have to be selected for analyzing the parameters like path losses, data rates, throughputs and signal quality and strength. Recently, various platforms have developed to analyse the practical scenario with respect to different propagation models.

1.3 Problem Definition

Fifth Generation or 5G, is the contemporary new release of cellular generation, engineered to drastically increase the speed and approachability of wireless networks. 5G performance objectives high data rate, increased capacity, low latency and large device connectivity. 5G enables massive increase in amount of data handling capacity due to its broad spectrum allocation covering both sub 6GHz range and mm-wave frequency bands. Massive MIMO (additionally referred to as huge-Scale Antenna structures, Very large MIMO, and Hyper MIMO) is an electrifying concept in wireless communications studies that promises to deal with the huge capacity requirement demanded by means of 5G systems. Massive multiple-input multiple-output (MIMO) technology, where a base station is installed with huge number of antennas serves large number of users by utilizing time-frequency resource will meet the requirements for 5G. Hence, MIMO is selected as promising candidate technology for upcoming generations of wireless systems. The selection of antenna and building the MIMO base stations which address both spatial and polarization diversity is one of the major task. Thus, antenna configurations for use in Massive MIMO schemes for 5G should be investigated and analyzed. Several antenna element such as dipoles, horn antenna and printed antennas could be used for 5G communications.

1.4 Objectives

Formulated objectives are:

- To design and develop a novel compact 2×2 dual slant 45^0 polarized MIMO antenna with low mutual coupling and high isolation for 4G LTE Band 40 base station applications.

- To design a AMC surface based low profile, miniaturized wide band dual polarized MIMO antenna with FSS decoupling technique for reducing mutual coupling in 1×2 MIMO antenna.

- To design a compact dual polarized MIMO antenna with wave propagation models for practical 5G scenario.

  To design and analyze a metasurface surface based radome for 5G MIMO antenna in sub 6 GHz range.

1.5 Methodology

Dual polarized antennas with extensive properties of MTMs are used to achieve the proposed objectives. Different methods are adopted to mitigate the mutual coupling among the designed MIMO antenna elements. Proposed MIMO antennas are deployed for practical scenario as well to meet the upcoming 5G requirements. The designs are simulated, fabricated and measured by using the both far field and facilities available at the lab.

- A novel dual polarized antenna using compact rectangular bow-tie antenna are designed. The two different antennas are fed with marchand balun feed with same amplitude and opposite phase to provide dual polarization. The design is extended for 2×2 MIMO with dual slant 45^0 polarization. To mitigate the mutual coupling between the two dual slant 45^0 polarized antennas in both azimuth and elevation planes a transmission line loaded with an array of split ring resonators are inserted. The designs are optimized to achieve low mutual coupling and high isolation focusing 4G LTE Band 40 base station applications.

10

- The low profile dual polarized antenna is obtained by utilizing zero phase reflective property of an artificial magnetic conductor (AMC). The wideband characteristics are obtained by incorporating the rectangular slots on the radiators which also suppress the surface currents when extended for 1 × 2 MIMO antenna. FSS decoupling structure is implemented with wideband stop characteristics to cover the entire band of operation. With the FSS wall mutual coupling reduction is reduced drastically between the two dual polarized antenna elements.

- In practical scenario the base station antennas have to deployed to achieve maximum range of coverage and data rates. The designed compact dual polarized antenna operating for 5G sub 6GHz range is deployed for practical geographical terrain with different wave propagation models. The designed MIMO antenna analyzed for various configurations to obtain the maximum data rate and area of coverage for 5G requirements. To protect the antennas from abnormal environmental conditions suitable radomes are to be designed. A metasurface based radome for 5G MIMO antenna in sub 6GHz range with gain enhancement properties is designed.

1.6   Organization of the Thesis

The motto of thesis is to design and implement MIMO antenna systems for 5G base station applications. It also focuses on mitigation of mutual coupling between the designed MIMO antenna systems. This thesis is organized into several chapters based on the various designs proposed and obtained results. Introduction section of the thesis describes the history of mobile communication, their evolution with various generations and technologies to upcoming 5G. Motivation to design the novel antennas which is followed by problem definition. The focusing objectives, work methodology and thesis organization are provided as each separate sections.

The second chapter discusses the basic concepts of MIMO and massive MIMO antennas for 5G communications. Dual polarized antennas and its importance for 5G base station antenna applications. The effect of mutual coupling and reduction

techniques in MIMO antenna system designs. Also, a brief explanation of MTMs, MTSs and split-ring resonators, frequency selective surfaces, are discussed, which are used to mitigate the mutual coupling. Also, it provides a explanation of the wave propagation models for 5G practical deployment. A brief literature survey is included in the next section. The first section of the literature survey gives dual polarized antennas and its contribution to design various types of antennas for 5G applications. Also, advantages of low profile and compact structures for base station antennas. The upcoming sections describe the literature works on metasurface based radomes for gain enhancement including the wave propagation models for practical deployment.

In the third chapter, a compact design of dual slant 45^0 polarized bow-tie antenna, effect of mutual coupling and its reduction techniques by implementing periodic array of SRRs loaded transmission line in both azimuth and elevation planes. The complete planar structure by implementing the printed feed network to feed the dual polarized bow-tie antennas with fabricated prototype and results.

The fourth chapter provides the design and implementation of MIMO and Massive MIMO antennas with two different configurations. The mitigation of mutual coupling with U shaped strips for both azimuth and elevation planes. The fabricated prototype of the designs focusing base station applications.

In the fifth chapter, low profile, wideband dual polarized antenna with FSS decoupling technique for 5G applications are discussed. Arc shaped dual polarized antenna with coaxial feeding and novel wideband antenna for 5G applications. The FSS decoupling technique to mitigate the mutual coupling when implemented for MIMO and complete MIMO performance analysis are also discussed.

The sixth chapter discusses wave propagation models for practical 5G deployment in any selected geographical terrains. The radio network planning with var-

ious modulation schemes and wireless standards to meet the 5G requirements. Also, metasurface based radome analysis for practical deployment of 5G MIMO antenna. Metasurface radomes utilizing for gain enhancement along with covering of antenna from environmental conditions.

The seventh chapter gives conclusions about the contributions provided through different designs in the thesis. Also, it discusses future scope to develop intelligent reflecting surfaces(IRS) for antennas with improved performances for future 6G applications.

CHAPTER 2

BACKGROUND AND LITERATURE SURVEY

2.1 MIMO Systems and Massive MIMO Antennas in 5G

2.1.1 MIMO Systems:

There are different types of antenna technology configuration concerning the multiplicity of inputs and outputs. The easiest figuration on radio link system is defined a **Single-Input-Single-Output (SISO)**, where both the transmitter and receiver operate with a single antenna, there is no diversity and no additional processing required. SISO systems are used in multiple systems such as Bluetooth, Wi-Fi, radio broadcasting and TV. However, these systems are limited on their performance. Rates above 1 Gbps rate can only be obtained by using wide input power and bandwidth. In addition, multipath is unavoidable using these systems and fading reveals to not be constant in time. This causes several issues like losses and attenuation and also the reduction in data speed, packet loss and increased errors. Exploiting different kinds of diversity, both on the receiver and transmitter terminals, two solutions have raised. Ferreira (2016).

Single-Input-Multiple-Output (SIMO) systems, which apply spatial diversity on the receiver, is often used to combat effects of fading and interference. Despite being easy to implement, SIMO systems require processing in the receiver

which may limit the performance in several applications as mobile communications (by size, cost and battery drain). Futhermore, the channel capacity on the link does not increase when applying this technology.

Multiple-Input-Single-Output (MISO) systems, also termed transmit diversity, take advantage specially on cellphone communications (in which less power is used and processing is required at the user end or receiver end). The same amount of data is transmitted from several transmitter antennas. Then, the receiver gets the optimum signal and extracts the required data. The main benefit of this technology is that the multiple antennas and the necessary coding and processing is shifted to the receiver, which helps to reduce the effects of multipath wave propagation, delay and packet loss. However, MISO systems particularly utilise time diversity, which doesn't represent a good solution by not increasing the channel capacity and high data rates.

The basic block diagram of MIMO system is shown in Figure 2.1.
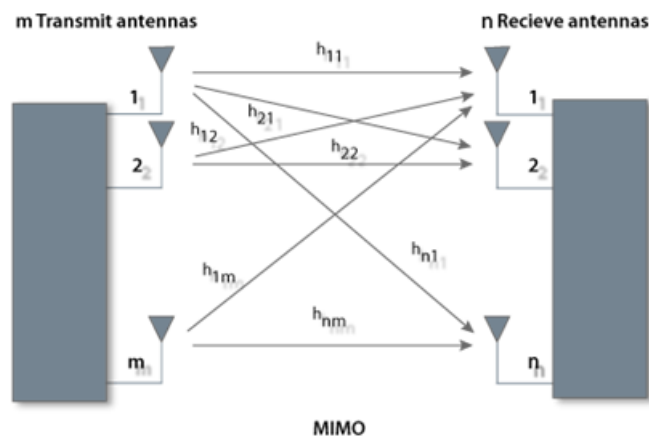
Figure 2.1: Block Diagram of MIMO System

2.1.2 MIMO Antenna Solutions:

MIMO (multiple input, multiple output) is an antenna technology in which multiple antennas are build at both transmitter and receiver end. At each end the communication circuits of antenna are combined to minimize errors and optimize the data speed. Electromagnetically printed antennas are developed to provide every wideband impedance characteristics. Many parameters optimize the impedance bandwidth of this antenna which has to be investigated. These antennas are built up for modern wideband wireless applications like mobile phones or Wireless LAN, Bluetooth, UWB and RFID technologies. MIMO systems perform best when they can answer to the issues related to antenna theory such as array configuration, radiation pattern, type of polarization and mutual coupling. Ferreira (2016).

To find out the proper design and configuration of the MIMO antenna, it's important to satisfy the requirements concerning its final wireless application. However, it is acceptable to define some essential properties that must be confirmed to ensure a good performance and to operate in the best possible manner. Some of the requirements are to be considered in order to optimize the antenna performance like size, bandwidth, efficiency, polarization, power handling. MIMO antenna design are established in order to optimize aspects such as array configuration, radiation pattern, type of polarization and mutual coupling. The topology is decided in order to maximize the channel capacity and minimize the error rate. In MIMO arrays, the channel capacity degradation is taken care by controlling the correlation between the multiple signals.

- Spatial Diversity: different elements are spaced with optimum distance to increase the number of channels in the link. In this technique, the smaller the distance, the more the mutual coupling between antennas, which result in a reduction of the channel capacity.

16

- Spatial multiplexing: This form of MIMO is used to provide additional data capacity by utilising the different paths to carry additional traffic, that is increasing the data throughput capability.

- Polarization Diversity: elements in the array are fed with differently polarized signals.

- Pattern Diversity: the signals with different angles are given to each one of the antennas present in the array.

MIMO antenna systems can be used in order to achieve different goals such as increasing the overall gain, cancelling out the interference from a particular set of directions and maximizing the Signal to Interference Pulse Noise Ratio (SINR) - to establish the maximum limit concerning to channel capacity. Ferreira (2016).

2.1.3 Dual Polarized Antennas For 5G:

The radiowave is an electromagnetic waveform composed of both electric and magnetic fields. In free space, the fields are mutually perpendicular and are also perpendicular to the direction of propagation. The term polarization commonly refers to the electric field component of the radiowave. In terrestrial microwave antennas, the polarization of the radio waves will be either horizontal or vertical. That is, the electric field will be either horizontal or vertically orientated. The transmission characteristics of both polarizations are very similar at microwave frequencies. However, the effects of obstacles and reflections within the microwave link are more likely to degrade system performance in horizontal polarization than in vertical polarization and thus vertical polarization tends to be the first polarization of choice.

Microwave antennas will generally be either single polarized or dual polarized. A single polarized antenna is one that responds only to one orientation of

polarization – either horizontal or vertical. Thus radio waves that are received or transmitted by a single polarized antenna will be either horizontal or vertical polarized. A dual polarized antenna, however, can respond to both horizontally and vertically polarized radio waves simultaneously. The use of both polarizations in this way increases the traffic handling capacity of the system.et al. (2014). The block diagram of dual polarization is shown in Figure 2.2
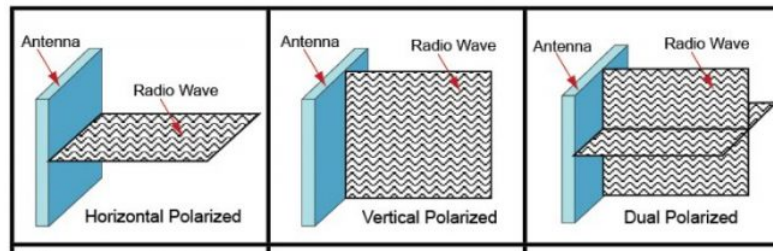
Figure 2.2: Block Diagram of Dual Polarization

2.2 Mutual coupling in MIMO Antennas

Mutual coupling defines as the energy absorbed by a proximate antenna when another antenna is radiating. Mutual coupling has a tendency to change the radiation pattern, reflection coefficient and input impedance of the MIMO antennas. The simplified mutual coupling, MC_{ij} empirical models can be presented as

$$MC_{ij} = exp(-(2d_{ij}/\lambda)(\alpha + j\pi)), i \neq j \tag{2.1}$$

$$MC_{ij} = 1 - 1/N \sum_{i} \sum_{i \neq j} MC_{ij} \tag{2.2}$$

where d_{ij} is the distance between ith and jth antenna elements. Further, α is

the coupling level controlling parameter and N is the number of array elements.

In practice, mutual coupling depends on the array configuration as well as on the excitations of other elements. It is usually calculated in dB-valued S-parameter between ith and jth antenna elements and the isolation of $-20\log10(|S_{ij}|)$ between them. However, the detailed mechanism of mutual coupling depends largely on the transmitting and receiving modes. Nadeem and Choi (2018). The simple diagram of the mutual coupling mechanism between the adjacent antenna elements for both transmitting and receiving mode are shown in Figure 2.3.
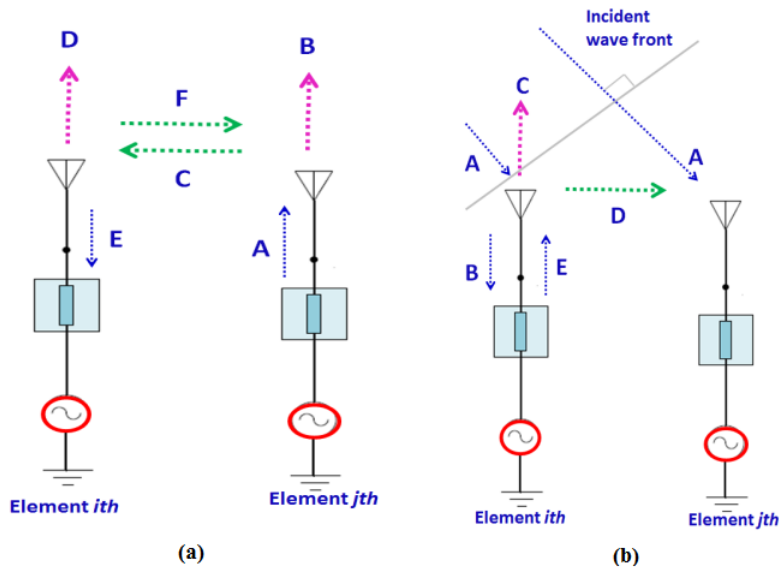
Figure 2.3: Diagram of mutual coupling mechanism (a)Transmitting mode (b)Receiving mode

Envelop Correlation Coefficient(ECC): ECC is the relationship between the incoming signals at the ports of a MIMO or array antenna. In MIMO antennas, ECC is used as a performance metric to characterize and measure the system performance and efficiency. Moreover, ECC evaluation is necessary for uncorre-

lated channels to find channel quality. Several methods are present in the literature to calculate ECC for MIMO antenna systems. The mutual coupling effect between numbers of ports of MIMO can be observed as two scattering parameters S_{ij} and S_{ji}. High mutual coupling can affect the antenna characteristics adversely. Hence, ECC is increased significantly. Higher value of ECC leads to high correlation and mutual coupling. Therefore, lower ECC values are expected in the MIMO antenna systems. Furthermore, ECC shows combined effect over all the scattering parameters of a designed MIMO antenna to illustrate their effect on correlation coefficients. In typical cellular phone application, ECC value must be less than 0.5 to achieve better diversity Nadeem and Choi (2018).

The correlation coefficients for S-parameter calculation method can be approximated as below.Network analyzer is used to extract these parameters from the antenna ports of the MIMO system. This approach does not require the computation and measurement of the radiation pattern of the antenna system. It also offers a clear understanding of the effects of mutual coupling and input impedance match on the diversity performance of the antenna system. This is a simple and fast method to calculate ECC which depends on the port parameters of the antenna. The ECC calculation methods and performance in MIMO antenna designs flow chart is shown in Figure 2.4.

$$P_{(ij)}(e) = \frac{|\sum_{n=1}^{N} S_{ni}^* S_{nj}|}{\sqrt{(1 - \sum_{n=1}^{N} |S_{ni}|^2)(1 - \sum_{n=1}^{N} |S_{nj}|^2)}} \tag{2.3}$$

where i and j are antenna ports, n is the number of radiating elements, S_{ni} and S_{nj} are scattering parameters of antenna elements. This scattering parameters are also knows as reflection coefficients.

Far-field radiation pattern method uses azimuthal and elevation radiated field

components for ith and jth elements, respectively. Anechoic chamber is used to extract these parameters. The correlation coefficients based on this method is written as

$$P_{(ij)}(e) = \frac{|\iint_{4\pi} F_i(\theta, \phi) \times F_j(\theta, \phi) d\Omega|^2}{\iint_{4\pi} |F_i(\theta, \phi)|^2 d\Omega \iint_{4\pi} |F_j(\theta, \phi)|^2 d\Omega} \qquad (2.4)$$

where $F_i(\theta, \phi)$ and $F_j(\theta, \phi)$ are field patterns of two radiating elements with respect to θ. Additionally, θ and Ω are the solid angles.
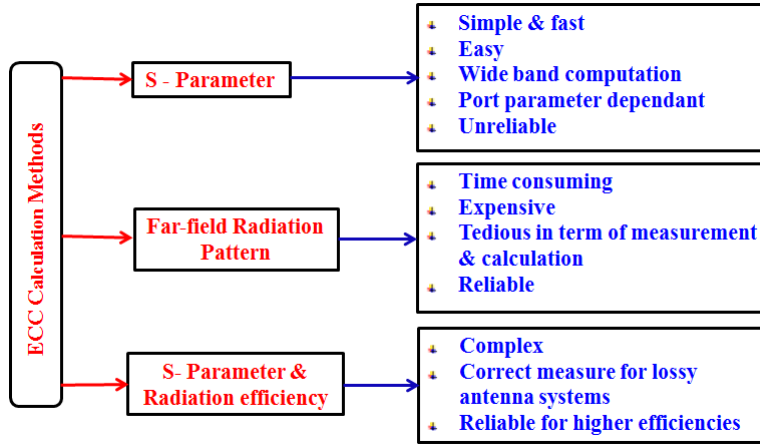
Figure 2.4: ECC calculation methods and performance in MIMO antenna designs

Diversity Gain(DG):   Diversity gain (GDG) is another important factor that must be taken into account while evaluating the MIMO performance. It gives an idea about the reliability of the MIMO system. The higher the value of diversity gain the isolation is better. It is dependent on the correlation coefficients between antenna signals is written as

$$DG = 10 \times \sqrt{(1 - |P_{(ij)}(e)|^2)} \qquad (2.5)$$

21

2.3 Wave Propagation Models

For the installation of mobile radio systems, wave propagation models are necessary to determine propagation characteristics for any arbitrary configuration. WinProp software ProMan component includes wave propagation models for different scenarios and network planning simulators for various air interfaces. The ProMan software package is designed to predict the path loss accurately between transmitter and receiver including all important parameters of the mobile radio channel. Propagation models for rural, urban, and indoor scenarios are available as well as the unique CNP mode for hybrid scenarios. Terrestrial, as well as satellite transmitters, can be considered. It offers network planning modules for 2G/2.5G, 3G/B3G, WLAN, WiMAX networks and more.

Different wave propagation models (computational methods) exist to simulate the propagation environment. These models are necessary to determine propagation characteristics for any arbitrary configuration. The predictions are required for a proper coverage planning, the determination of multipath effects as well as for interference and cell calculations, which are the basis for the high-level network planning process. The environments where these systems are intended to be installed, are ranging from indoor up to large rural areas. Hence wave propagation prediction methods are required covering the whole range of macro-, micro- and pico-cells including indoor scenarios and situations in special environments like tunnels or along highways.

- Rural and Suburban

- Urban

- Indoor

Rural and Suburban Propagation Models

WinProp offers various wave propagation models for rural and suburban environments.

Empirical models without consideration of the terrain profile between transmitter and receiver

- Hata-Okumura model
- Empirical two ray model
- ITU P.1546 model

Basic topographical profile prediction models (2D vertical plane models)

- Deterministic two ray model
- Longley-Rice model
- Parabolic equation method
- Knife edge diffraction model

Deterministic 3D models (3D topography)

- Rural Dominant path model
- Ray-tracing model

Urban Propagation Models

Radio transmission in urban scenarios is subject to strong multipath propagation. Dominant characteristics in these scenarios are reflection, diffraction, shadowing by discrete obstacles and the wave guiding in street canyons. To consider these effects in a propagation model, it is necessary to gain knowledge of all dominant propagation paths. These paths depend primarily on the base station antenna height with respect to the building heights around.

- COST 231 Walfisch-Ikegami Model

- Urban Dominant Path Model

- 3D Intelligent Ray Tracing

Indoor Propagation Models

The phenomena which influence radio wave propagation can generally be described by four basic mechanisms: Reflection, diffraction, penetration and scattering. For the practical usage of propagation models in real scenarios these mechanisms must be described by approximations. The predictions are required for a proper coverage planning, the determination of multipath effects as well as for interference and cell calculations, which are the basis for the high-level network planning process. The basis for any propagation model is a data base which describes the propagation environment. Considering indoor propagation suggests, for the purpose of propagation modeling, that each building element should be categorized into classes (wall, floor, door, window) and specified by its coordinates and finally its material properties (thickness, permittivity, conductivity).

- One Slope Model (Modified Free Space Model)

- Motley-Keenan Model (MK)

- COST-Multi-Wall Model (MW)

- Indoor Dominant Path Model

- Indoor Intelligent Ray Tracing

- 3D Standard Ray Tracing

2.4 Metamaterials

MTMs are periodic arrangements of sub-wavelength engineered materials, which exhibit electromagnetic properties that are not found in natural substances. J.C Bose first explored the concept of artificial materials in 1898 on twisted structures(Frenkiel (2009)). The material medium plays a key role in the propagation of the EM wave. The materials are classified based on their effective parameters called effective permeability and permittivity, as shown in Figure 2.5 (Caloz and Itoh (2005)). In the figure, the first quadrant represents right-handed (RH) materials, which support froward wave propagation and the third quadrant represents left-handed (LH) materials, which exhibit backward wave propagation. In the second and fourth quadrant, wave decays exponentially with time as it propagates through a medium.

2.4.1 Frequency Selective Surface(FSS)

The FSS is a particular class of MTM, and it is periodic to obtain specific reflection and transmission property. The FSS finds applications in stealth and aerospace technology as an absorbing medium or reflecting surface(Munk (2000)). Also, FSS is used in low observable platforms to enhance the characteristics of an antenna like gain, bandwidth and radar cross-section(RCS) reduction. The FSS structures are categorized into two types based on the periodic structure of the geometry. The periodic patches are etched on the substrate called capacitive FSS and the substrate with metallic ground comprises of apertures called inductive FSS. The specific spectrum is selected by the careful design of these periodic structures. Figure 2.6 shows some of the FSS structures.

μ

II.
$\varepsilon < 0, \mu > 0$:
$n = \sqrt{\varepsilon\mu} \in \mathbb{I}, n < 0$
plasmas ($\omega < \omega_{pe}$)
metals at optical frequencies
evanescent wave

I.
$\varepsilon > 0, \mu > 0$:
$n = +\sqrt{\varepsilon\mu} \in \mathbb{R}, n > 0$
isotropic dielectrics
right-handed (RH) /
forward-wave propagation

r

ε

r

III.
$\varepsilon < 0, \mu < 0$:
$n = -\sqrt{\varepsilon\mu} \in \mathbb{R}, n < 0$
Veselago's materials
left-handed (LH) /
backward-wave propagation

IV.
$\varepsilon > 0, \mu < 0$:
$n = \sqrt{\varepsilon\mu} \in \mathbb{I}, n < 0$
ferrites ($\omega < \omega_{pm}$)
(ferrimagnetic materials)
evanescent wave
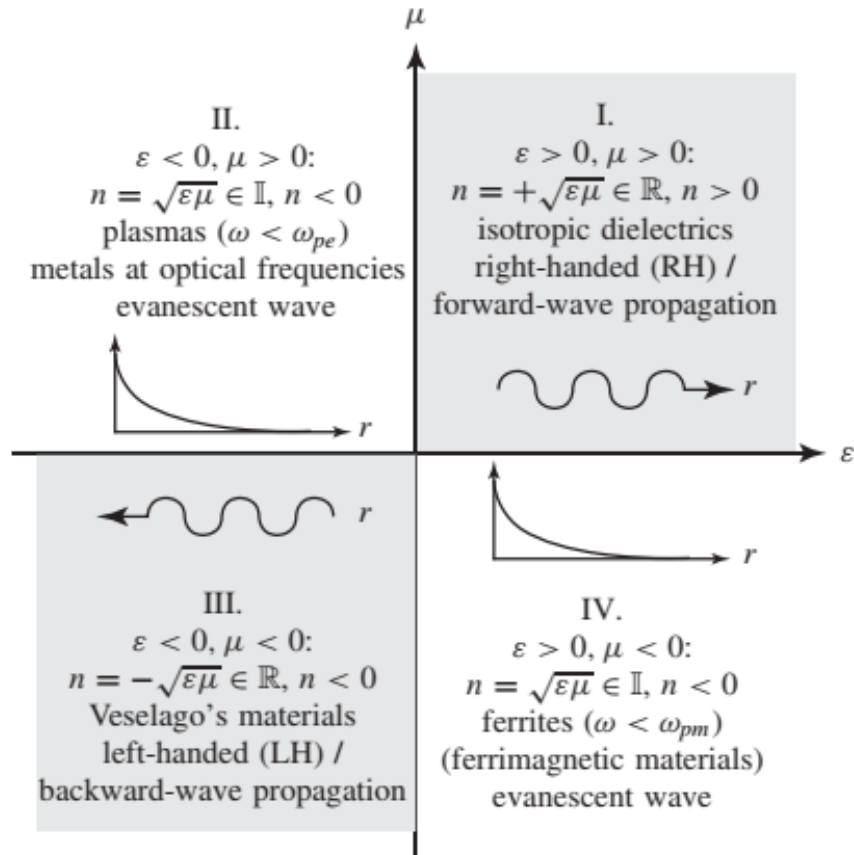
Figure 2.5: Material classification based on permeability- permittivity and refractive index (Caloz and Itoh (2005))

2.5 Literature Survey

In previous sections the introduction and background of few technologies are studied. In this section the literature survey for the selected objectives is divided into different subsections, the first section is mentioned on dual polarized MIMO antennas for 5G with list of recent works and how the proper dual polarized antenna element is selected for 5G applications. The second section gives details on low profile AMC based MIMO antennas which reflects the list of recent studies on importance of low profile and miniaturization in MIMO antennas for base station
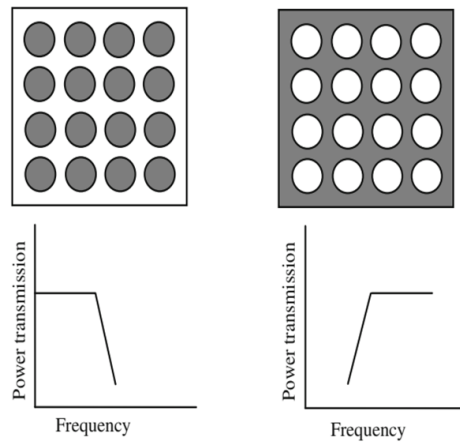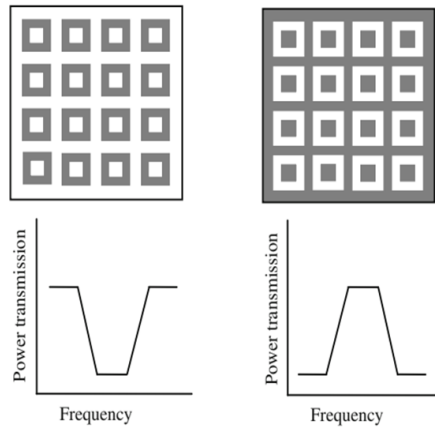
Figure 2.6: (a) array of circular metallic patches and array of circular apertures
(b) array of square metallic loops and array of square aperture rings

applications. The third section elaborates on metasurface based radomes for 5G
MIMO antennas by which the significance of radomes and its effect on MIMO
antennas are studied.

2.5.1 Dual Polarized MIMO Antennas for 5G

In recent years, multiple-input and multiple-output (MIMO) technology has also become the focus of radars and wireless communications. MIMO wireless communication systems may increase channel capacity, enhance data rate, and reduce multipath fading. Since strong mutual coupling between antennas will degrade the performance of MIMO systems seriously, design of high-isolation MIMO antennas is always desired. Different structures have been applied to suppress mutual coupling between MIMO antennas. By using parasitic elements, neutralization lines, decoupling networks, coupled resonator decoupling networks, defected ground structures, and electromagnetic (EM) bandgap structures. Deployment and polarization diversity MIMO antennas have also been considered to increase the isolation.

In Huiqing Zhai (2018) , a low profile MIMO antenna array with high isolation was implemented. In Jihoon Bang (2018),a miniaturized extremely close-Spaced four-Element dual-band MIMO antenna system with polarization and pattern diversity is analysed. In et al. (2016), an integrated dual MIMO antenna system with dual-function ground-plane frequency-agile Antenna is designed. In Saeidi-Manesh and Zhang (2018), an integrated four-element slot-based MIMO and a UWB sensing antenna system for CR platforms is proposed. In Kong and Xu (2018), a substrate integrated magneto-electric dipole antenna and its 3D MIMO system with metasurface for 5G/WiMAX/WLAN/X-Band applications is analysed. In et al. (2018b), a novel wide-band MIMO antenna system for smart phones is designed. In et al. (2018a), a reconfigurable MIMO antenna system for wireless communications is proposed. The different applications considered for designing MIMO antennas is observed for incorporating the various ideas in our research.

Dual Polarized antennas are widely used in modern communication systems.

A common feeding technique for dual polarized patch antennas is based on slot coupling, where micro-strip feeding lines are coupled to the radiating driver patches through slots in metallic ground. Two feed lines are usually needed to get a dual polarized antenna. To avoid overlapping between the two lines, a double layer substrate, or an air bridge, or via holes and a short strip is needed. All of them increase the realization cost of large arrays. In search of low cost single layer feed networks, antenna designers have developed several dual polarized slot-coupled patch configurations. In et al. (2018c), a low profile 45^0 dual-polarized antenna based on metasurface and its arrays for base station applications is designed. In Rifaqat Hussain and Shamim (2018), tri-band dual polarized patch antenna system for next generation cellular networks is proposed.

Recently, various designs of dual-polarized antennas have been developed for base station applications among them the design with arc shaped slots with high isolation and low cross polarization is selected for designing a single element. Initially the design is realized by implementing the dual polarized antenna with arc shaped slots by using coaxial cable feed and further analysed by using two orthogonal dipoles in cross pair feed baluns to get enough bandwidth and isolation.

To suppress the mutual coupling with good isolation is very stringent in closely spaced MIMO antennas. The mutual coupling degrades the overall performance of the entire MIMO antenna system and causes spectral regrowth X. Chen and Li (2018). Several methods are developed to suppress the mutual coupling between antenna elements. Some of the proposed techniques like decoupling networks, etched parasitic elements, complementary split ring resonators, electromagnetic band gap and defected ground structures are already reported Son Xuat Ta (2018). By using a wall like structure with SRR inclusion designed in between the monopole antennas almost 20 dB reduction is achieved M. M. Bait Suwailam and Ramahi

(2009). With two $\lambda/4$ slots in the ground plane acting like a wave trap utilized for coupling reduction of -33dB between two monopole antennas S. Zuo and Ma (2010). Another technique with folded SRR for very closely spaced patch antennas a reduction of 30 dB is obtained A. Habashi and Ghobadi (2011). Modified CSRR are printed on the decoupling substrate slab to achieve suppression of 27 dB to 11 dB on high and low permittivity substrates for densely packed patch antennas Z. Qamar and Shafique (2016).

In R. Hafezifard and Sadeghzadeh (2016), with elliptical split ring resonators placed horizontally between closely spaced meander lines antennas coupling reduction of 19 dB is obtained. A broadband neutralization line is used for decoupling between ultra wide band MIMO antennas to achieve coupling reduction lower than -22 dB Zhang and Pedersen (2016). Coupling reduction of -25 dB is achieved in E and H planes by using meta-structures for wideband dual polarized patch antenna array et al. (2017). With a pair of parallel coupled line resonators with band stop characteristics are used as decoupling element between microstrip antennas to obtain -26.2 dB coupling suppression K. S. Vishvaksenan and Raj (2017). A series of CLL meta-materials superstrate wall structures are designed for the coupling reduction of over 55 dB for patch antenna array A. Jafargholi and Choi (2019). By using periodic multi layered electromagnetic band gap structures between MIMO antennas mutual coupling reduction of 30 dB is achieved T. Jiang and Li (2018). The metalized via walls along with neutralized networks are designed for mutual coupling reduction of 28 dB between two patch antenna elements K. D. Xu and Xue (2018).

A metamaterial structure is designed for closely spaced microstrip patch antennas to lower the mutual coupling around -24.5 dB Iqbal (2018). Modified ADS(MADS) and H shaped DGS(HDGS) are adopted as decoupling structures

for closely spaced MIMO antennas which resulted -34.2 dB and -36.3 dB for MADS and HDGS respectively Z. Niu and Zhong (2019). As the side by side placement of antennas additionally needs a decoupling technology to minimize the surface currents flow, a novel approach on frequency selective surface (FSS) is developed for coupling reduction of -20 dB in E and H planes Y. Zhu and Yang (2019). By changing the shape of the ground plane under each antenna element the coupling from free space and the ground plane make out of phase and cancel with each other, which obtains more than 10 dB coupling reduction S. Zhang and Pedersen (2019). A metasurface based decoupling method is used to improve the isolation over 25 dB at two independent bands for two coupled MIMO antennas F. Liu and Yin (2020). Recently, a decoupling slot strip array for two dimensional microstrip antennas is proposed for coupling reduction in E, H and D planes D. Gao and Chen (2020).

2.5.2   Low Profile AMC Based MIMO Antennas

Artificial magnetic conductors (AMC) were proposed for the first time in 1999, and since then have been extensively explored and widely used in antenna and electromagnetic applications. The unique property of AMCs is their in-phase reflection coefficient at a certain frequency which makes them similar to magnetic conductors. The perfect magnetic conductors do not exist in nature, image theory indicates that a perfect magnetic conductor (PMC) surface would be an efficient candidate in the applications where the radiating element is very close to the ground plane, unlike a perfect electric conductor (PEC) surface whose radiation efficiency is very poor. AMCs exhibit a unique dispersive reflection response, which varies from 180^0 to -180^0, in the designed frequency band.

In Xue-Yan Song and Lian (2016) a low profile wideband bowtie antennas

is designed using AMC ground plane. The distance between the bowtie antenna and the AMC surface is maintained at $\lambda/10$. Bow-tie antenna, loaded with an open stub has broadband property. The good stable gain is achieved by utilizing the AMC ground plane. In A. Foroozesh and Shafai (2008) an artificial ground planes is designed for compact cavity-resonance dual-band high-gain antennas. A code based on method of moment (MoM) is developed to analyze and design such artificial ground planes. The reflection parameters obtained using the MoM code are employed to characterize the surface impedance of the artificial ground plane for different incident angles and both TE and TM polarizations. In Min Li and Cheun (2018) a low-profile dual-polarized dipole antenna using wideband artificial magnetic conductor (AMC) reflector with stable radiation pattern for use in 2G,3G,4G base stations operating from 1.7 to 2.7 GHz is presented. The antenna consists of a pair of crossed-dipoles and a wideband AMC reflector which consists of an AMC surface, a metallic ground plane and the air substrate between them. Six metallic ground walls are used to stabilize the radiation patterns. In Wei Hu and Yin (2016) A wideband dual-polarized slot antenna loaded with artificial magnetic conductor (AMC) is proposed for WLAN,WIMAX and LTE applications. The slot antenna mainly consists of two pairs of arrow-shaped slots along the diagonals of the square patch. Stepped microstrip feed lines are placed orthogonally to excite the horizontal and vertical polarizations of the antenna. To realize unidirectional radiation and low profile, an AMC surface composed of 7 $\times$ 7 unit cells is designed underneath a distance of 0.09λ from the slot antenna.

In Rola Saad (2012) a design methodology to reduce inter unit cell mutual coupling in a miniaturized dual band Artificial Magnetic Conductor (AMC) is described. The AMC features miniaturization using lumped component loading and flexible dual band design with minimum mutual coupling between subunit AMC cells. The advantages and disadvantages of four methods of designing a multi-

band AMC in terms of the minimum difference between the resonant frequencies of the two frequency bands is analyzed. In Marco Salucci (2014) the design of a low-profile narrowband antenna that is tunable over a wide frequency range is presented. A spline-based Ultra-Wideband (UWB) antenna is synthesized by means of time-domain-based PSO and is mounted on top of a reconfigurable Artificial Magnetic Conductor (AMC) obtained by replicating a square unit cell in a 15×15 periodic lattice. The AMC is composed by a planar array of periodic metallic strips printed on top of a PEC-backed dielectric substrate, connected by tunable capacitors (varactors), and has been designed to work within the (1-4)GHz bandwidth. In this design the reflection coefficient of the resulting narrowband antenna system can be easily controlled inside a wide frequency range by tuning the capacitance of the varactors inside the AMC groundplane. In J.Wu et al. (2017) a low-profile dual-polarized wideband omnidirectional antenna with artificial magnetic conductor (AMC) reflector is proposed. The antenna is designed to operated in the LTE band (1.7 - 2.7 GHz), and has a compact size. The antenna structure consists of a horizontally polarized (HP) circular loop antenna, a vertically polarized (VP) low-profile monopole antenna, and an AMC reflector. It is observed by carefully designing the reflection characteristics of the AMC reflector, the profile height of the proposed antenna is significantly reduced as compared with those of antennas backed by conventional PEC ground planes.

In R. Dewan and Yusoff (2015) a coplanar waveguide (CPW) wideband antenna operates from 2.69 GH to 6.27 GHz which act as reference antenna (RA) has been designed. A Dual Band AMC (DBAMC) unit cells have been proposed to operate at 2.45 GHz and 5.8 GHz. AMC is a metamaterial which mimics the behavior of zero reflection phase of Perfect Magnetic Conductor (PMC) at resonance frequency which not naturally existed in nature. Subsequently the antenna is incorporated with AMC unit cell, herein referred as Antenna with Dual Band AMC

33

(ADBAMC). In Yong-Wei Zhong and Zhong (2015) A novel fractal wideband artificial magnetic conductor (AMC) structure is designed as the ground plane of a printed bow-tie antenna for gain enhancement and low profile. The distance between the antenna and the AMC is reduced to one-eighth of the wavelength in free space at 1.7 GHz. In Kristou et al. (2017)a compact AMC unit cell achieving a 37% reduction in the largest dimension is proposed. Numerical technique is applied to simulate the behavior of the considered AMC and the conventional one based on mushroom-like unit cell. In Nagata et al. (2016) an AMC (Artificial Magnetic Conductor) composed of a FSS (Frequency Selective Surface) and the ground plane, and describes the design method of the unit cell of the AMC to realize PMC (Perfect Magnetic Conductor). The FSS that consists of a patch type FSS and a medium is proposed to realize broadband PMC characteristics. A frequency characteristics of the relative permittivity of the medium is calculated by equivalent circuit analysis. In addition, a near-ideal reflection phase is obtained by applying the medium.

In Dewan et al. (2012) AMC operates in three operating frequencies which are 2.3 GHz, 5.8 GHz and 8.36 GHz with the bandwidth of 5.64%, 1.73% and 3.58 % respectively. The size of AMC unit cells is relatively smaller compare to the previous designs. Parametric results for the reflection phase diagram is also analyzed. In Zhang et al. (2019) a dual-band dual-polarized wearable array is presented, based on a miniaturized innovating button radiator topology. A small-size rigid PCB is used as a basis for the button element. A flexible conducting textile (clothes) acts as the antenna ground, and a semi-rigid coaxial cable is used to feed the proposed antenna. In Liu et al. (2020)a low-profile dual-band dual-polarized antenna with an artificial magnetic conductor (AMC) reflector is designed for 5G communications. The antenna consists of a pair of crossed dual-polarized dual-band bowtie dipoles and a dual-band AMC reflector. By introducing trapezoidal

slots and U-shaped slots on the bowtie dipoles, miniaturization and dual-band characteristics are achieved. Moreover, T-shaped feeding structures are utilized to broaden the bandwidth of the bowtie dipoles. By adopting a dual-band AMC reflector instead of a conventional perfect electric conductor (PEC) reflector, the distance between the radiator and the reflector is reduced. In Liu et al. (2019) a low-profile differentially fed dual-polarized slot antenna is proposed for base station application. Its radiator is an octagon patch etched with two normal H-shaped slots. The folded feeding line is introduced to accommodate the differentially fed scheme and tune impedance matching. Both high isolation and stable radiation patterns are realized by using the differential feeding technique.

2.5.3 Metasurface Based Radomes for 5G MIMO Antennas

Frequency selective surface (FSS) is a kind of one or more layers of periodic metal patch on the dielectric substrate. FSS can effectively control the transmission and reflection of electromagnetic waves, so the function of frequency selection and polarization selection can be achieved for propagation of electromagnetic waves on different frequencies. Frequency selective surfaces (FSS) are periodic structures composed of a one- or two-dimensional lattice and they are usually designed to exhibit a band-pass or a band-stop response. For more than four decades, FSSs have been attractive options because of their comprehensive applications ranging from microwave antennas, radars and satellite communication systems. Unlike traditional microwave filters, the frequency responses of FSSs are not only functions of frequency, but also functions of the incident angle and polarizations of the incident electromagnetic waves.

In Thummaluru et al. (2018) a new frequency selective surface (FSS)-based isolation technique is proposed for multiple-input-multiple-output (MIMO) an-

tennas. This method has a conventional ground plane of monopole-based MIMO antenna which is replaced with FSS to improve the isolation between the antenna elements as well as to reduce MIMO antenna radar cross section (RCS). With FSS, isolation enhancement and RCS reduction have been achieved by altering antenna characteristics. The RCS reductions of 25 and 20 dBsm have been achieved by replacing the PEC ground plane with FSS and M-FSS, respectively. Also, by using the FSS, a stable RCS reduction up to 60^0 for TE polarization and up to 45^0 for TM polarization also achieved. In Li et al. (2016) a novel frequency selective radome (FSR), which is "transparent" within the operating band of the antenna while absorbing out-of-band incoming waves in a very wide band, is given in this article. In order to absorb undesired signals out of the band, square loops loaded with lumped resistors are used. The pass-band property is realized by employing meandering square slots with a smaller period to enhance the stability under large incident angles. The equivalent circuit method is also introduced to explain the working principles of the FSR and verify the full-wave simulation results based on the FEM codes. The structure's performances under oblique incidences are also presented. In Hamza Ahmad and Seman (2020) a miniaturized frequency selective radome with wideband absorption is presented. The design consists of bandpass FSS and a resistive FSS. Both FSS's are combined together through a foam spacer. A slotted miniaturized form of the conventional Jerusalem cross structure is employed as the bandpass FSS. A meandered form of the basic square loop with lumped resistors incorporated in each side of the loop is used as the resistive FSS. The bandpass FSS ensures the transmission in the X-band, which is the operating band of the radome. The resistive FSS absorbs the out-of-band signals and thus reduces RCS at higher frequencies.

In Costa and Monorchio (2011)a frequency selective radome is presented, acting as a pass band filter at a given frequency band, while behaving as an absorber

out of the operating band. The reflection band of the FSS filter is used as the ground plane of a outer wideband absorber based on resistive high-impedance surfaces. The absorber, which reduces the signature of the antenna system illuminated by out of band signals, comprises a resistive FSS designed to minimize losses within the transmitting band of the radome. The composite structure is thoroughly analyzed by an efficient equivalent circuit approach and by full-wave numerical simulations. In Tu et al. (2017)a novel miniaturized frequency selective rasorber (FSR) with tunable passband is presented. The unit cell dimension of designed structure is miniaturized to $\lambda/30$. Miniaturization of the FSR unit cell is achieved by using convoluted elements, introducing varactors, and adopting nonresonant elements. The property of tunable passband is obtained from the variable capacitance of loaded varactors. In Han et al. (2017) aS switchable low-profile broadband frequency rasorber/ absorber based on slot arrays is presented. An equivalent circuit model is proposed to synthesize a rasorber with the transmission window within the absorption band. Based on the slot arrays, simple design guidelines for rasorber design are developed. Low-profile broadband rasorber and high-selectivity rasorber are respectively, designed and analyzed to verify the design strategies. By loading the switching diodes, a switchable rasorber/absorber is presented and analyzed, which exhibits small insertion loss at the transmission window and a bandwidth around 100% while the thickness is less than 10% of the free-space wavelength at the lowest operating frequency. Moreover, one extension of dual-polarized rasorber is also designed and analyzed to further validate the design strategy. For demonstration, the rasorber prototypes are fabricated and measured, good agreement between the simulation and measured results is observed.

In Wang et al. (2014)a composite radome with wideband transparent and absorbing properties is presented. The composite unit of this radome is a multilayer

37

structure combining metallic and resisitive components. The unit is studied thoroughly. Under the TE and TM incident waves' illumination separately from different directions, its transmission/reflection coefficients are given. In Zhu et al. (2017) a miniaturized and tunable frequency selective structure with wideband absorbing property is designed for the application of radar radome. To avoid the problem that the periodicity of the bandpass FSS should larger than that of resistive FSS, in this design, the varactor diodes are loaded on the band-pass FSS to achieve the operating frequency adjustability and miniaturize the periodicity of FSS. In Shang et al. (2014) a novel design of a transmission window within the absorption band of a circuit analog absorber, named as frequency-selective rasorber (FSR), is presented. Based on an equivalent circuit model, the conditions are formulated to produce a passband with small insertion loss and to reduce the reflection at frequencies below and above the passband in the meanwhile. Simple design guidelines of our proposed FSR are then developed. With loaded lumped elements, the arrays of square-loop and cross-dipole are combined to realize its implementation. In Weiwei Wu (2018) an ultrathin K-band Frequency Selective Surface with one narrow passband and wide reflection bands is presented. FSS structure is very insensitive to different polarizations and a large variation of the RF incident angle. Working as a low-profile radome for its covered antenna, this FSS is electromagnetic transparent within its passband; out of this passband, it helps the antenna achieve Radar Cross Section (RCS) reduction or protects the antenna from interference. It can be a good candidate for the applications such as antenna radomes and spatial filters, in which a wide frequency range of electromagnetic interference needs to be suppressed.

In Costa and Monorchio (2012) a frequency selective radome is presented, acting as a pass band filter at a given frequency band, while behaving as an absorber above the transmission band. The pass band behavior is obtained by a metallic

FSS realized through a compact interdigitated Jerusalem cross element characterized by a very large rejection band. The metallic FSS is used as the ground plane of a thin wideband absorber based on resistive high-impedance surfaces within the total reflection band. The outer absorber reduces the signature of the antenna system when the radome is illuminated by out of band signals. The resistive FSS which comprises the absorber is designed so to minimize losses within the transmitting band of the radome. The composite structure is thoroughly analyzed by an efficient equivalent circuit approach and by full-wave numerical simulations. In Liguo Liu (2013) a novel radome is presented, which is transparent at operating frequency and is invisible out of band. In order to prevent reflection of the incoming power, frequency selective surfaces loaded with the lumped resistors are employed. To obtain the pass-band properties in lower frequencies, the convoluted slots are utilized. It performs with high transmission characteristics in band, and broadband absorbing properties out of band simultaneously. The oblique incidences are also given for both transmission coefficients and reflection ones. In Xianjun Sheng and Liu (2019) a low-frequency transmissive frequency selective rasorber (FSR) with high in-band transmission and wideband absorption characteristics is presented. It comprises the top resistive sheet and the bottom bandpass FSS. For resistive sheet, the tiny strip-type parallel LC resonator composed of square spiral inductor and its two-sided capacitors is inserted between the resistor-loaded crosses to achieve lower insertion loss (IL) by cutting off the lossy path. The bandpass FSS with high selectivity consists of Jerusalem cross slot array and capacitive metallic patches.

2.6   Summary

With the overview of the basic terminologies and its recent literature survey the following chapters discusses in detail about the research work carried out in accordance with the existing literature by implementing the novel techniques to obtain the desired results and to meet the 5G standard requirements.

CHAPTER 3

COMPACT 2×2 DUAL SLANT 45^0 POLARIZED MIMO ANTENNA WITH LOW MUTUAL COUPLING AND HIGH ISOLATION FOR 4G LTE BAND 40

3.1 Introduction

In this chapter, initially compact dual slant 45^0 polarized MIMO antenna element is designed and extended for 2×2 MIMO antenna system. A radio wave is made up of both electric and magnetic fields. In free space, the electric and magnetic fields are mutually perpendicular and are also perpendicular to the direction of propagation. The direction of oscillation of the electric field component, when a radio wave is propagating in a medium, is called the polarization of the radio wave. Antennas are usually developed to receive and transmit radio waves that are polarized in a specific way. The different types of polarizations are discussed below.

- Linear Polarization When the electric field is oscillating in the horizontal or vertical direction, the radio wave is said to be linearly polarized as shown in Figure 3.1.

- Slant Polarizartion When the electric field oscillates at –45 degrees and +45 degrees from a reference plane of 0 degrees, the polarization is said to be slant as shown in Figure 3.2. It is another form of linear polarization, it is equivalent to taking a linearly polarized radio wave and rotating it 45 degrees.
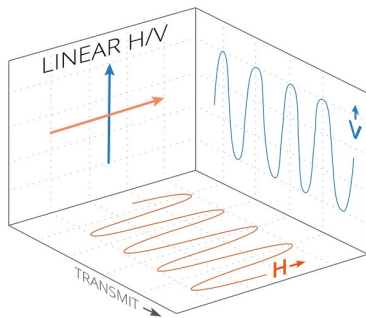
Figure 3.1: Linear Polarization.
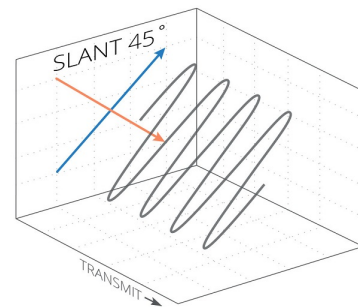
Figure 3.2: Slant Polarization.

- Circular Polarization When the polarization of a radio wave rotates while the signal propagates. Based on the direction the signal is rotating, circular polarization can be classified as two types: Right Hand Circular Polarization (RHCP) and Left Hand Circular Polarization (LHCP). A Circularly Polarized signal consists of two perpendicular electromagnetic plane waves of equal amplitude, which are 90 degree out of phase as shown in Figure 3.3.
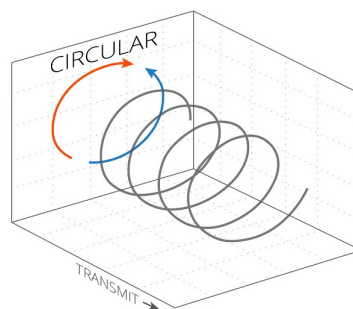
Figure 3.3: Circular Polarization.

- Elliptical Polarization Elliptically polarized radio signals consist of two perpendicular waves of unequal amplitude which differ in phase by 90 degree.

The orientation of the base station antennas with respect to linear an slant 45^0 polarization are shown in Figure 3.4 and 3.5 respectively.

Figure 3.4: Base Station Antennas with Linear Polarization.

Figure 3.5: Base Station Antennas with Slant 45^0 Polarization.

3.2 Dual Slant Polarized Bow-Tie Antenna Element:

In this design, a novel dual slant polarized bow-tie antenna element operating at Band 40 (2.3 to 2.4 GHz) is designed using FR4 substrate of size 50 mm, relative permittivity of 4.4, height (h) of 1 mm and loss tangent of 0.02. The two bow-tie antenna elements are excited by the two separate printed balun feed network designed using FR4 substrate. The bottom ground plane is also designed by using same FR4 substrate of size 100 mm, relative permittivity of 4.4, with height (h) of 1.6 mm and loss tangent of 0.02.

The geometry of the design with the two printed feed networks arranged in slant 45^0 gives high isolation and low mutual coupling between the elements when implemented for MIMO designs. Initially the design is implemented with normal patches and later on introduced the L-shaped slots and U-shaped notches on the radiator elements to obtain high isolation. The different stages of the DPA are shown below in Figure 3.6. The geometry and isometric view of the proposed dual slant polarized antenna (DSPA) are shown in Figure 3.7 and 3.8.

Stage 1: Geometry of the DPA Antenna   Stage 2: Geometry of the Dual Polarized Antenna with L-Shaped Slots   Stage 3: Geometry of the Proposed Dual Polarized Antenna
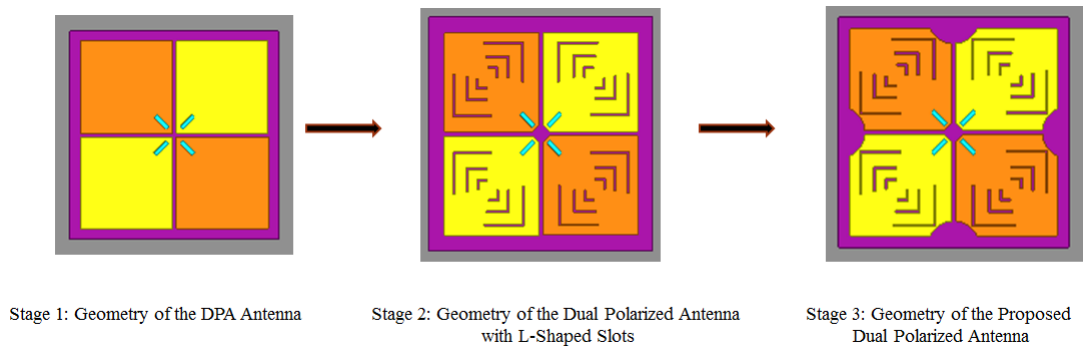
Figure 3.6: Different Stages of the Proposed DSPA.
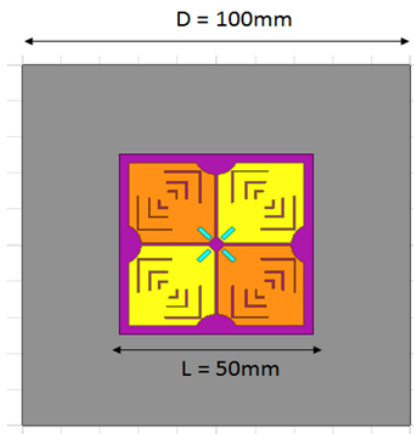
Figure 3.7: Geometry of Proposed DSPA.
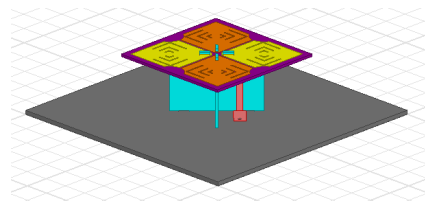
Figure 3.8: Isometric View of Proposed DSPA.

3.2.1 Printed Feed Network:

For dual polarized antennas, port isolation is one of the most important factors that influence the sensitivity of the receiving channel and the stability of receiver. Consequently, miniaturized base station antennas with high port isolation are becoming one of the hottest issues in modern wireless communication. Due to the complexity in soldering on the top and bottom of bow-tie dipoles with coaxial cables. The alternative approach is used to design the dual polarized antenna which consists of two perpendicularly crossed bow-tie dipoles printed on FR4 substrate.

Each bow-tie dipole is excited by a microstrip stub that is directly fed by coaxial line, enabling the antenna to be fully planar.

The configuration of the baluns is designed initially with single microstrip line feed on front side and two patches on the back of substrate which will be connected to the printed dipoles and ground plane at top and bottom respectively. The design is simulated in ANSYS HFSS 19.0 for desired frequency. The two printed feed networks are matched at desired frequency with 180^0 phase shift. The two feed networks are integrated with the help of slits provided in two substrates are shown in Figure 3.9 and 3.10.
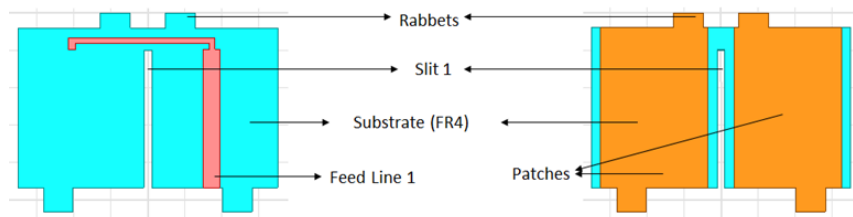
Figure 3.9: Front and Back View of Feed Network 1 .
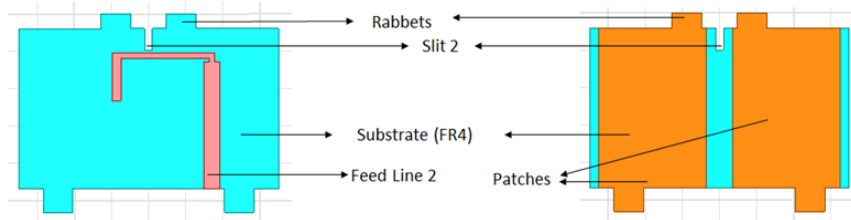
Figure 3.10: Front and Back View of Feed Network 2.

The simulation results are shown from Figure 3.11 to 3.13. From the simulated results it is observed that the proposed dual slant polarized antenna covers -10 dB impedance bandwidth from 2.2 GHz to 2.8 GHz. A high port to port isolation of around 36 to 40 dB is observed for entire Band 40. The simulated radiation

patterns are obtained for both E and H planes. The co-cross polarization levels resulted around 25 dB for both E and H planes.
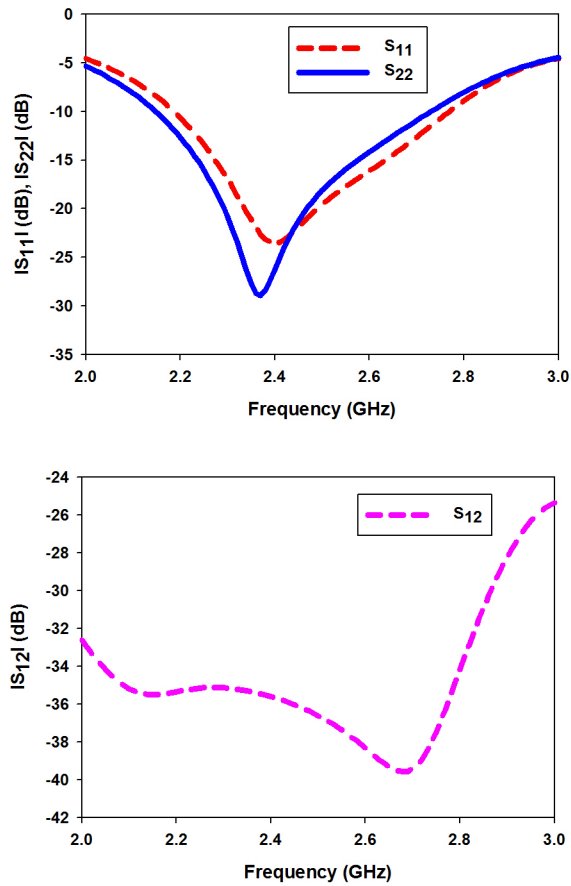
Figure 3.11: Simulated Scattering Parameters.

The designs are fabricated and tested. The measured results are in agreement with the simulated results. The details of the fabricated antenna are shown in Figure 3.14 and 3.15.

The measured plots of the fabricated dual slant polarized antenna with printed feed network are shown in Figure 3.16. From the measured plots it is observed
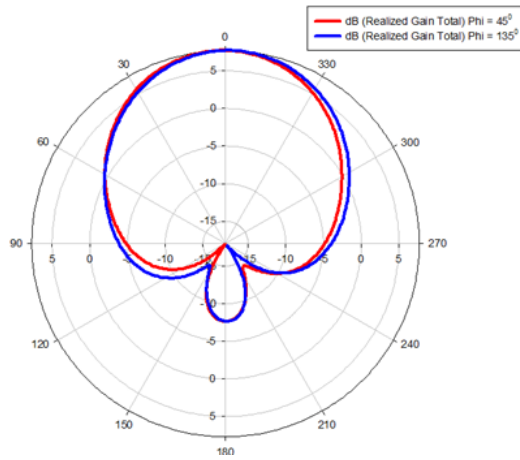
Figure 3.12: Simulated Realized Gain.
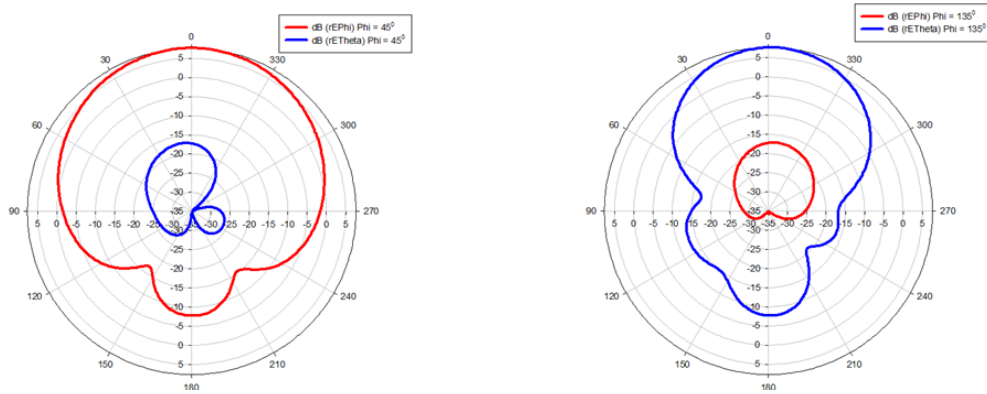
Figure 3.13: Simulated Radiation Patterns for both E and H Planes.

that the DSPA covers the frequency band from 2.2 GHz to 2.6 GHz which is the required Band 40 for the 4G LTE requirements. The high isolation resulted to be below 35 dB for the proposed dual slant polarized antenna element.

The radiation pattern measurements are done separately when transmitting is placed in both horizontal and vertical polarization. The receiving dual slant polarized antennas are named as antenna1 and antenna2 while taking measurements.
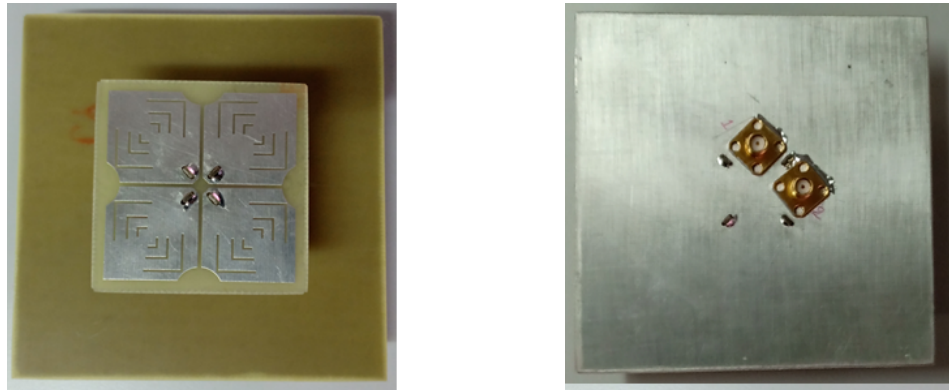
Figure 3.14: Top and Back View of the Fabricated DSPA.
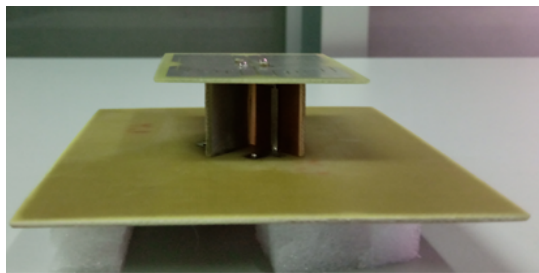
Figure 3.15: Side View of the Fabricated DSPA.

The far field measurement setup for the dual slant polarized antenna with standard horn antennas is shown in Figure 3.17. The measured radiation patterns for antenna 1 when transmitting in both vertical and horizontal polarization are shown in Figure 3.18 and 3.19, for antenna 2 it is shown in Figure 3.20 and 3.21.

The setup for measurement of gain for dual slant polarized antennas with two standard gain horn antennas is shown in Figure 3.22. The measured gain for the dual polarized antenna is shown in Table 3.1.
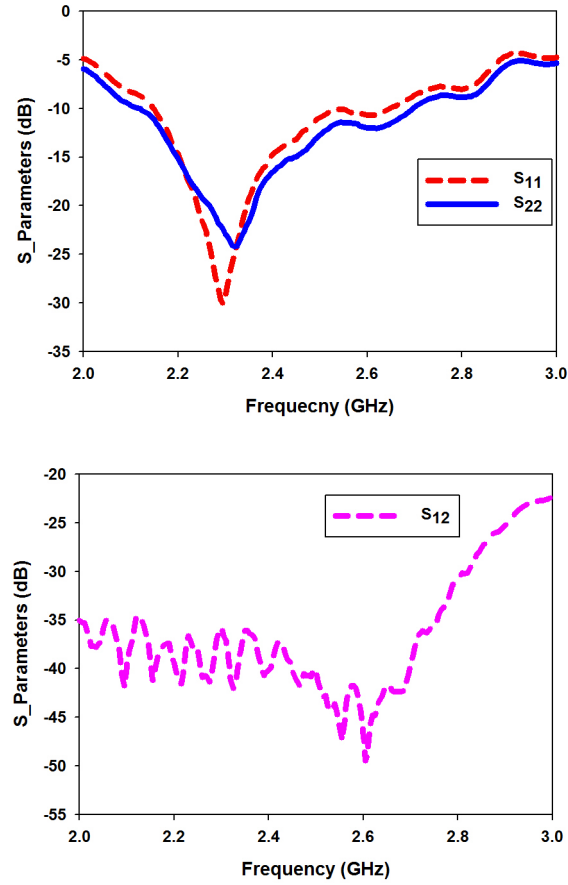
Figure 3.16: Measured Scattering Parameters.

Table 3.1: Measured Gain for Antenna 1 and Antenna 2.

Frequency(GHz)	Antenna 1(dB)	Antenna 2(dB)
2.2	7.65	7.57
2.25	7.54	7.81
2.3	7.62	7.52
2.35	7.58	7.46
2.4	7.84	7.61
2.45	7.02	7.25
2.5	7	7.45

The comparison of simulated and measured results are shown in Table 3.2.

49

Figure 3.17: Far Field Measurement Setup of Dual Slant Polarized Antenna.

A. Transmitting Antenna in Vertical Polarization for Antenna 1

At 2.3 GHz   At 2.35 GHz   At 2.4 GHz

Co-Pol
Cross-Pol
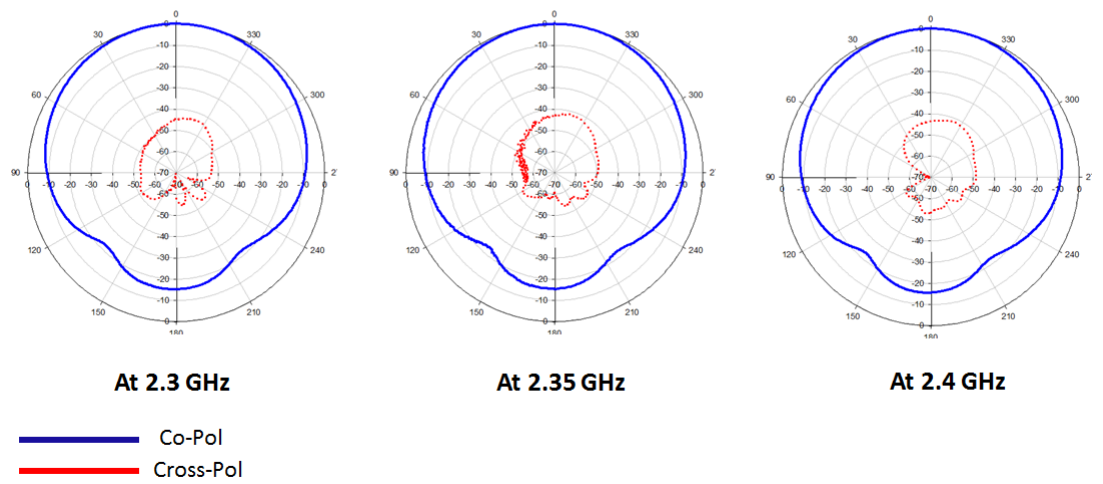
Figure 3.18: Measured Radiation Patterns for Antenna 1 with Tx. Antenna Vertically Polarized.

B. Transmitting Antenna in Horizontal Polarization for Antenna 1

At 2.3 GHz   At 2.35 GHz   At 2.4 GHz

Co-Pol
Cross-Pol
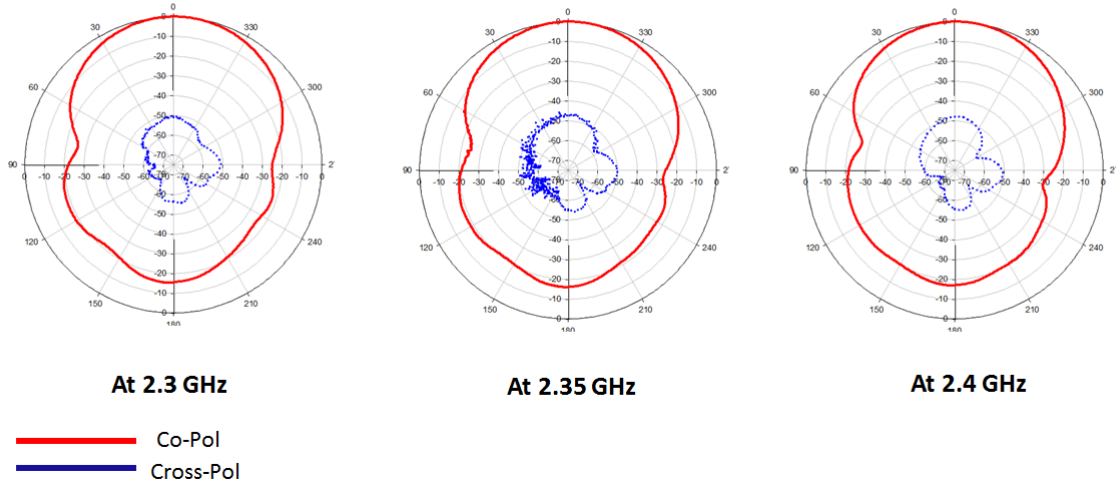
Figure 3.19: Measured Radiation Patterns for Antenna 1 with Tx. Antenna Horizontally Polarized.

A. Transmitting Antenna in Vertical Polarization for Antenna 2

At 2.3 GHz   At 2.35 GHz   At 2.4 GHz

Co-Pol
Cross-Pol
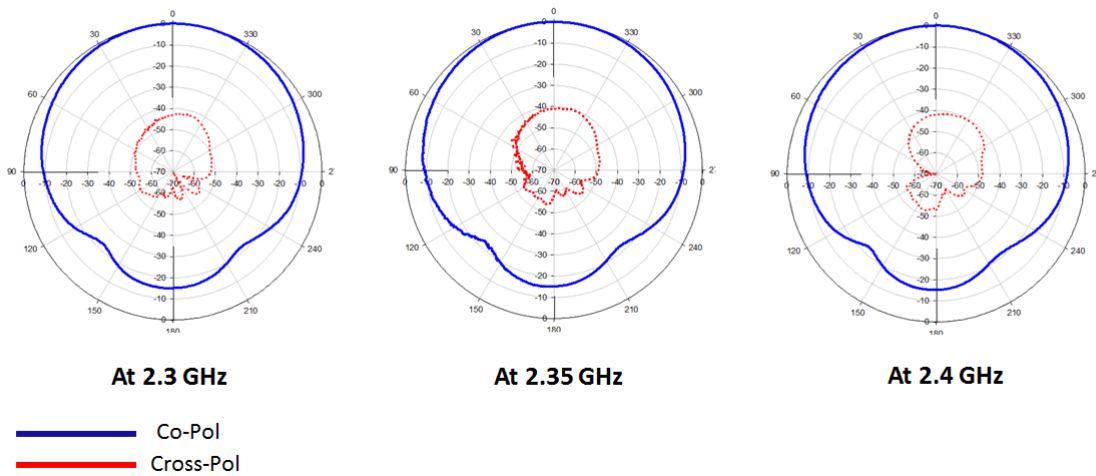
Figure 3.20: Measured Radiation Patterns for Antenna 2 with Tx. Antenna Vertically Polarized.

At 2.3 GHz   At 2.35 GHz   At 2.4 GHz

Co-Pol
Cross-Pol
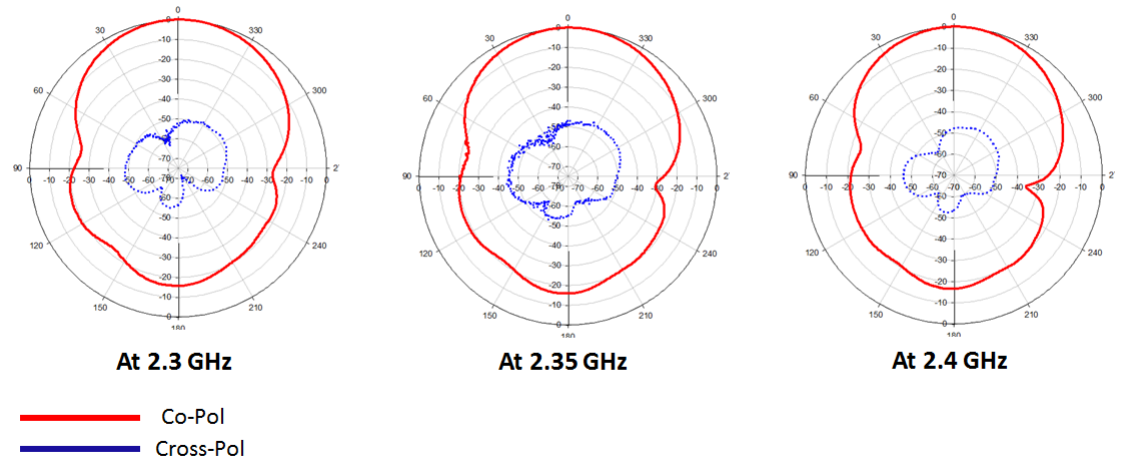
Figure 3.21: Measured Radiation Patterns for Antenna 2 with Tx. Antenna Horizontally Polarized.

Figure 3.22: Gain Measurement Setup with Standard Gain Horn Antennas .

3.3 Compact 2×2 MIMO Antenna System with Dual Slant 45^0 Polarized Antenna Element

3.3.1 Dual Slant 45^0 Polarized MIMO Antenna Element

The geometry of the proposed dual slant 45^0 polarized antenna is shown in Figure 3.23. The antenna consists of radiator, printed feed structure and a PEC reflec-

Table 3.2: Comparison of simulated and measured results at 3.5 GHz.

Parameters	Simulated Results(dB)	Measured Results(dB)
Reflection Coefficient	-23.57 , -26.27	-18.94,-21.05
Isolation	-35.30	-39.47
Gain	7.66 , 7.70	7.58 , 7.46
Front to Back Ratio	15.27	17.25

tor.The main radiator of the proposed antenna is made up of two printed dipoles in orthogonal orientation and fabricated on FR4 substrate with relative dielectric constant of 4.4. The arrangement of two such antennas in cross-pairs provides 45^0 polarization radiations. To improve the isolation, three pairs of L-slots are introduced on each arm of the radiator. The geometry of the each arm with L shaped slots on the radiators enhance the port to port isolation and suppress the cross polarization levels between the two dipole antenna elements.

Antenna Element 1   Antenna Element 2   PEC Reflector
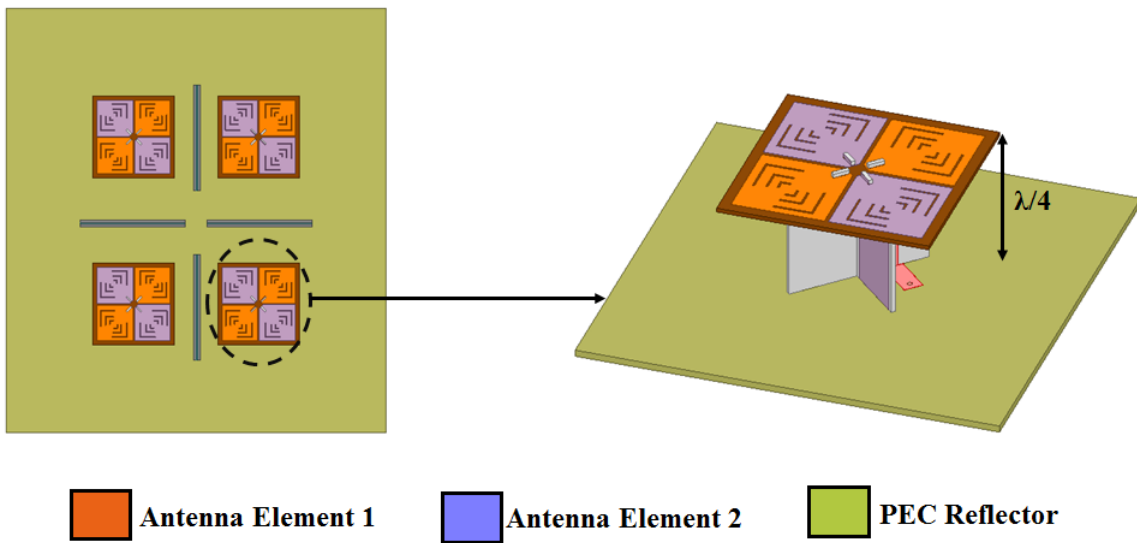
Figure 3.23: Geometry of the Proposed Dual Slant 45^0 Polarized MIMO Antenna Element.

The feed structure is printed on two vertical substrates with shaped feed lines, which are properly designed for good impedance matching on FR4 substrate. The

extra bumps called rabbets on each edge of the vertical substrates of the feed structure are utilized to feed the antenna elements as shown in Figure 3.24. Each feed substrate is provided with a slit in the middle so as to make orthogonal feeding network. The bottom PEC reflector contains the extended feed lines of the two vertical substrates where the two 50Ω coaxial cables for the feed structures are connected. It is also observed that the two individual ports of dual polarized antennas with this arrangement provide better port to port isolation. The compactness of the structure is obtained by optimizing the size of radiator for C-RAN applications. Optimizations are carried using FEM based 3D electromagnetic (EM) simulation software Ansoft HFSS 19.0.
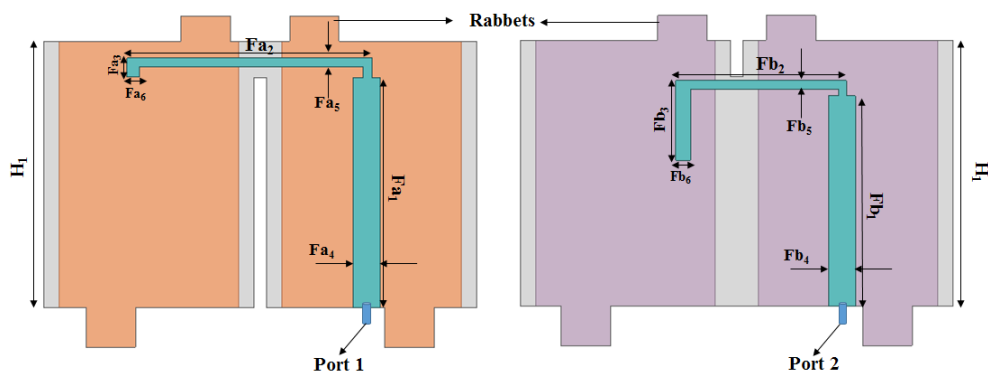
Figure 3.24: Geometry of the Printed Feed Network.

54

The fabricated prototype of the dual slant 45^0 polarized MIMO antenna element is shown in Figure 3.25. Measured and simulated S-Parameters for the fabricated prototype are shown in Figure 3.26. It is observed with reflection coefficient below -15 dB for the entire band 2.3 to 2.4 GHz. A high isolation of -30 dB is measured for the entire band. Measured radiation patterns for the single dual polarized MIMO antenna in both E and H planes are shown in Figure 3.27. The measured gain for both the antenna elements are shown in Figure 3.28. An gain of 7.5 dB is observed for both polarized antenna elements. The optimized dimensions of the fabricated prototype antenna are given in Table 3.3.

Table 3.3: Optimized Dimensions of the Proposed 2×2 MIMO Antenna.

Parameters	Value(λ_0)	Parameters	Value(λ_0)
L	2.03	W	1.84
L1	0.51	L2	0.4
L3	0.17	L4	0.07
L5	0.04	L6	0.019
W1	0.004	W2	0.08
W3	0.025	g1,g2	0.04
d	0.02	c	0.006
h	0.008	g3,g4	0.01
Fa1	0.22	Fa2	0.14
Fa3	0.02	Fa4,Fb4	0.018
Fa5,Fb5	0.006	Fa6,Fb6	0.007
H	0.19	H1	0.24

The designed dual slant 45^0 polarized antenna element can be used to build MIMO for C-RAN applications. The spacing between the elements in both azimuth and elevation planes play a very stringent role for observing the effect of mutual coupling between the antenna elements in MIMO. To obtain the high isolation and low mutual coupling for the dual slant 45^0 polarized antenna elements is a difficult task. The proposed technique and compactness of the proposed antenna element makes it suitable for building MIMO and Massive MIMO antenna
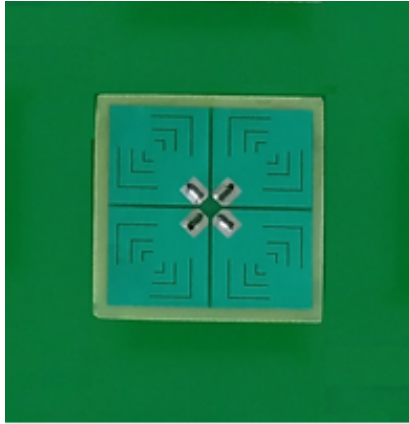
Figure 3.25: Fabricated Prototype of the proposed antenna.
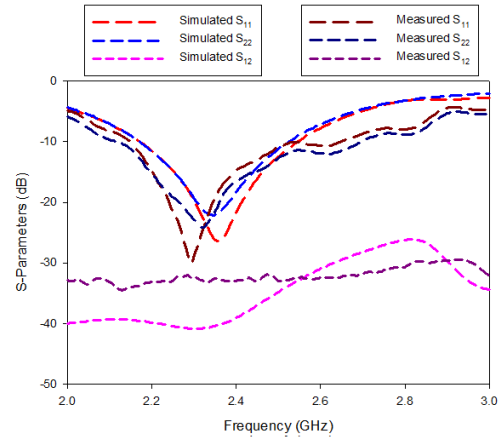
Figure 3.26: Simulated and Measured S-Parameters of the Proposed Antenna.

systems with both and polarization diversity.
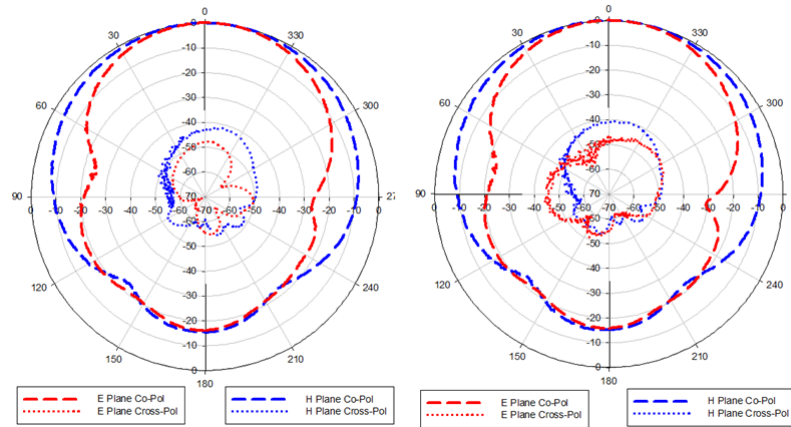
Figure 3.27: Measured Radiation Patterns in E and H Planes.

3.3.2 Periodic Array of SRRs Loaded with Transmission Line

Split Ring Resonator(SRR)   A split-ring resonator(SRR) is a type of meta-material used to produce desired magnetic response in different structures. It con-
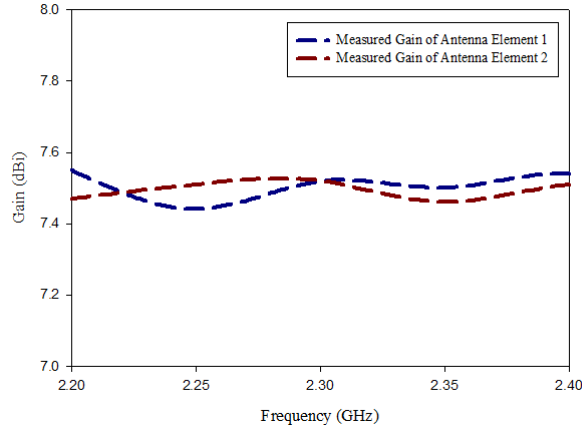
Figure 3.28: Measured Gain of the Proposed Antenna.

sists of two concentric metal rings, etched on a dielectric substrate, with slits etched on opposite sides. The designed SRR unit cell with boundary conditions are shown in Figure 3.29. Each SRR creates a strong magnetic field so as to induce resonating currents in the loop and generate equivalent magnetic dipole moment. The two SRR rings are coupled by the strong distributed capacitance caused by the gap between the rings. Total capacitance of the SRR arises from the splits and gap between the two rings whereas the inductance arises from the conducting rings. Therefore, the total intensity of currents flowing through the rings remains the same for any angular co-ordinates. The simulated S-parameters for the designed SRR unit cell are shown in Figure 3.30.

The schematic view of the square SRR and its equivalent circuit are shown in Figure 3.31. The resonant frequency of the square SRR is given by the following formula where L_{eq} and C_{eq} represents the total inductance and conductance of the square SRR.

57
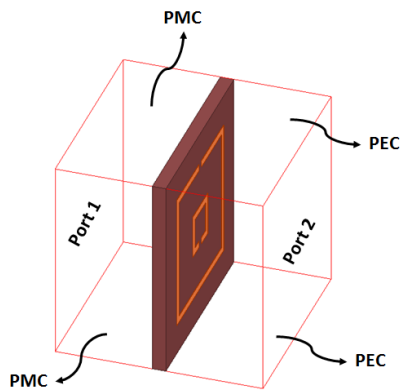
Figure 3.29: Model of SRR With Boundary Conditions.
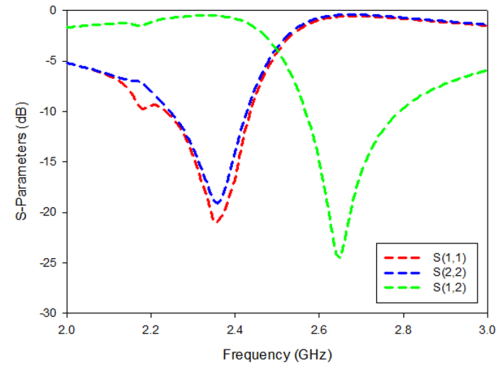
Figure 3.30: Simulated S-Parameters of SRR.

$$f_0 = \frac{1}{2\pi\sqrt{L_{eq}C_{eq}}} \tag{3.1}$$
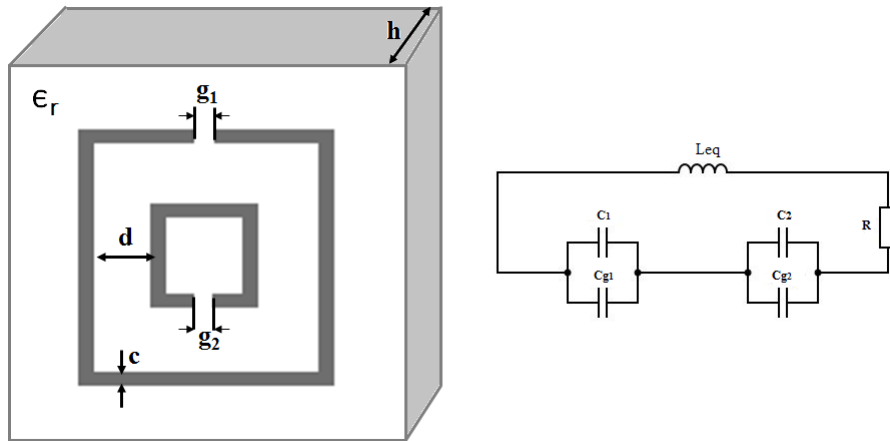
Figure 3.31: Schematic view of square SRR and its equivalent circuit
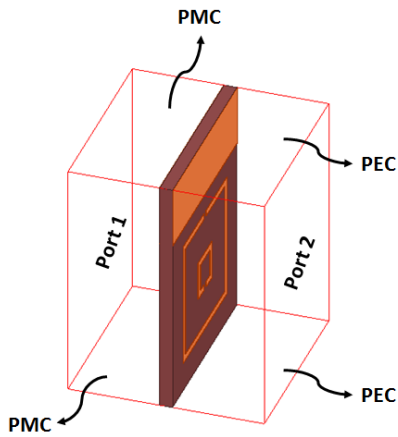
Figure 3.32: Model of SRR loaded with transmission line.
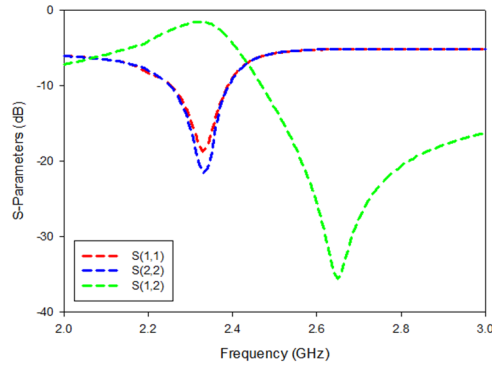
Figure 3.33: Simulated S-Parameters of SRR unit cell loaded with transmission line.

Split Ring Resonator Loaded with Transmission Line   The vertical strips are considered by utilizing FR4 substrates with relative dielectric constant of 4.4 on which array of split ring resonators and copper strips are embedded on either sides of the FR4 substrate. When an array of electrically small SRRs is excited by means of a time varying magnetic field, the structure behaves as an effective medium with negative effective permeability in a narrow band above SRR resonance. The mutual coupling between the two dual polarized dipole antennas is reduced by the copper strips and the SRR embedded on the vertical strips in both azimuth and elevation planes. The model of SRR loaded with transmission line is shown in Figure 3.32. The simulated S-parameters for the designed SRR unit cell loaded with transmission line are shown in Figure 3.33. The fabricated prototype of the vertical strips used in 2×2 MIMO configuration is shown in Figure 3.35. The designed vertical substrates are inserted at 0.6λ and 0.8λ in azimuth and elevation plane respectively.

The schematic view and equivalent circuit of periodic array of SRRs loaded with tranmission line is shown in Figure 3.34. From the equivalent circuit model

59
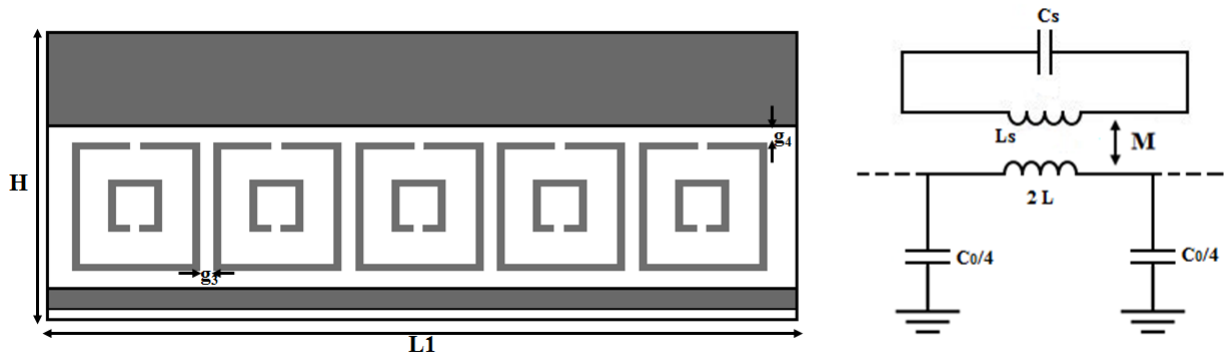
Figure 3.34: Schematic view and equivalent circuit of periodic array of SRRs loaded with transmission line.

the resonant frequency is calculated by using the following formula. For the desired resonant frequency resultant inductance and capacitance resulted to be 0.30μH and 0.015ρF. The mutual inductance between the SRR and loaded transmission line is indicated by 'M' which is given by using the below formula where L indicates per section inductance and the fraction f is the slot area occupied by the square rings.

$$\omega_0 = \frac{1}{\sqrt{L_s C_s}} \tag{3.2}$$

$$M = 2Lf \tag{3.3}$$

60
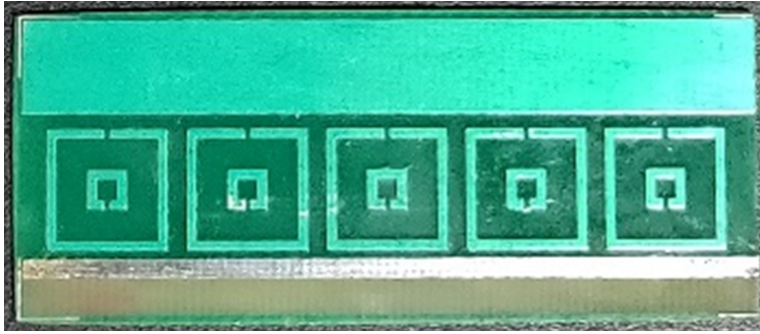
Figure 3.35: Fabricated Prototype of the Proposed Printed Periodic Array of SRRs Loaded with Transmission Line.

3.3.3 Implementation of 2×2 Dual Slant Polarized MIMO Antennas with Periodic Array of SRRs

2×2 MIMO Antenna Configuration 2×2 MIMO antenna configuration with dual slant polarized antennas is implemented. The spacing between the elements is considered as 0.6λ by 0.8λ in azimuth and elevation plane respectively. Dual slant 45^0 polarized antenna elements are considered to build the MIMO. To analyse the effect of mutual coupling between the each polarized antenna element in azimuth and elevation planes specific nomenclature is given for the 2×2 MIMO configuration as shown in Figure 3.36.

The row 'A' contains the two antenna elements with A1-1, A1-2, A2-1, A2-2 and row 'B' contains B1-1, B1-2, B2-1, B2-2 giving eight individual ports for the entire 2×2 MIMO. The complete view of the 2×2 MIMO Antenna with vertical strips is shown in Figure 3.37 and 3.38.

Effect of Periodic Array of SRRs Loaded With Transmission Line When the elements are placed closely the changeling task in MIMO antenna system is to suppress the mutual coupling between the adjacent antenna elements. To anal-
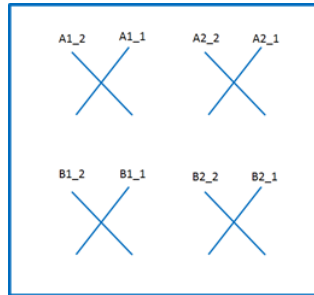
Figure 3.36: Nomenclature of the 2×2 MIMO Configuration.
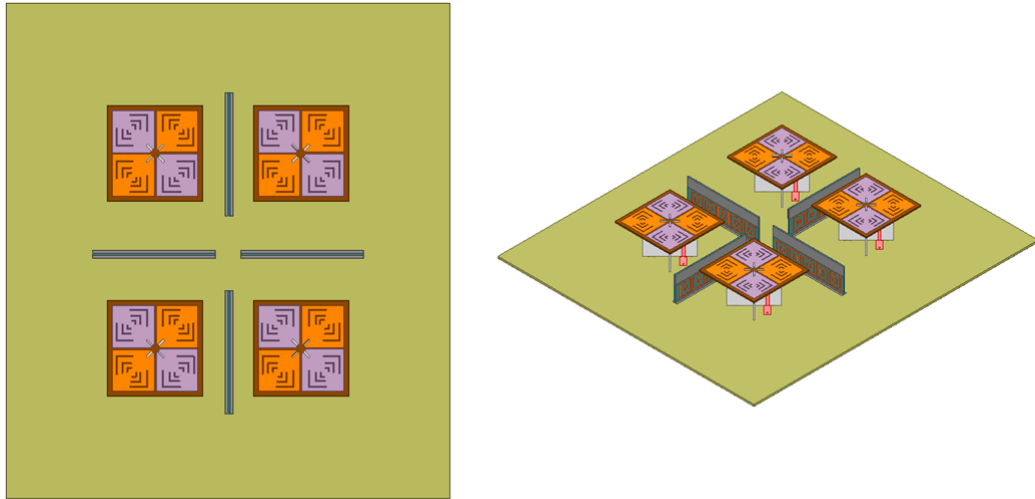
Figure 3.37: complete view of the 2×2 MIMO Antenna Configuration.

yse the effect of mutual coupling between the each polarized antenna element in azimuth and elevation planes specific nomenclature is given for the 2×2 MIMO configuration as shown in Figure 3.36. By introducing the planar printed periodic array of SRR loaded with transmission line, the effect of mutual coupling is analysed in both azimuth and elevation planes.

The coupling effects between the array of SRR and the loaded transmission lines reduces the mutual coupling between the two adjacent antenna elements. The additional horizontal strip at the bottom of periodic array of SRR is utilized for
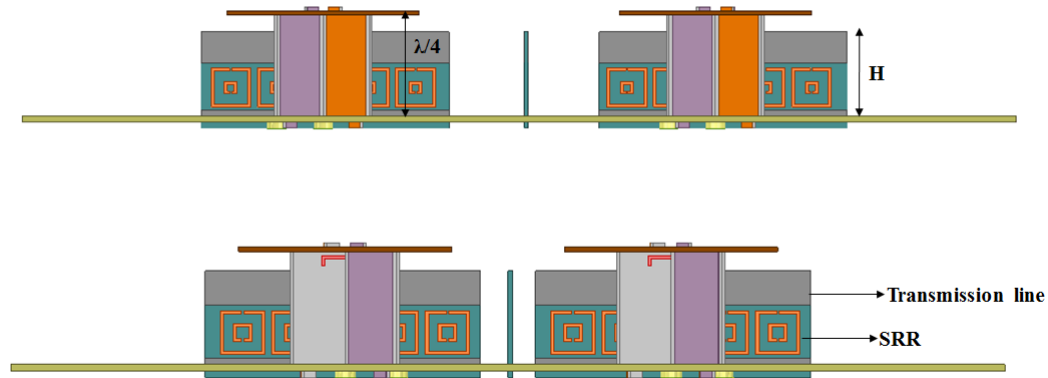
Figure 3.38: Side view of the 2×2 MIMO Antenna Configuration.

mounting the FR4 vertical strips in between the MIMO antenna elements which also provides the return path to the ground plane by isolating the each MIMO antenna element. Various techniques have been performed to suppress the mutual coupling in MIMO antennas but for the dual slant 45^0 polarized antenna elements with printed feed structure so far has not been reported. By optimizing the dimensions and position of the periodic array of SRR loaded with transmission line it is observed there is significant reduction of mutual coupling. The fabricated prototype of the complete 2×2 MIMO antenna configuration is shown in Figure 3.39.

The designed MIMO antenna system and the impact of surface currents distributions with and without periodic array of SRR loaded transmission line when port A1-1 is activated are analyzed in Figure 3.40. It is observed that the surface current mostly concentrates at the edges of the bow-tie antenna elements and at the center where the two printed feed structures are inserted. Hence the field lines mainly occurs between those of edges and across the printed feed structures in both cases. In the case without the periodic array of SRR loaded transmission
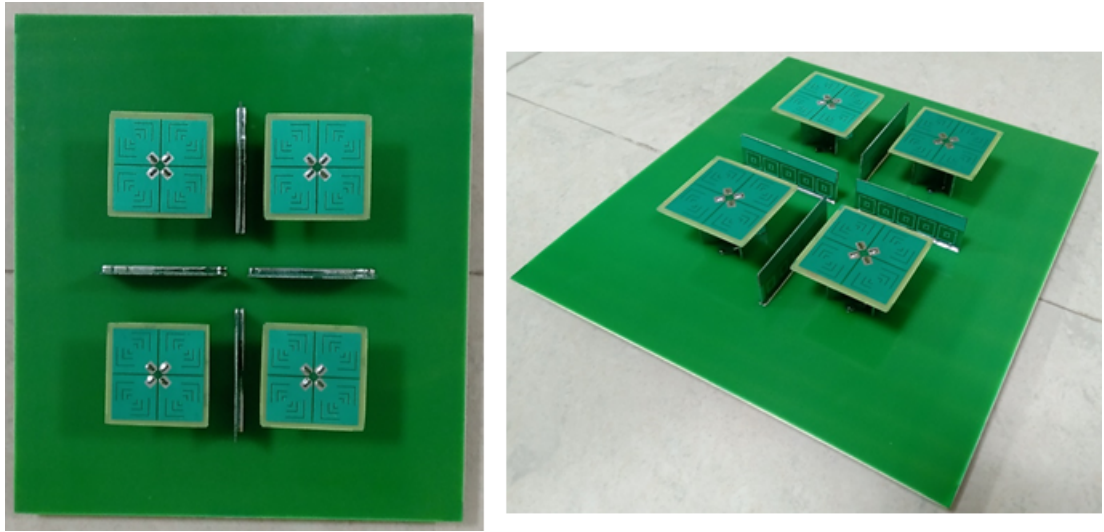
Figure 3.39: Fabricated Prototype of the Proposed 2×2 MIMO Antenna System

line, a significant amount of current mutually induces on the other antenna element and also some current transfers through the excited planar printed feed structure. In the cases with the periodic array of SRR loaded transmission line, less current induces on the other antenna elements in both the planes due to the presence of planar printed periodic array of SRRs loaded with transmission line. Since the array of SRR couples the majority of mutual field with the loaded transmission line it enables to minimize the surface currents generated between the adjacent antenna elements in both azimuth and elevation planes. The height of the FR4 vertical substrates is also optimized for effective mitigation of mutual coupling among the MIMO antenna elements.

For the designed 2×2 MIMO antenna system Figure 3.41 and 3.42 depicts the simulated and measured S-parameters plot for row A and row B antenna elements respectively. It is observed that the antenna operates for the entire (2.3 – 2.4 GHz) Band 40 with VSWR of ¡ 2. The corresponding port to port isolation between the each antenna element is shown in Figure 3.43. Antenna provides a good
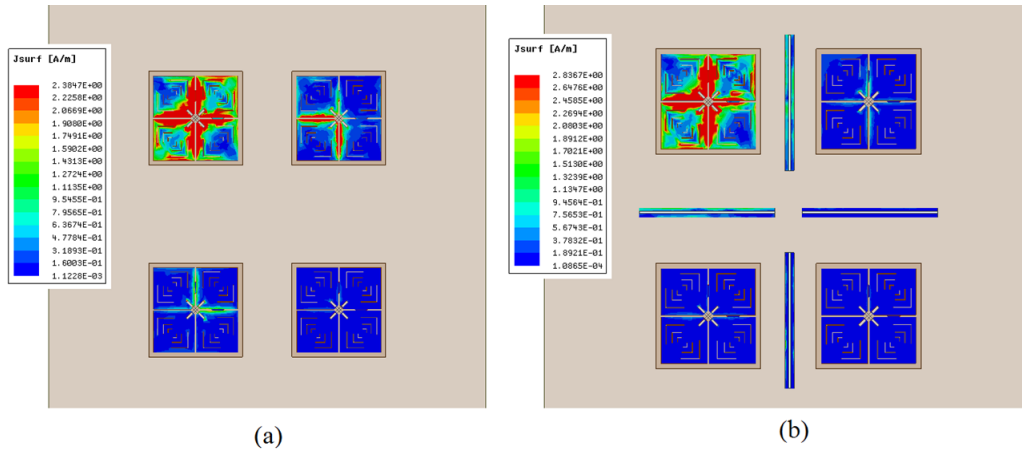
Figure 3.40: Surface Currents Distribution of the MIMO Antenna When Port A1-1 is activated (A) Without Periodic Planar Printed SRR. (B)With Periodic Planar Printed SRR.

isolation of 30 to 40 dB as observed from both simulated and measured results. The effect of mutual coupling in both scenarios that is with and without planar printed periodic array of SRR loaded transmission line is studied for each dual slant 45^0 polarized antenna element. As per the considered nomenclature given in Figure 3.36. Each polarized antenna element focuses the other three co-polarized antenna elements in E-plane, H-plane and D-plane. The E-plane and H-plane are the planes in 0^0 and 90^0 and the D-plane is considered as the plane 45^0 to both E and H planes.

The effect of periodic array of SRR loaded with transmission line mitigates the mutual coupling for the each polarized antenna element in 2×2 MIMO configuration. Figure 3.44, depicts the measured and simulated results for reduction of mutual coupling between antenna elements A1-1 and A1-2 with respect to other three polarized antenna elements A2-1, A2-2, B1-1; B1-2, B2-1 and B2-2 respectively. Similarly, for the other polarized antenna elements A2-1, A2-2, B1-1, B1-2, B2-1 and B2-2 in the MIMO antenna configuration the reduction of mutual

65
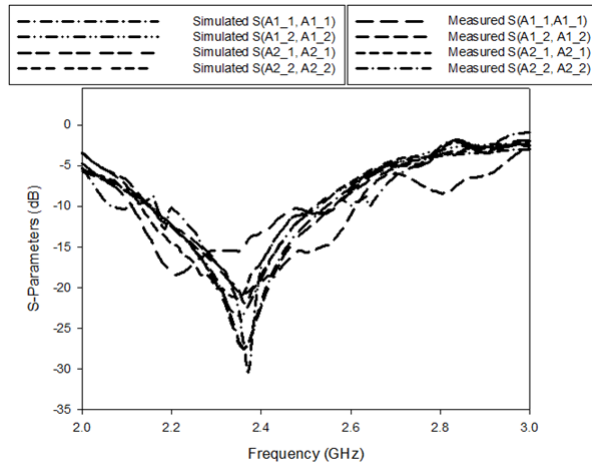
Figure 3.41: Measured and Simulated Reflection Coefficient for Row A Elements in 2×2 MIMO Configuration.
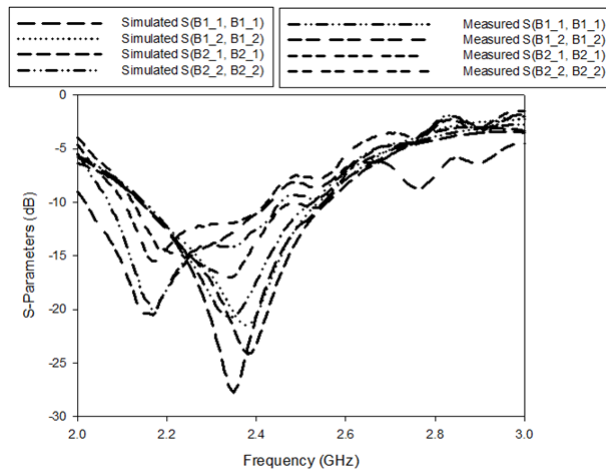
Figure 3.42: Measured and Simulated Reflection Coefficient for Row B Elements in 2×2 MIMO Configuration.

coupling are shown from Figure 3.45 to Figure 3.47. From the measured and simulated results the difference over the range of 25 to 50 dB suppression is observed in E-plane, H-plane and D-plane for with and without periodic planar printed array of SRRs loaded with transmission line over the entire band of operation. By
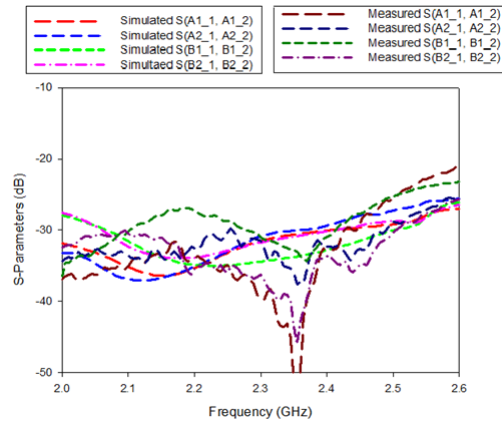
Figure 3.43: Measured and Simulated Port to Port Isolation in 2×2 MIMO Configuration.

optimizing the dimensions and position of the periodic array of SRR loaded with transmission line it is observed there is significant reduction of mutual coupling.
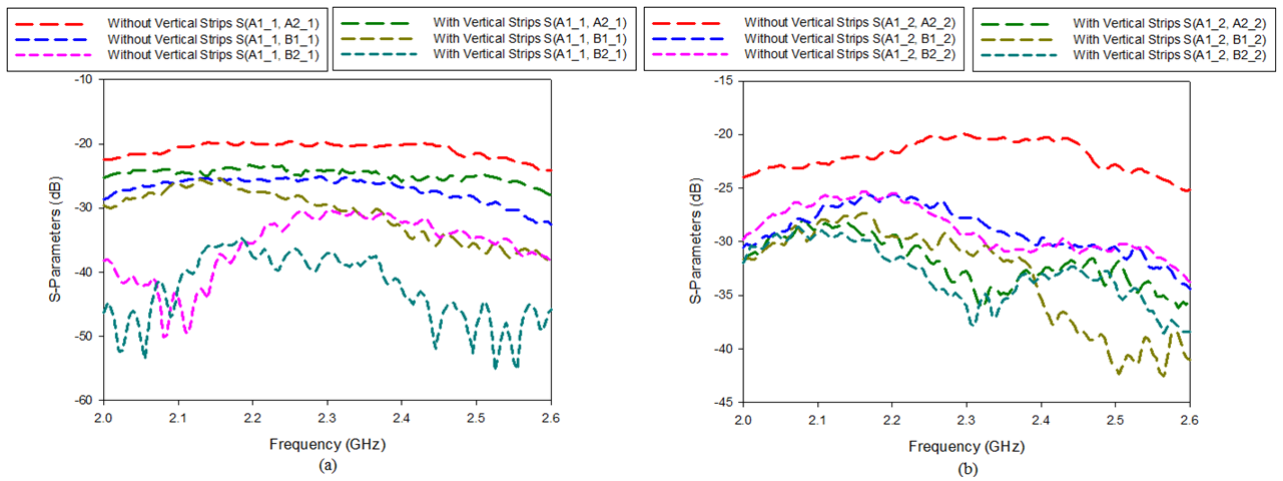
Figure 3.44: Comparison of Mutual Coupling With and Without Periodic Array of SRRs Loaded with Transmission line for (A) A1-1. (B) A1-2.

MIMO Performance Analysis   Envelope correlation coefficient (ECC) and diversity gain (DG) are the important parameters for evaluating the performance
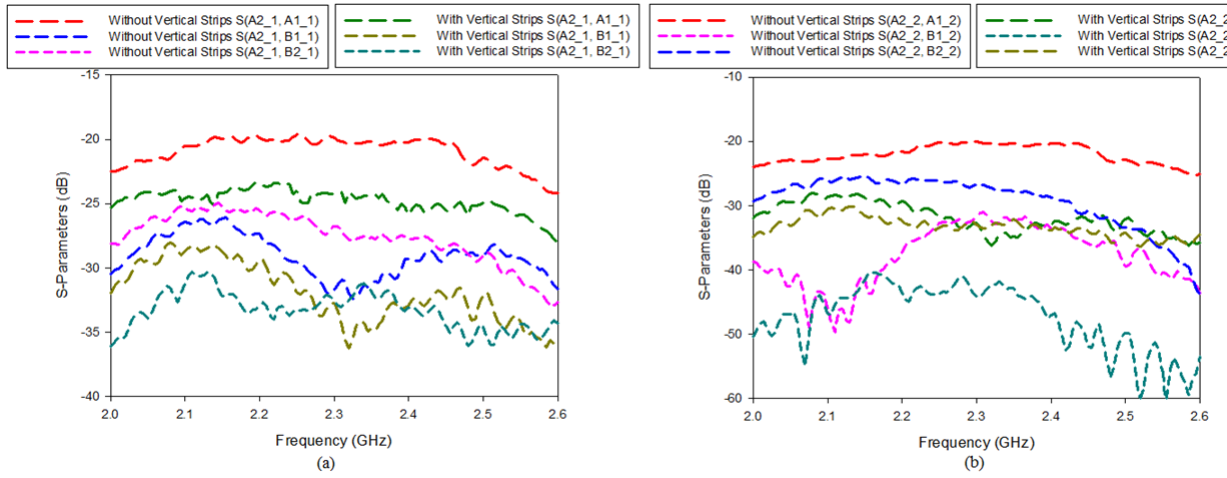
Figure 3.45: Comparison of Mutual Coupling With and Without Periodic Array
of SRRs Loaded with Transmission line for (A) A2-1. (B) A2-2.
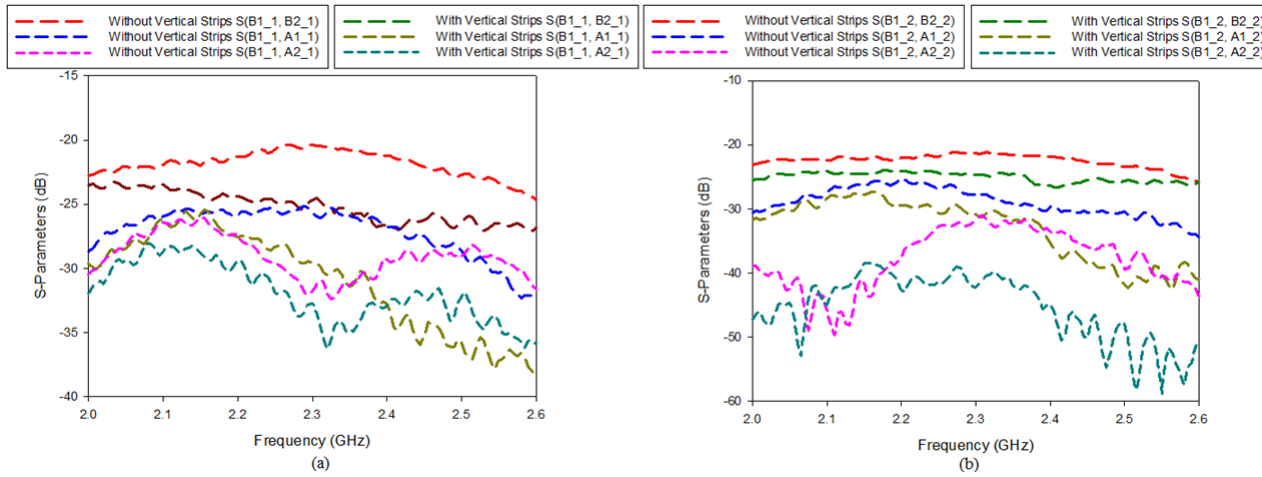
Figure 3.46: Comparison of Mutual Coupling With and Without Periodic Array
of SRRs Loaded with Transmission line for (A) B1-1. (B) B1-2.

of MIMO antenna system. The correlation between the communication channels
is observed from the ECC value. ECC can be computed by using either far field
radiation patterns or by using scattering parameters method. ECC is computed by
using measured S-Parameters. ECC is computed by using the following formula.

68
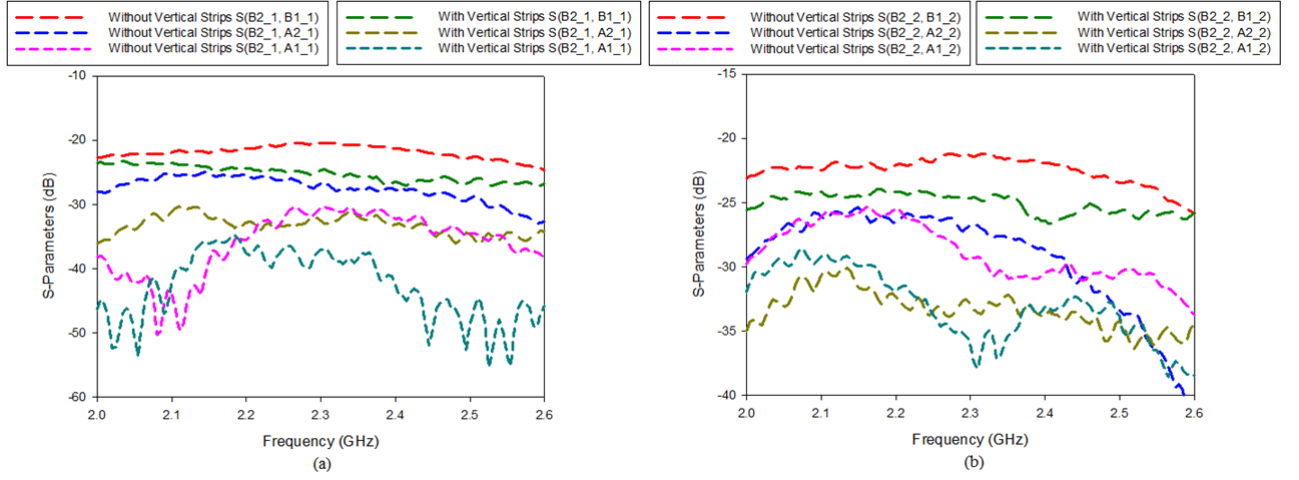
Figure 3.47: Comparison of Mutual Coupling With and Without Periodic Array
of SRRs Loaded with Transmission line for (A) B2-1. (B) B2-2.

$$P_{(ij)}(e) = \frac{|\sum_{n=1}^{N} S_{ni}^* S_{nj}|}{\sqrt{(1 - \sum_{n=1}^{N}|S_{ni}|^2)(1 - \sum_{n=1}^{N}|S_{nj}|^2)}} \qquad (3.4)$$

where i and j are antenna ports, n is the number of radiating elements, S_{ni} and S_{nj}
are scattering parameters of antenna elements. This scattering parameters are also
knows as reflection coefficients.

In ideal case ECC ought to have zero value, but practically for an uncorrelated
MIMO antenna it is less than 0.5. The measured ECC of the proposed MIMO
antenna is shown in Figure 3.48 which is well maintained below 0.5. Another
important parameter diversity gain can be related to ECC by using the following
formula given below. Practically diversity gain should be nearly 10 dB. The pro-
posed MIMO antenna system attained a diversity gain more than 9.5 dB for the
entire band as shown in Figure 3.49.

$$DG = 10 \times \sqrt{(1 - |P_{(ij)}(e)|^2)} \qquad (3.5)$$
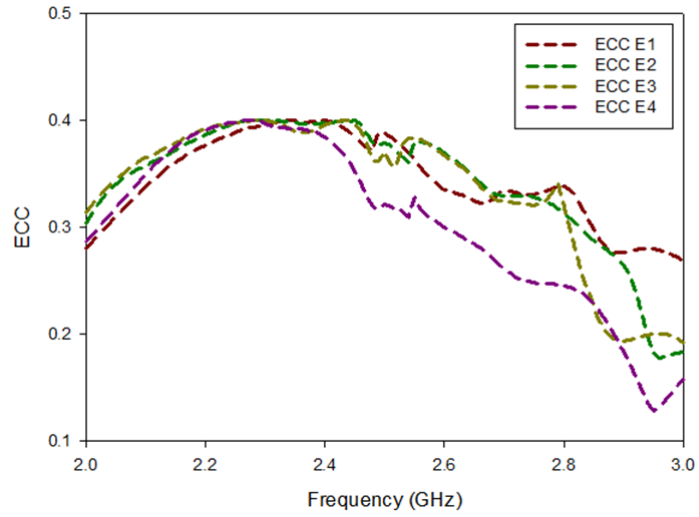
Figure 3.48: Measured ECC of the proposed MIMO antenna system.
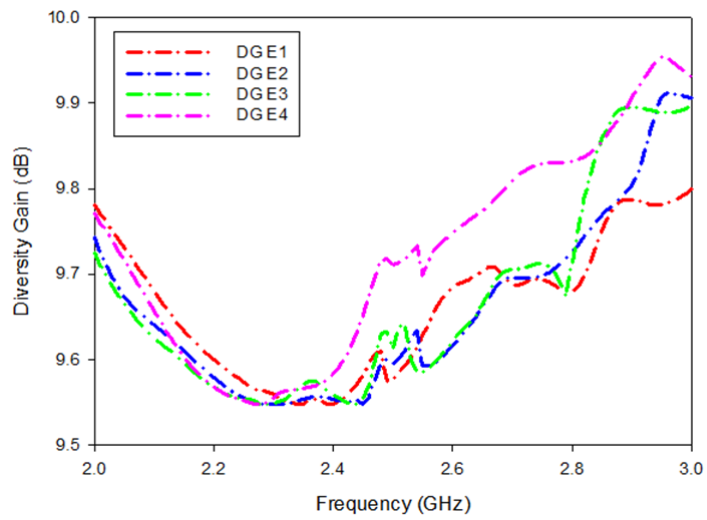
Figure 3.49: Measured DG of the proposed MIMO antenna system..

3.4 Summary

2×2 multiple input multiple output (MIMO) antenna system with low mutual coupling is discussed for polarization and spatial diversity. MIMO antenna operates for (2.3 – 2.4 GHz) Band 40 with a VSWR of < 2. A very good isolation of 30 dB between the two ports and gain of 7.5 dB for dual slant 45^0 polarized antenna is measured. By introducing the planar printed periodic array of SRRs loaded with transmission line on FR4 vertical substrates the mutual coupling can be significantly suppressed in both E and H planes. From the measured and simulated results it is observed mutual coupling reduction of 25 dB to 50 dB in both E and H planes. The miniaturized structure of the radiator to 0.4λ in dual slant 45^0 polarized antenna and further investigation of MIMO parameters in terms of ECC and DG makes the entire 2×2 MIMO antenna system suitable for future wireless communication.

CHAPTER 4

MIMO AND MASSIVE MIMO ANTENNAS FOR BASE STATION APPLICATIONS

4.1 Introduction

In general wireless engineers probably know that the acronym MIMO stands for Multiple-Input/Multiple-Output, but often that is where the understanding ends. The name usually describes an information theory concept and enables the idea of streams of information through propagation channels. The MIMO wireless system can be visualized as a black box between a transmitter connected to multiple inputs to the black box and a receiver connected to multiple outputs of the black box. Each input and output are expected to carry different information. As inside the black box, we have the antennas on the transmitter and receiver and the intervening environment through which the signals propagate. By definition, MIMO is a system level concept, and it implies that there is an independent transmitter and receiver on each input/output.

MIMO is an emerging technology which offers major advantages when compared with single user MIMO. It works with each single antenna terminals inside the black box both at the transmitter and receiver end. The other benefits of massive MIMO consists of low power components, reduced latency and robustness. The upcoming challenges for future 5G increased data rate, low latency and maximum area of coverage with upmost data speeds makes MIMO a promising technology. Massive MIMO addresses the spatial multiplexing which in turn relies on

base station with good enough channel knowledge for both uplink and downlink data streams.

4.2 4×4 MIMO Antenna System

In the previous chapter 2×2 MIMO configuration is extended to implement the massive MIMO antenna for 4G LTE base station applications. Dual slant 45^0 polarized antenna elements are considered to build the massive MIMO. 4×4 MIMO antenna configuration with 16 dual slant 45^0 polarized antenna elements is shown in Figure 4.1. The spacing between the elements is considered as 0.6λ by 0.8λ in azimuth and elevation plane respectively. For base station antenna designs three important principles are to be considered wide band impedance match, stable radiation patterns in wide frequency band and high cross polarization ratio in wide angle range. The feed network of the proposed design is same as the dual feed network of the dual polarized antenna element as shown in Figure 4.2. The optimized dimensions of the fabricated prototype antenna are given in Table 3.3.

The simulated and measured S-parameters of the proposed single DPA antenna element which has been extended to implement the 4×4 MIMO configuration is shown in Figure 4.3.

The effect of mutual coupling between the dual slant 45^0 polarized antenna elements is analysed with various decoupling techniques for 4×4 MIMO antenna configuration. After examining the different decoupling structures the U shaped aluminium structure is giving feasible results for the each polarized antenna elements in both azimuth and elevation planes. The U shaped strips are placed both in azimuth and elevation planes as shown in Figure 4.2. The selected configuration with U shaped strips and slotted ring at the ground plane for adjacent
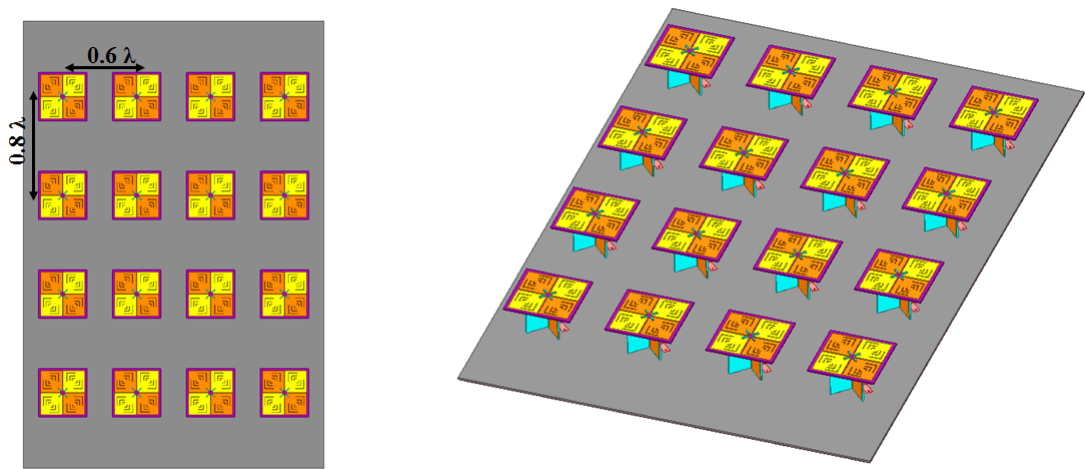
Figure 4.1: Geometry of 4 × 4 MIMO Antenna Configuration.
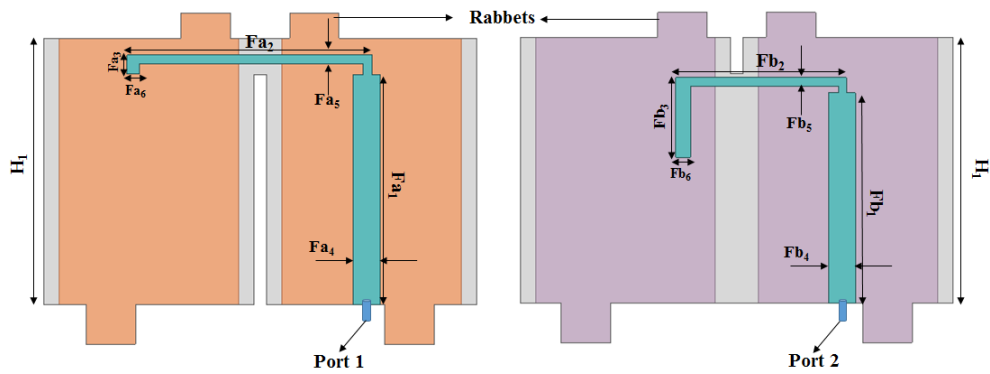
Figure 4.2: Geometry of the Printed Feed Network.

antenna elements coupling reduction is shown in Figure 4.3. When the elements are placed closer with co-polarization the coupling reduction becomes stringent in many configurations. To overcome that effect apart from the U shaped strips a slotted ring like structure is etched in the bottom ground plane for the elements placed in middle two rows. The height of the U shaped strips is optimized in ANSYS HFSS 19.0 for efficient coupling reduction.
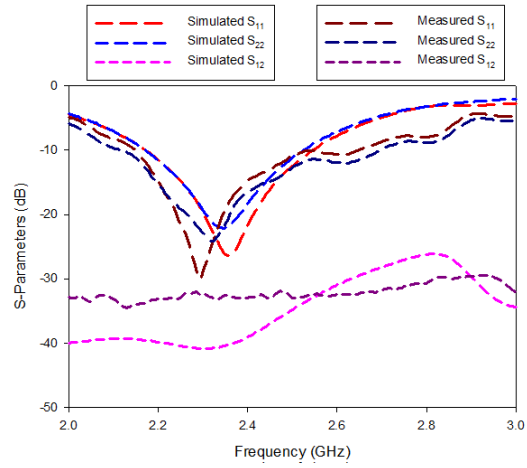
Figure 4.3: Simulated and Measured S-Parameters of the Proposed Single DPA
Element.
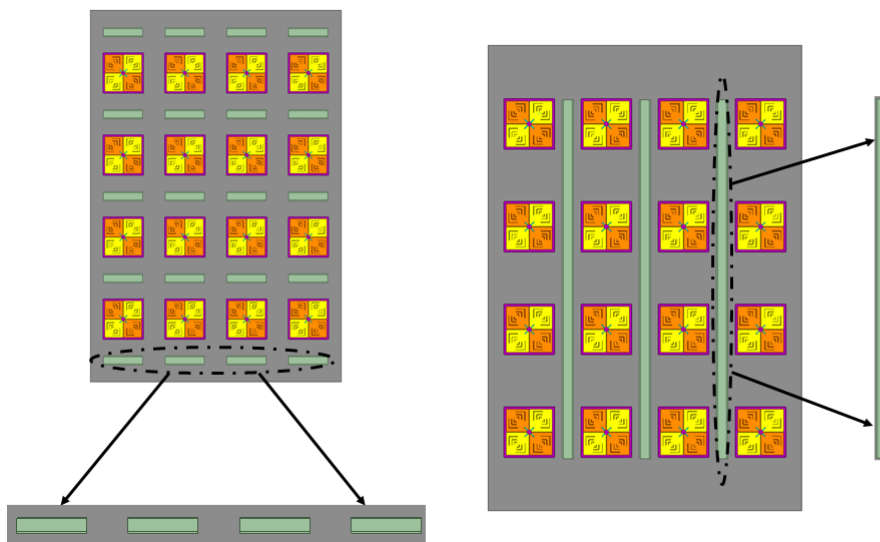
Figure 4.4: Geometry of U Shaped Strips in 4×4 MIMO Antenna Configuration.
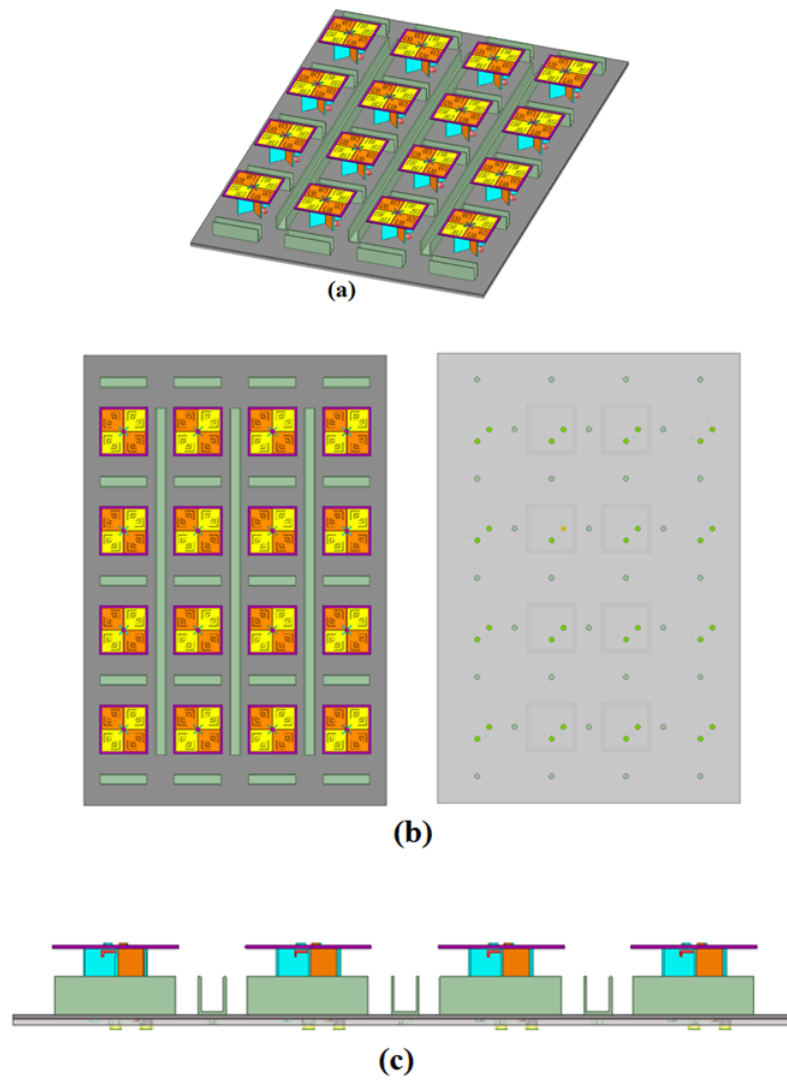
Figure 4.5: (a) Isometric View (b) Top and Bottom View (c) Side View of 4×4 MIMO Antenna Configuration.

The fabricated prototype of the 4×4 MIMO antenna configuration is shown in Figure 4.4. The MIMO antenna measurement is complex so initially the basic element of the 4×4 MIMO is measured VSWR for the two polarized antenna elements as shown in Figure 4.5. The isolation between the two dual polarized antenna elements also measured as and resulted 30 dB as shown in Figure 4.6.
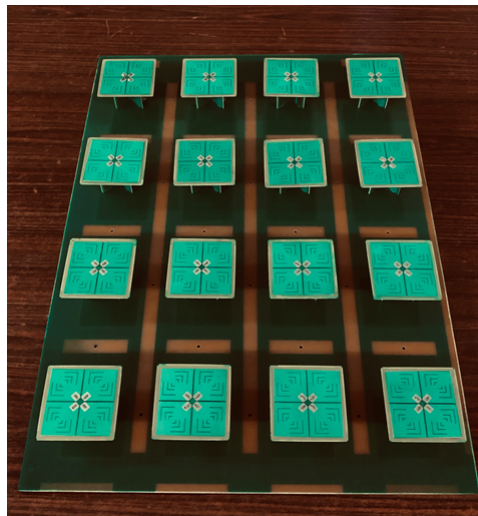
Figure 4.6: Fabricated Prototype of 4×4 MIMO Antenna Configuration.
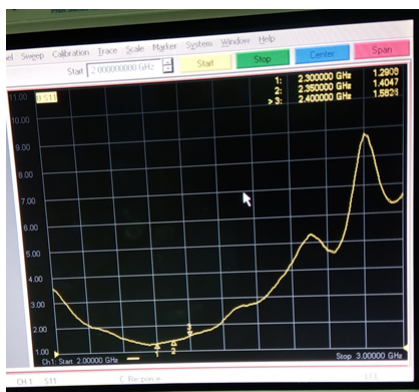
(a)
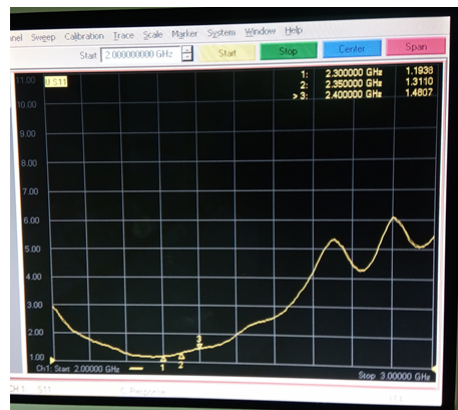
(b)

Figure 4.7: Measured VSWR for First Antenna Element in 4×4 MIMO Antenna Configuration.
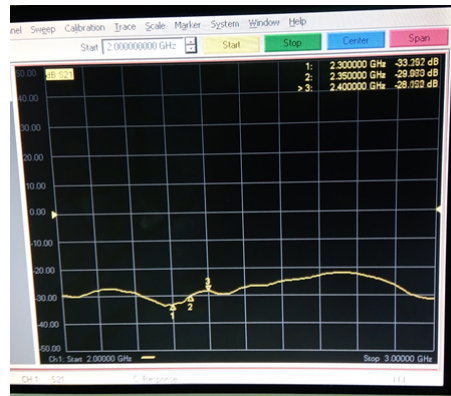
Figure 4.8: Measured Isolation for First Antenna Element in 4 × 4 MIMO Antenna Configuration.

4.3   8 × 8 Massive MIMO Antenna System

Massive MIMO technology utilizes the simple processing of the signals among all the antennas installed in the base stations. Massive MIMO increases the capacity of the channels by 10 times more by simultaneously improving the energy efficiency on the order of 100 times. The spatial multiplexing and polarization diversity makes dramatic increase in channel capacity with large number of antennas.

The selected configuration of 4 × 4 MIMO Antenna with U shaped strips is extended to implement 8 × 8 massive MIMO as shown in Figure 4.7. The fabricated prototype without inserting the U shaped strips is shown in Figure 4.8. The complete assembly of the U shaped strips with radome enclosure also completed for utilizing in base station applications.
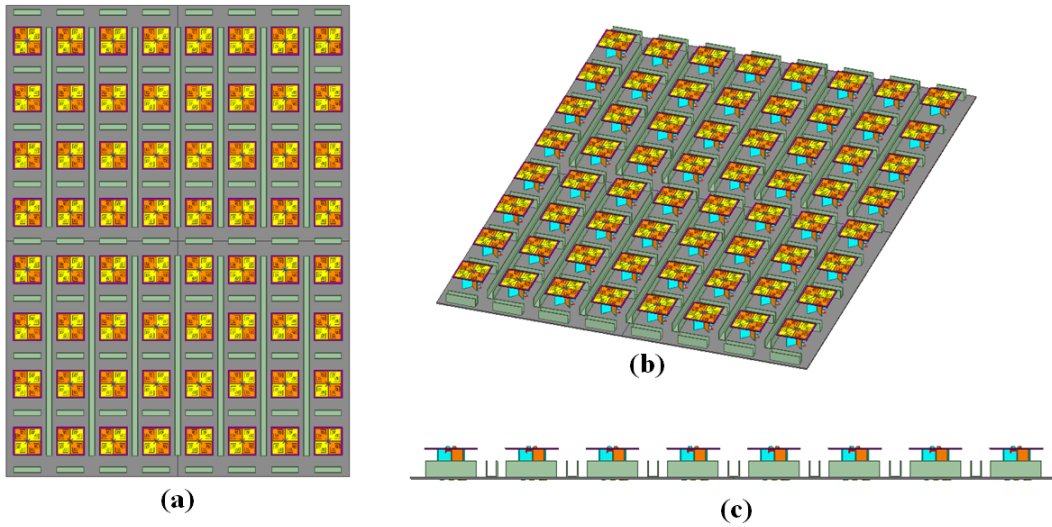
Figure 4.9: Geometry of 8×8 Massive MIMO Antenna Configuration.

4.4 Summary

In this chapter, MIMO and Massive MIMO antennas are designed with 4×4 and 8×8 configurations for base station applications. The mitigation of mutual coupling is carried out with U shaped strips placed at both azimuth and elevation planes for the designed MIMO antenna configurations. Optimizations are carried out with respect to practical deployment of the base station antennas. The designs are fabricated and tested for the functionality of both the polarized antenna elements. The radome analysis also done with proper materials for practical deployment to overcome the environmental conditions. The design and implementation of 8×8 massive MIMO antenna for C-RAN applications is a part of End-to-End Indigenous 5G Test Bed under SAMEER Chennai.
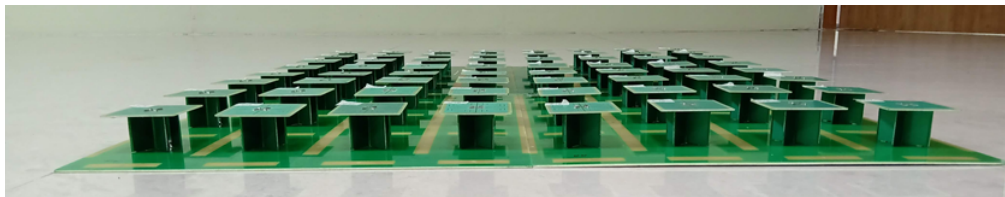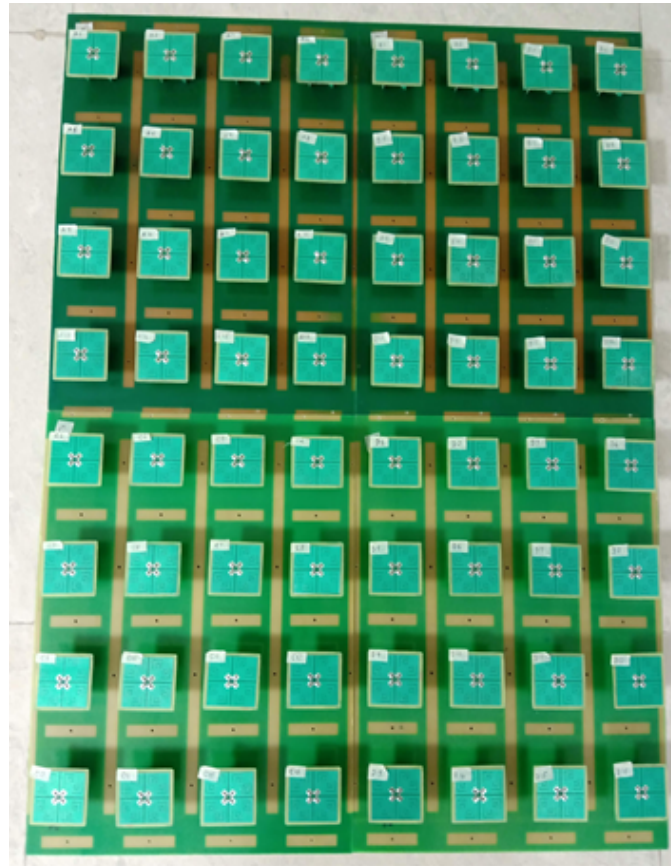
Figure 4.10: Fabricated Prototype of 8×8 Massive MIMO Antenna Configuration.

CHAPTER 5

LOW PROFILE, WIDEBAND DUAL POLARIZED ANTENNA WITH FSS DECOUPLING TECHNIQUE FOR 5G APPLICATIONS

5.1 Introduction

The rapid development of the mobile communication technology paved the way for the upcoming 5G technology. Multiple antennas are needed to cover the wide range of frequencies and simultaneously to meet the high data rates for the future 5G wireless standards. The requirement of wideband dual polarized antennas is needed in many applications of the next generation wireless communication systems. To meet these requirements various kinds of bow-tie antennas have been developed. Bow-tie antennas exhibits broadside radiation patterns which makes them suitable for future wireless communication. Dual polarized antennas has a very wide range of applications in modern wireless communication systems as they effectively increase the channel capacity. For obtaining wide band generally aperture coupled, stacked patches are used recently T shaped bow-tie antenna elements are used with coaxial feed.

In this chapter, low profile, wideband dual polarized bow-tie antenna element is designed. In the first section, the wideband dual polarized bow-tie antenna element is presented. The performance of the dual polarized antenna (DPA) element is discussed with fabricated prototype supporting with measured results.

The second section discusses the low profile DPA with chessboard based artificial magnetic conductor (AMC) loaded with wideband operation. The designed unit cell is extended for 1×2 MIMO antenna with frequency selective surface (FSS) decoupling technique to mitigate the mutual coupling between the two DPA elements. MIMO antenna performance is evaluated with and without FSS wall. Finally, both designs are fabricated and measured experimentally. The simulated and experimental results are presented in terms of bandwidth, impedance bandwidth, gain, isolation, mutual coupling and radiation patterns.

5.2 Arc Shaped Dual Polarized Bow-Tie Antenna with Coaxial Feed

In this design, initially the two bow-tie antenna elements were implemented without any slots and then it was modified with arc shaped slots by calculating the dimensions using Matlab code for desired frequency. The antenna was designed using Rogers 5880 substrate, permittivity of 2.2, height (h) of 0.8 mm and loss tangent of 0.0009. The two bow-tie antenna elements are arranged such that two radiator elements sits on the top and bottom side of the substrate as shown below in Figure 5.1 and 5.2.
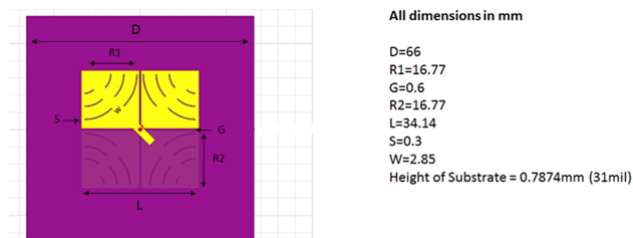
Figure 5.1: Geometry of the Proposed Dual Polarized Antenna(DPA) with dimensions.
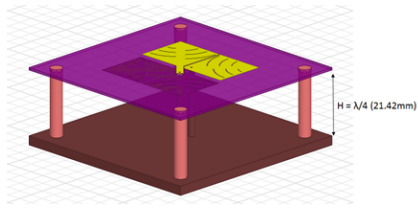
Figure 5.2: Isometric View of Proposed DPA.
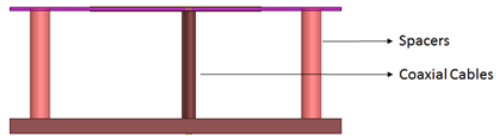
Figure 5.3: Side View of Proposed DPA.

The designs has been simulated by using ANSYS HFSS 19.0 and the results observed for dual polarized antenna with arc shaped slots are shown in Figure 5.4 and 5.5.
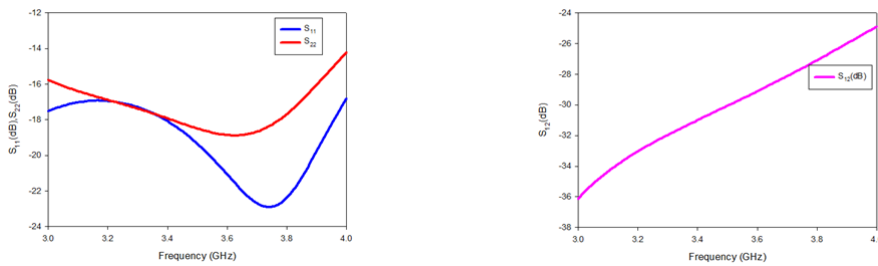
Figure 5.4: Simulated S-Paraemters of Proposed DPA.
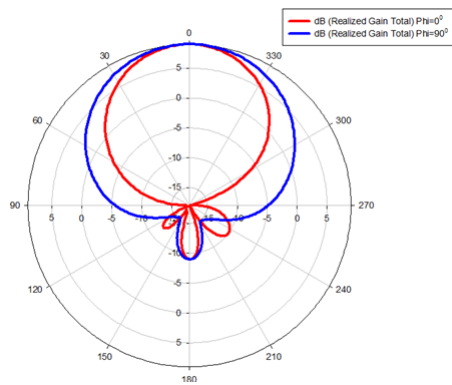
Figure 5.5: Simulated Radiation Pattern of Proposed DPA.

83

5.3   Wideband Dual Polarized Bow-Tie Antenna with Coaxial Feed

A wideband dual polarized bow-tie antenna excited with two coaxial line feeding. The novelty of the structure is obtained by incorporating the rectangular slots and chamfering at the edges and optimizing the size of radiator for 5G applications. The proposed antenna makes suitable for building MIMO systems.

The geometry of the proposed dual polarized bow-tie antenna is shown in Figure 5.6 and 5.7. The antenna consists of radiator, coaxial feeds and a PEC ground plane reflector. The main radiator of the proposed antenna is made up of two planar printed bow-tie elements in orthogonal orientation. The arrangement of the two arms of bow-tie elements are placed on either side of the FR4 substrate thickness of 0.8 with relative dielectric constant of 4.4.To improve the isolation, rectangular slots are introduced on each arm of the radiator. In addition to the rectangular slots, chamfering are also included on the edges and in between two adjacent arms of the bow-tie antenna. The chamfering on the each arm and the slots enhances the port to port isolation and also supress the cross polarization levels. The two bow-tie antenna elements are fed with two separate 50Ω coaxial cables.

The top patches on the substrate acts as radiator and the corresponding two patches at bottom side of substrate refers to ground for both the bow-tie antenna elements. The PEC ground plane is fabricated on FR4 substrate thickness of 1.6 with relative dielectric constant of 4.4. The two patches on the bottom gets the ground connectivity to the PEC ground plane by using the two 50Ω coaxial cables. The four supporting rods are placed on four sides of the radiator to the bottom ground plane.
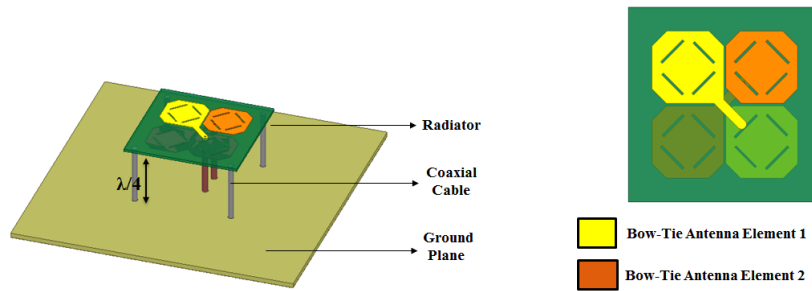
Figure 5.6: Antenna Congfiguration With Antenna Radiator Elements.
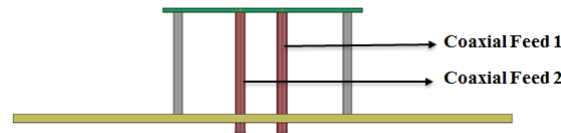
Figure 5.7: Side View of the Proposed Antenna.

The simulated and measured S-parameters for the proposed design are shown in Figure 5.8. It can be observed that the proposed design covers the 5G frequency band from 3.3-3.7GHz with 15 dB impedance matching bandwidth. The percentage bandwidth of 42.85% covering the frequencies from 3.1-4.6 GHz at centre frequency of 3.5 GHz is obtained with 10dB impedance matching bandwidth. A high port to port isolation of about 28 dB is achieved for the proposed dual polarized antenna. The simulated and measured gain plots are shown in Figure 5.9. From the measured results an average gain of 8.4 dB to 6 dB is observed for entire band from 2.8 – 4.6 GHz. The difference can be attributed to the fabrication error and test errors of the antenna system.

The measured radiation patterns for the proposed antenna are shown from Figure 5.10 to Figure 5.15. The corresponding plots for both the E- and H- Planes are plotted individually for 3.3, 3.5 and 4.2 GHz with co and cross polarization levels
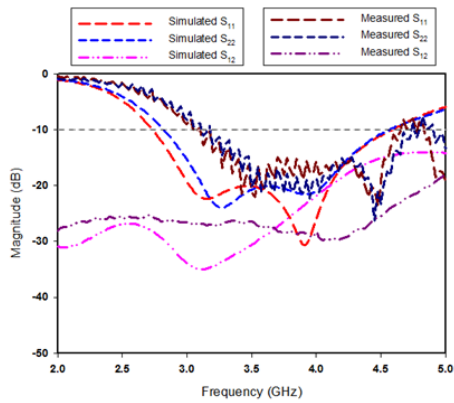
Figure 5.8: S-Parameters of the Proposed Dual Polarized Bow-Tie Antenna.
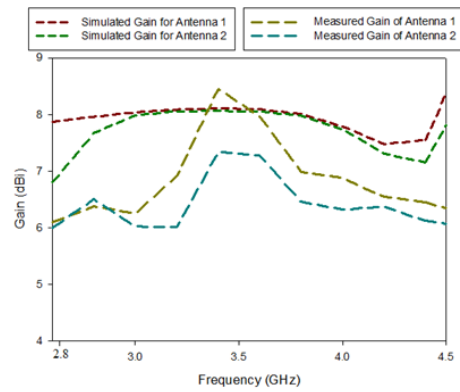
Figure 5.9: Gain Plot for the Proposed Dual Polarized Bow-Tie Antenna.

for both the antenna elements. By introducing the rectangular slots and chamfering at the edges of both arms of the bow-tie antenna the cross polarization level less than 30 dB is obtained in both E- and H- planes. The front to back ratio of 18 dB is observed over the band.
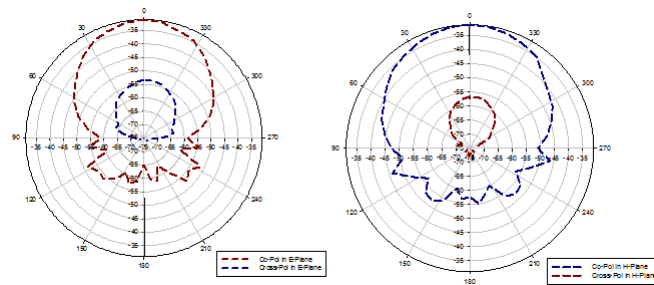
Figure 5.10: Measured radiation patterns for Antenna Element 1 at 3.3 GHz.

The fabricated prototype of the proposed dual polarized bow-tie antenna and measurement setup are shown in Figure 5.16 and 5.17. respectively. Optimizations are carried using FEM based 3D electromagnetic (EM) simulation software Ansoft HFSS 19.0.

86
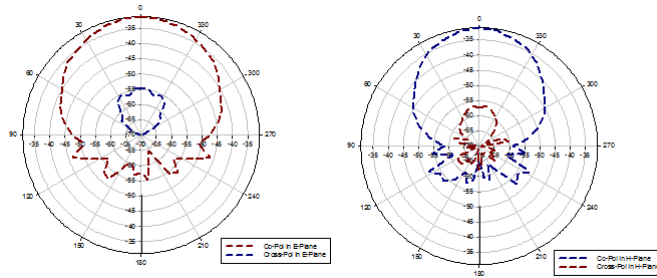
Figure 5.11: Measured radiation patterns for Antenna Element 2 at 3.3 GHz.
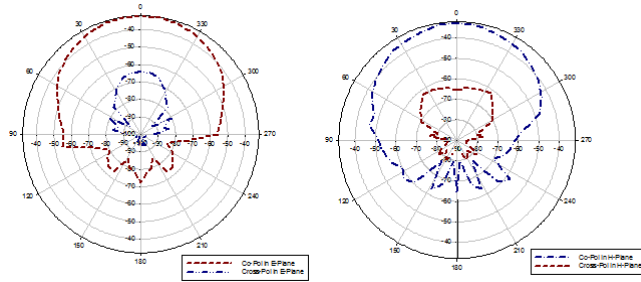
Figure 5.12: Measured radiation patterns for Antenna Element 1 at 3.5 GHz.
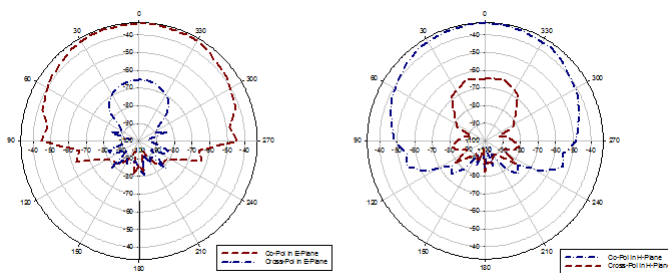
Figure 5.13: Measured radiation patterns for Antenna Element 2 at 3.5 GHz.
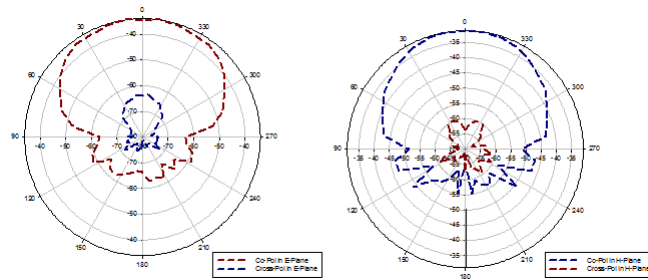
Figure 5.14: Measured radiation patterns for Antenna Element 1 at 4.2 GHz.
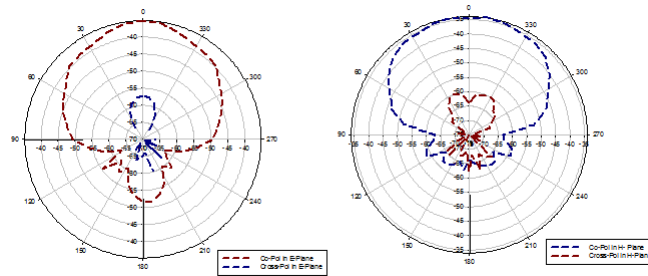
Figure 5.15: Measured radiation patterns for Antenna Element 2 at 4.2 GHz.
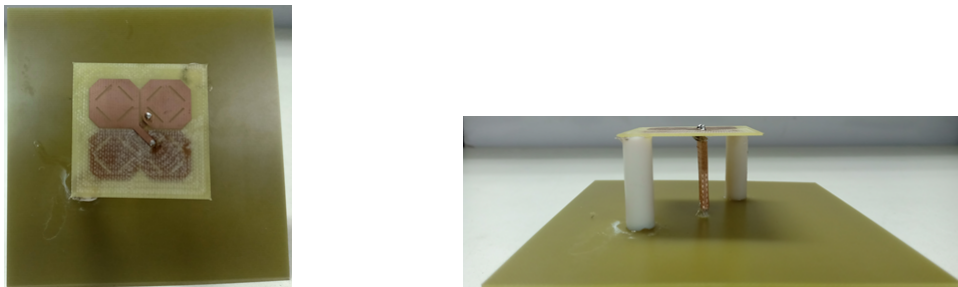
Figure 5.16: Fabricated Prototype of Proposed Dual Polarized Bow-Tie Antenna Top view and Side View.

5.4 Low Profile, Wideband Dual Polarized MIMO Antenna on Chessboard AMC Surface

Dual polarized wideband antennas are widely needed in both radar and communication systems that needed polarization diversity, and many dual-polarized an-
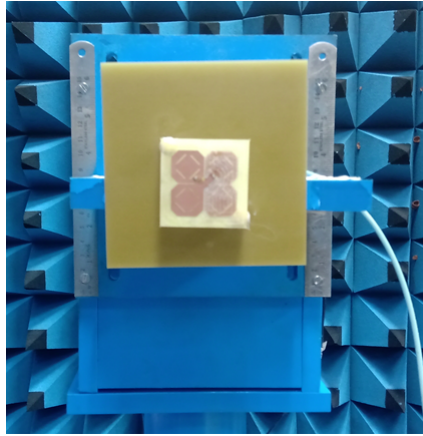
Figure 5.17: Measurement Setup for the Proposed Antenna.

tennas have been reported till now. For low-profile requirement, the microstrip class of antennas is the usual choice. However, the cross polarization and isolation performance of a traditional microstrip antenna may not be good enough for some applications. There are several techniques to improve the isolation and cross polarization. However, the antennas using an aperture-coupled feed generally need a reflector plane behind the antenna to reduce the effects of the platform and to eliminate back lobe radiation due to the coupling aperture. This typically increases the overall antenna height. The "dual feed" technique is also used to improve the isolation and cross polarization, and the introduction of a wideband balun improves the entire performance, at the expense of a more complicated design. The notched antenna can achieve wide bandwidth, but the height of this type of antenna is generally very large. So, here a wideband dual-polarized antenna comprising planar dipoles with slot cuts across the dipole's is implemented.

To reduce the height of the high profile antennas, an Artificial Magnetic Conductor (AMC) reflector is the good candidate for obtaining low profile antennas. AMC is a novel material which is comparable with the ideal magnetic conduc-

tor during a certain frequency band. Antennas can be very close to the AMC reflectors to reduce the height of the dual polarized antennas for the reason that the phase of the incident wave of the AMC reflector is consistent with that of the reflected wave. By designing the parameters of the AMC reflector carefully, it can be used to improve the radiation performances of the dipole antennas. The proposed antenna consists of two orthogonal bow-tie dipole antennas which are excited by coaxial cables, a square ring and an AMC reflector.

5.4.1   Structure of AMC Unit Cells

AMC Unit Cell for 3.5 GHz   The AMC reflector is placed under the radiation element as a metal ground plane. The geometry of the AMC unit cell designed for 3.5 GHz is shown below. The design of Artificial Magnetic Conductor (AMC) unit cell is designed in CST Microwave Studio. The unit cell is designed by considering the square and tuned to desired frequency for obtaining the zero phase shift at the desired frequency. Initially the design was implemented on Rogers 5880 and later on shifted to FR4 substrate for low cost. The single unit cell has been extended to array of 5×5 to check the similar characteristics with respect to unit cell design at desired frequency. The same AMC unit cell design is also implemented in HFSS to compare the results before integrating with the designed dual polarized antenna. The unit cell designs with boundary conditions are in shown below Figure 5.18.

Dual Band AMC Unit Cell for 3.1 GHz and 4.5 GHz   The geometry of the dual band AMC unit cell designed for 3.1 GHz and 4.5 GHz are shown below. The design of Artificial Magnetic Conductor (AMC) unit cell is designed in CST Microwave Studio. The unit cell is designed by considering the square and tuned
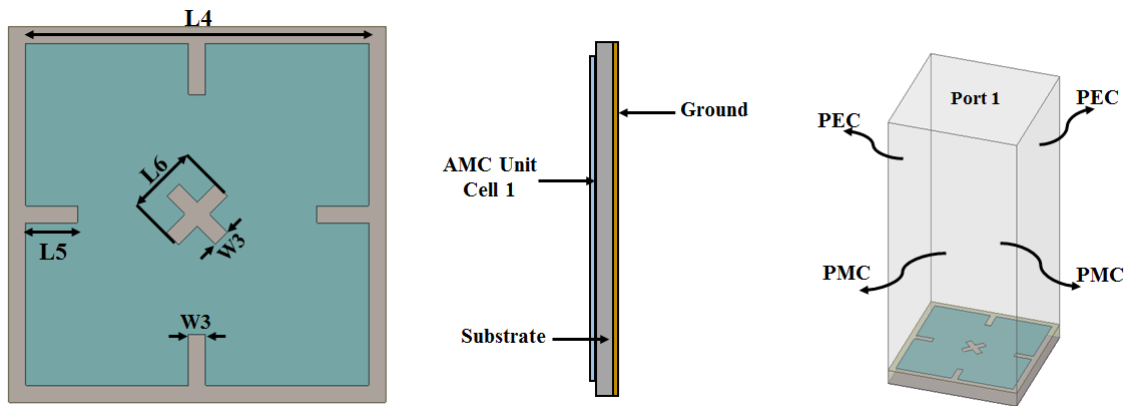
Figure 5.18: Geometry of the AMC Unit Cell at 3.5GHz with Boundary Conditions.

to desired frequencies for obtaining the zero phase shift at the desired frequencies. The design was implemented on FR4 substrate for low cost. The single unit cell has been extended to array of 5×5 to check the similar characteristics with respect to unit cell design at desired frequencies. The same AMC unit cell design is also implemented in HFSS to compare the results before integrating with the designed dual polarized antenna. The unit cell designs with boundary conditions are shown in below Figure 5.19. The reflection phase diagram of the AMC unti cell 1 at 3.5 GHz and AMC unit cell at 3.1 and 4.5 GHz with various incident angles are shown in Figure 5.20.

5.4.2   Structure of Band Stop FSS Unit Cell

Frequency selective surfaces (FSS) have been receiving enormous interest in communication systems applications. Numerous wide variety of resonant shapes have been utilized for FSS design, for example square, hexagon and fractal geometries. Various methods can be found in the literature for improving the characteristics
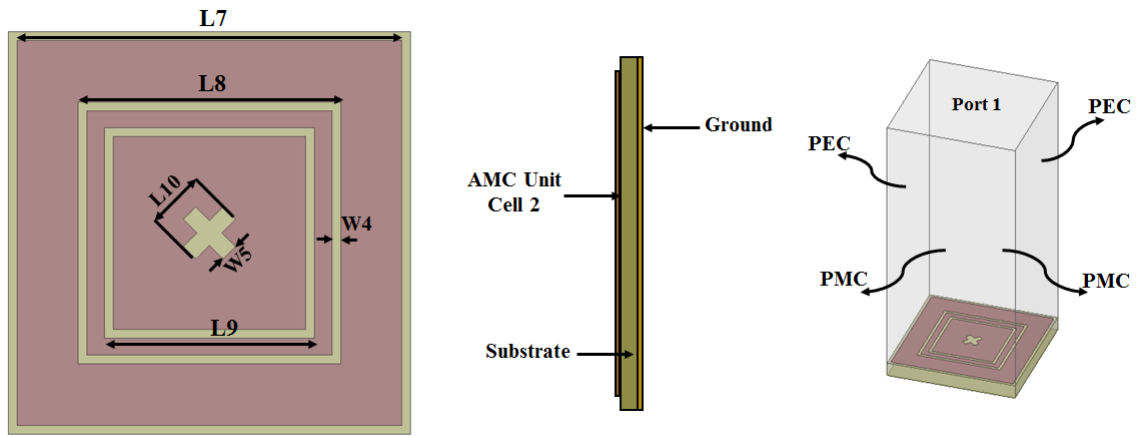
Figure 5.19: Geometry of the Dual Band AMC Unit Cell at 3.1GHz and 4.5GHz with Boundary Conditions.
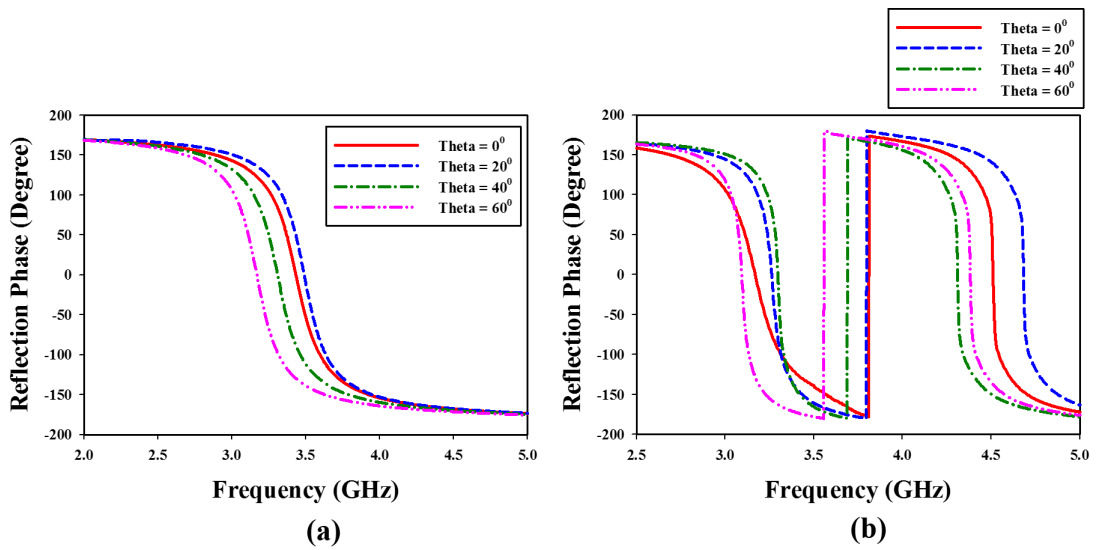
Figure 5.20: Reflection Phase Diagram of the AMC Unit Cells with Various Incident Angles (a) At 3.5 GHz (b) At 3.1 and 4.5 GHz.

of traditional 2D FSS's and even for 3D FSS. Multi-layered FSS are also been implemented rather than shortcoming conventional FSS.

Band Reject FSS Unit Cell for 3.5 GHz   A variety of novel structures were propose in literature with stop band as well as pass band performance for different applications. The structure of FSS unit cell for band reject of 3.5 GHz is shown in Figure 5.21(a). The design of FSS unit cell is designed in CST Microwave Studio. The unit cell is designed by considering the square and miniaturized to desired frequency for obtaining the band rejection at the desired frequency. The same FSS unit cell design is also implemented in HFSS to compare the results before integrating with the designed dual polarized antenna. The unit cell designs with boundary conditions are in shown below Figure 5.21(a). The simulated results of the band reject FSS unit cell for 3.5 GHz is shown in Figure 5.21(b).
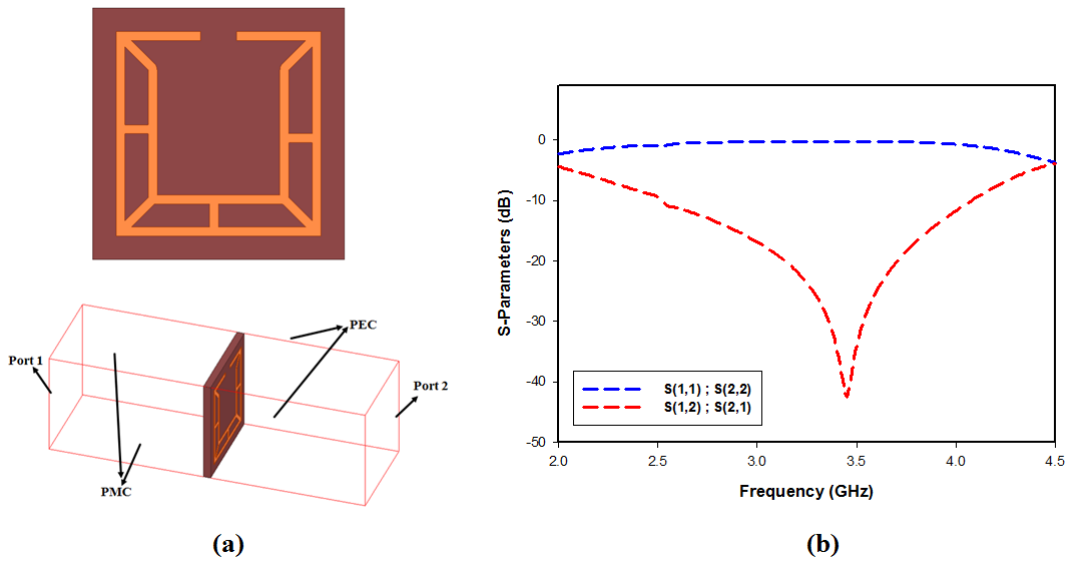
Figure 5.21: (a) Geometry of the Band Reject FSS Unit Cell with Boundary Conditions.(b) Simulated Results of Band Reject FSS Unit Cell.

Wide Bandstop FSS Unit Cell   A wide band stop frequency selective surface unit cell is designed in CST microwave studio with necessary periodic boundary conditions. The FSS unit cell is designed on the FR4 substrate with relative

dielectric constant of 4.4. The geometry of the FSS unit cell is shown in Figure 5.22(a). The square shaped fractal structures are designed on either side of the FR4 substrate with thickness of 0.012λ. Simulated result of the designed FSS unit cell with wide band stop from 2.85 – 4.75 GHz is shown in Figure 5.22(b). The designed wide band stop FSS unit cell is considered to build a FSS wall on the vertical substrate in between dual polarized 1×2 MIMO antennas.
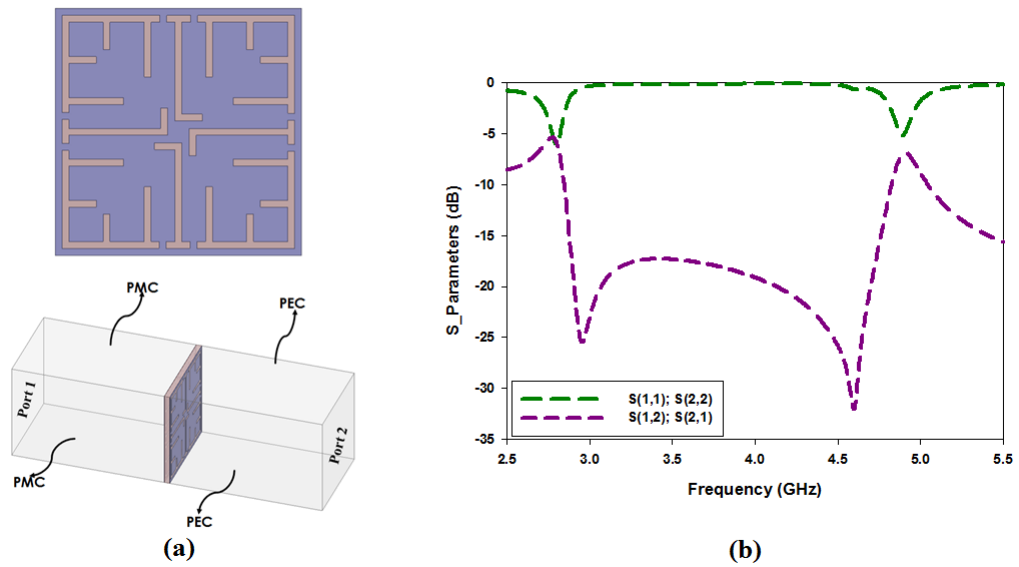
Figure 5.22: (a) Geometry of Wideband Stop FSS Unit Cell with Boundary Conditions. (b) Simulated Results of Wide Bandstop FSS Unit Cell.

94

5.5 1 × 2 Wideband Dual Polarized MIMO Antenna with FSS Decoupling Technique on Chessboard Based AMC Reflector

5.5.1 Wideband Dual Polarized MIMO Antenna Element

The geometry of the wideband dual polarized MIMO antenna loaded with chessboard based AMC surface is show in Figure 5.23. The dual polarized MIMO antenna consists of radiator, coaxial feeds and chessboard AMC surface. The main radiator consists of two printed bow-tie antenna elements in orthogonal orientation. The orthogonal arrangement of the two arms of bow-tie elements are placed on either side of the FR4 substrate thickness of 0.8 with relative dielectric constant of 4.4. To improve the isolation, rectangular slots are introduced on each arm of the radiator. The chamfering on each arm of the radiator enhances the port to port isolation and also suppress the cross polarization levels. The two 50Ω coaxial cables are utilized to feed the two independent bow-tie antenna elements. In addition, rectangular ring is designed around the radiator to give proper resonance at 4.5 GHz. The compactness of the radiator is achieved by miniaturizing the radiating structure to 0.4 λ.

The alternate placement of the AMC cells designed at 3.5 GHz, 3.1 GHz and 4.5 GHz gives the chessboard configuration as shown in Figure 84. The incident wave travels towards the AMC surface in Z direction and gets reflected with zero reflection phase below the dual polarized MIMO antenna resulting in unidirectional stable radiation patterns with low profile. By properly placing the AMC unit cells, a 5 × 5 periodic AMC array is developed and positioned underneath at a distance of 0.125 λ from the antenna as shown in Figure 5.24.
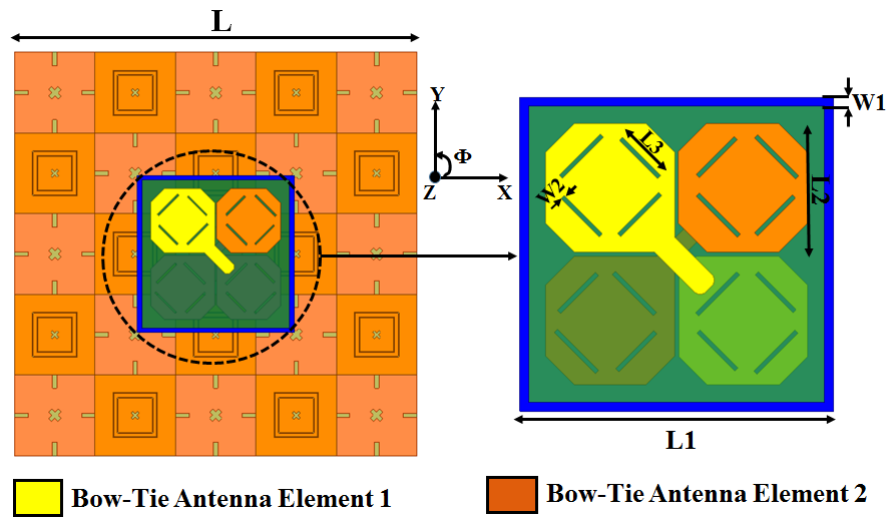
Figure 5.23: Geometry of the wideband dual polarized MIMO antenna.
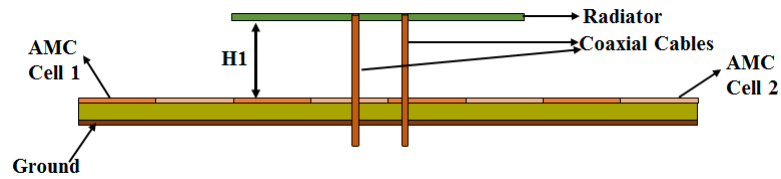
Figure 5.24: Chessboard Configuration of the AMC Unit Cells.

The simulated and measured S-parameters of the proposed dual polarized MIMO antenna are shown in Figure 5.25. The measured gain of proposed dual polarized MIMO antenna is shown in Figure 5.26. It can be observed the antenna covers the band from 3 - 4.6GHz with 10 dB impedance matching bandwidth. The port to port isolation of 20 dB is achieved for the designed low profile dual polarized MIMO antenna. Simulated radiation patterns for the proposed antenna are shown in Figure 5.27 and 5.28. The individual radiation patterns for 3.1, 3.5 and 4.5 GHz are plotted for both E and H planes. A high front to back ratio of 28 dB is observed from the simulation results.
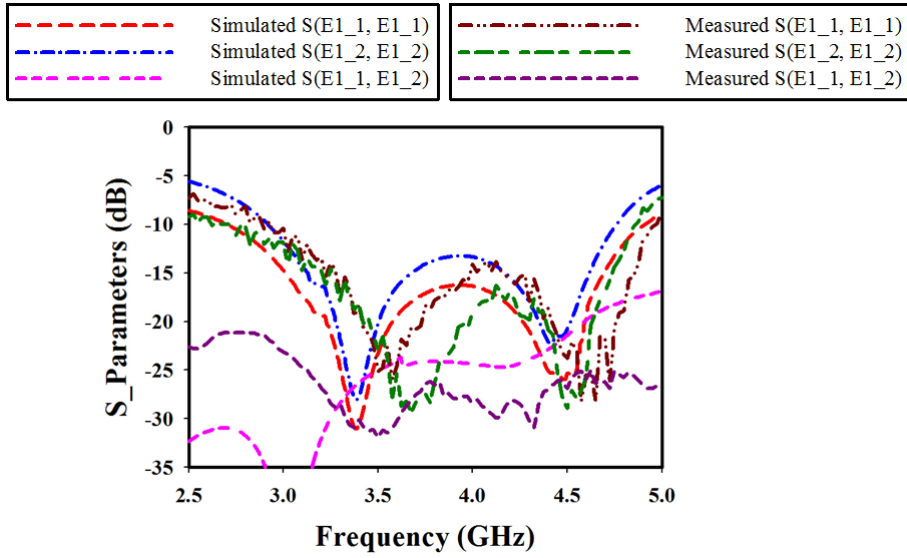
Figure 5.25: Simulated and Measured S-Parameters of the Proposed Wideband DPA.
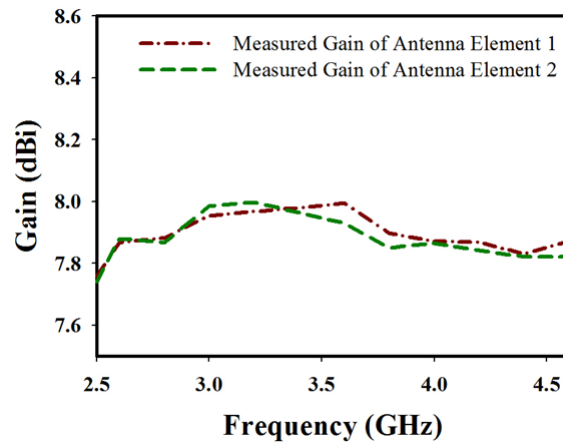
Figure 5.26: Measured Gain of the Proposed Wideband DPA.

97
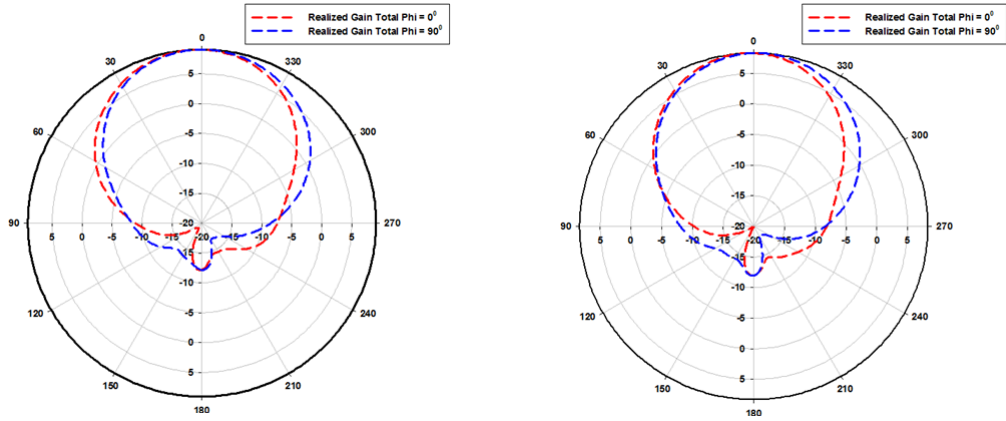
Figure 5.27: Simulated Radiation Patterns for Wideband DPA at 3.5 and 3.1 GHz.
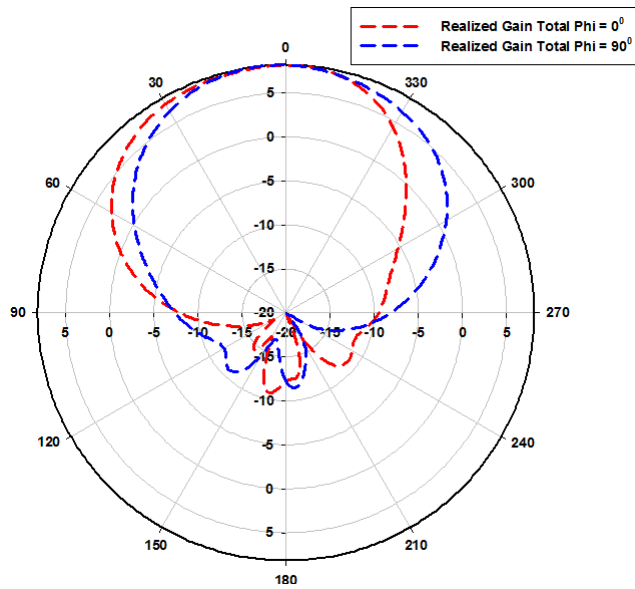
Figure 5.28: Simulated Radiation Patterns for Wideband DPA at 4.5 GHz.

5.5.2   1 × 2 MIMO Antenna With Wideband FSS Wall

When the elements are placed closely the changeling task in MIMO antenna system is to suppress the mutual coupling between the adjacent antenna elements. To analyse the effect of mutual coupling between the each polarized antenna element FSS wall is introduced in between the two dual polarized MIMO antennas. The spacing between the two antenna elements is considered as 0.6 λ. The entire configuration is loaded with chessboard based AMC surface with profile height of 0.125 λ. An array of FSS unit cell is created a wall like structure to suppress the mutual coupling between the two antenna elements. All the four dual polarized antenna elements are excited with four different 50Ω coaxial cables. The geometry of the designed 1 × 2 MIMO antenna is shown in Figure 5.29. The FSS wall which is inserted in between two dual polarized antenna elements is shown in Figure 5.30. The bottom strip line is utilized for fixing the FSS wall and for the return current path towards the ground plane. The fabricated prototype of the frequency selective surface wall is shown in Figure 5.31.
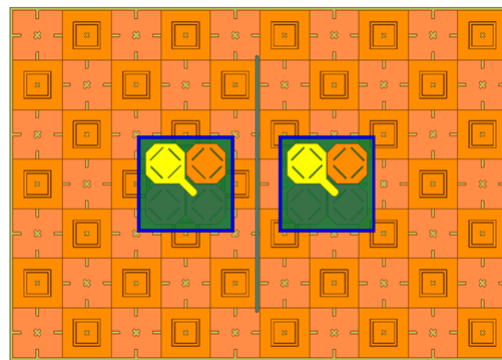
Figure 5.29: Geometry of the 1 × 2 dual polarized MIMO antenna.
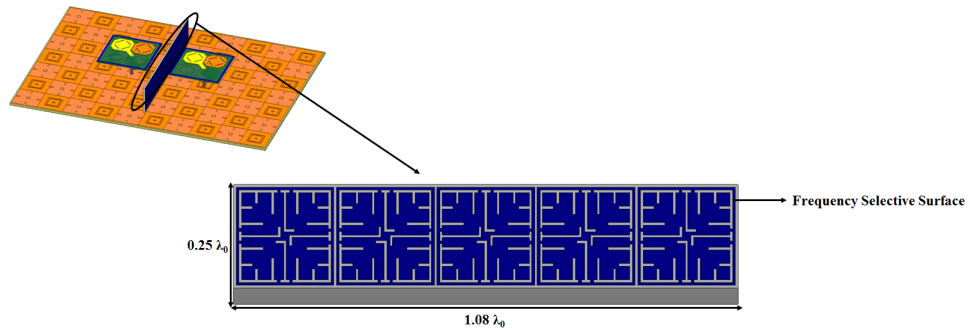
Figure 5.30: Geometry of the Frequency Selective Surface Wall.
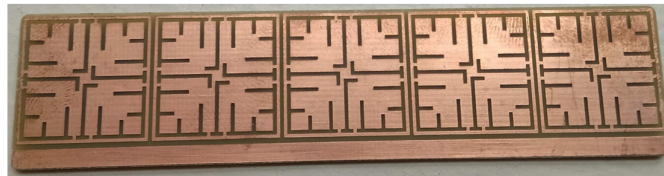
Figure 5.31: Fabricated Prototype of Frequency Selective Surface Wall.

5.5.3 Decoupling Mechanism of FSS Wall

As the surface current have great impact on port to port isolation and mutual coupling in MIMO antennas. The designed 1×2 MIMO antenna and its surface currents distributions with/without FSS wall when port E1-1 is activated are analyzed in Figure 5.32. It is observed that the surface current concentrates at bow-tie antenna elements and at the feed position where two coaxial feed structures are inserted. Hence the field lines mainly occurs around the square ring and bow-tie antenna elements in both cases. To understand the effect of FSS wall over the band of interest the current distributions are observed at various frequencies Figure 5.32(i), (ii) and (iii) depicts the surface current plots at 3.1, 3.5 and 4.5 GHz respectively.

In the case without the FSS wall Figure 5.32(a), a significant amount of cur-

rent mutually induces on the other antenna element. In the case with the FSS wall Figure 5.32(b), less current induces on the other antenna elements due to the presence of vertical FSS wall inserted in between two antenna elements. Since the array of FSS couples the majority of mutual field it enables to minimizes the surface currents generated between the adjacent antenna elements. The height of the FR4 vertical substrate is also optimized for effective mitigation of mutual coupling among the MIMO antenna elements.

The port to port isolation between the antenna ports with and without FSS wall is shown in Figure 5.33(a). Without FSS wall low isolation is reported (<22 dB) is observed between ports (E1-1,E1-2) and ports (E2-1,E2-2). However, noticeably there is improved isolation (<25 dB) between the ports (E1-1,E1-2) and ports (E2-1,E2-2) for entire band of interest. Effect of mutual coupling between each polarized antenna element in both the scenarios that is with and without FSS wall are shown in Figure 5.33(b). In absence of FSS wall between the antenna elements coupling is around 20 to 22 dB between ports (E1-1,E2-1) and ports (E1-2,E2-2). By introducing wide bandstop FSS wall the coupling reduction of 27 dB is achieved between ports (E1-1,E2-1) and ports (E1-2,E2-2) in band of interest. The fabricated prototype of the complete 1×2 MIMO antenna with FSS wall is shown in Figure 5.34.

5.5.4   Measured Results of 1×2 MIMO Antenna

Figure 5.35(a) depicts the simulated and measured S-parameters plot for both the antenna elements. It is observed that the antenna operates for wideband from 2.95 to 4.95 GHz with VSWR of < 2. From the measured results antenna provides a good isolation of 25 to 30 dB as shown in Figure 5.35(b). The simulated and measured radiation patterns at various frequencies of 3.1 GHz, 3.5 GHz and 4.5
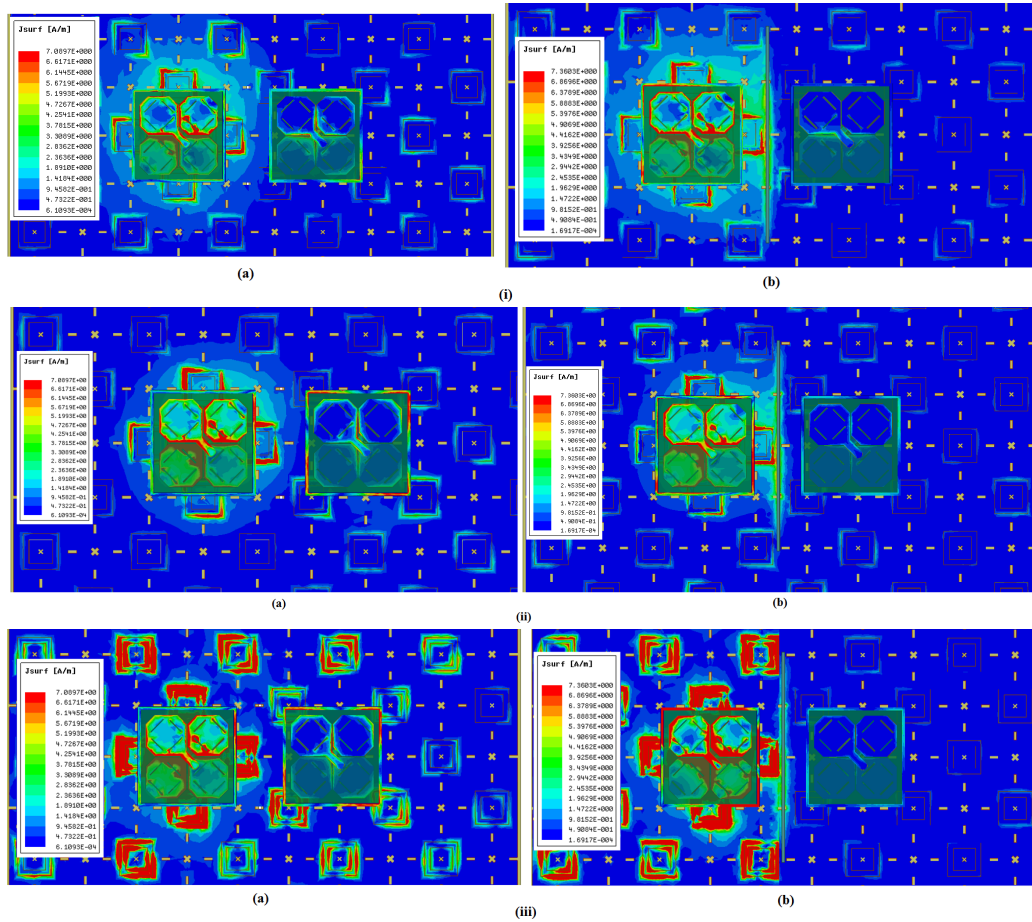
Figure 5.32: Surface currents distribution of the 1×2 MIMO antenna when port E1-1 is activated at (i) 3.1 GHz (ii) 3.5 GHz (iii) 4.5 GHz for (a) Without FSS wall and (b) With FSS wall.

GHz for dual polarized MIMO antenna element in both E and H planes when port E1-1 is excited are shown in Figure 5.36(a), 5.36(b) and 5.36(c) respectively. The measured cross polarization levels are less than -25 dB in both E- and H-planes with high front-to-back ratio of 28 dB. The difference in simulated and measured results may be attributed to the measurement and manufacturing errors. The measurement setup for the proposed MIMO antenna element is shown in Figure 5.37. The performance comparison of the proposed MIMO antenna with and without chessboard AMC surface is given in Table 5.1. The purpose of loading the dual
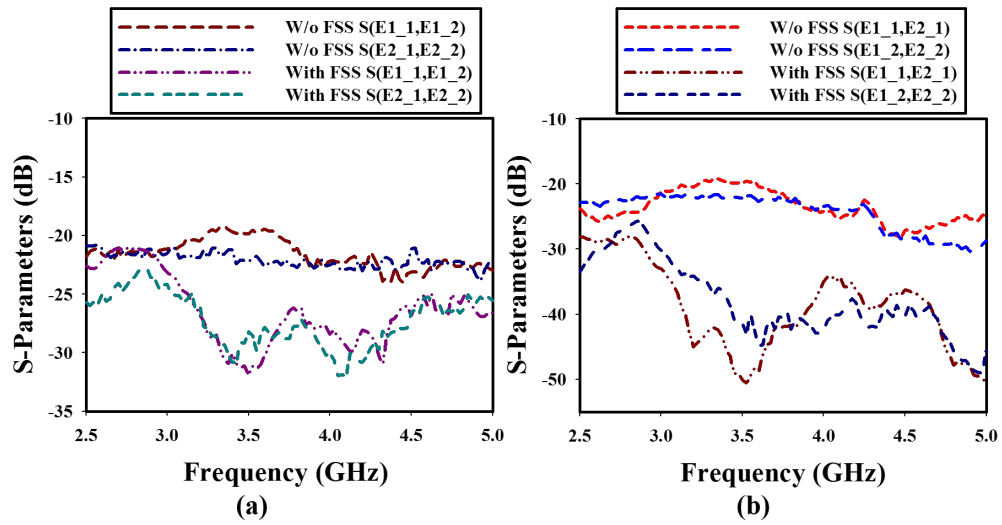
Figure 5.33: Measured (a) Port to port isolation and (b) Mutual coupling reduction with and without FSS wall in 1×2 MIMO antenna.
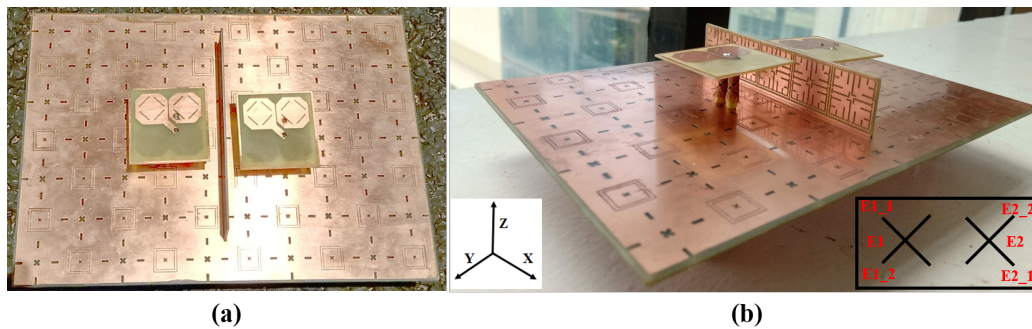
Figure 5.34: (a) Top view and (b) Isometric view of fabricated low profile 1×2 MIMO antenna with FSS wall.

polarized bow-tie antenna with chessboard AMC surface is to obtain low profile and enhance the gain over complete band of interest. The performance of the proposed MIMO antenna element with previous designed antennas from the literature survey are tabulated in Table 5.2.
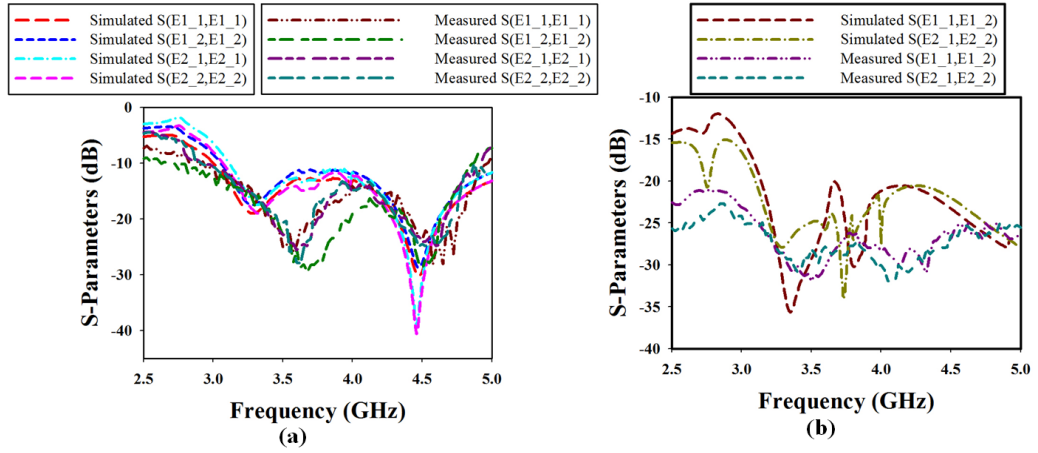
Figure 5.35: Measured and simulated results (a) Reflection coefficient, (b) Port to port isolation in 1×2 MIMO antenna.

Table 5.1: Performance of Proposed MIMO Antenna Element With and Without Chessboard AMC Surface

S.No	Parameters	With AMC Surface	Without AMC Surface
[1]	—S11— < -10 dB	(2.95-4.95)GHz	(3.1 - 4.6)GHz
[2]	Isolation(dB)	25 - 30	28
[3]	Peak Gain(dBi)	7.85 - 8	7.3
[4]	Height	0.125 λ_0	0.25 λ_0
[5]	Remarks	low profile, wide bandwidth, high isolation, high gain	medium bandwidth, high isolation, medium gain

Table 5.2: Performance Comparison of the Proposed MIMO Antenna Element with Previous Antenna Designs

Ref.	Size:L×W×H(λ_0)	Bandwidth(%)	Gain(dBi)
[12]	0.87×0.87×0.19	31% (3-4.1GHz)	7
[13]	1.8×1.8×0.27	40.7% (1.7-2.8GHz)	5.5
[14]	1.39×1.10×0.15	40% (1.7-2.7GHz)	7.3
[16]	1.01×1.01×0.07	22% (2.4-3GHz)	7
[17]	0.93×0.93×0.13	19.8% (3.14-3.83GHz)	7.1
		13.2% (4.4-5.02GHz)	8.2
Pro.	1.05×1.05×0.125	57.14% (2.95-4.95GHz)	7.85 - 8
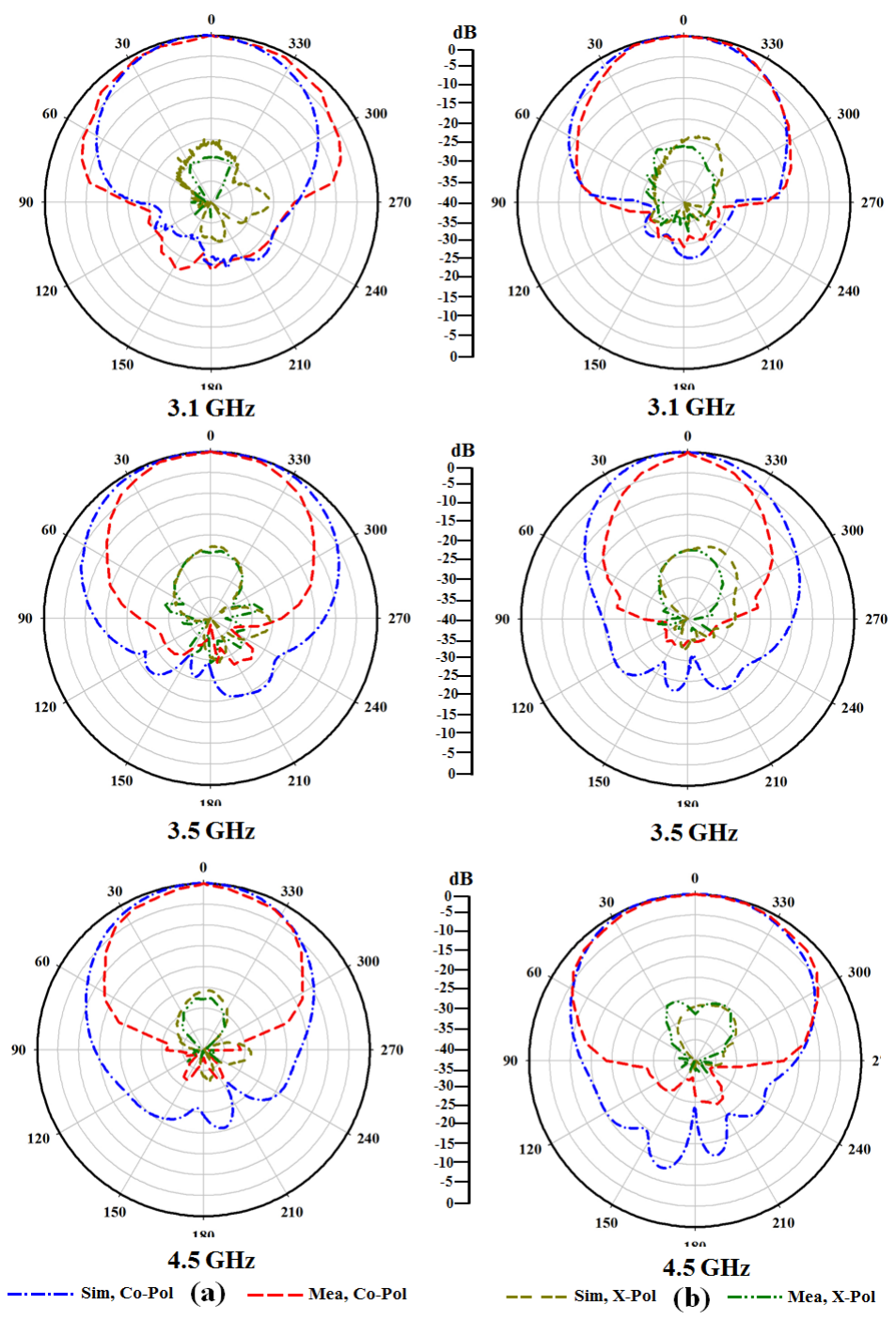
Figure 5.36: Simulated and measured normalized radiation patterns when port E1-1 is excited for MIMO Antenna Element (a) E-Plane (b) H-Plane.

105
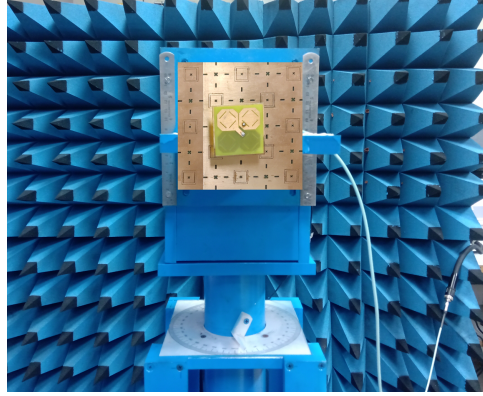
Figure 5.37: Measurement setup of MIMO antenna element.

5.5.5 MIMO Performance Analysis of 1×2 MIMO Antenna

To evaluate the performance of MIMO antenna system, the basic important parameters envelope correlation coefficient(ECC), diversity gain (DG) and total active reflection coefficient(TARC) are considered. Due to complex tedious far field measurement in this article ECC and DG are calcualted using measured S-parameters and supported by simulated far field radiation patterns. ECC by using S-parameters is computed by using the following formula.

$$ECC = \frac{|S_{ii}^* S_{ij} + S_{ji}^* S_{jj}|^2}{(1 - |S_{ii}|^2 - |S_{ij}|^2)(1 - |S_{ji}|^2 - |S_{jj}|^2)} \quad (5.1)$$

where $(i,j) \in (i,j) \mid 1 \leq i < j \leq 4, i,j \in N \mid$

ECC by using far field pattern of the antennas with both phase and polarization information is given by following formula.

$$ECC = \frac{|\int \int \vec{F_1}(\theta,\phi).\vec{F_2}(\theta,\phi)d\Omega|^2}{\int \int |\vec{F_1}(\theta,\phi)|^2 d\Omega \int \int |\vec{F_2}(\theta,\phi)|^2 d\Omega} \quad (5.2)$$

where F_i (θ,ϕ) is the radiated field of the 'i' antenna.

For far field measurement the simple equivalence principle IDM(Infinitesimal Dipole Models) technique along with Ansys HFSS field calculator are utilized. With source current distributions $J_m(\text{r}) = J_{mx}(\hat{x}) + J_{my}(\hat{y}) + J_{mz}(\hat{z})$ and m=1 to n; here n=4, ECC for MIMO antennas is computed by using the formula in [24]. By considering the functions are gaussian in elevation and uniform in azimuth the angular density functions $P_\theta = P_\theta(\theta,\phi)$ and $P_\phi = P_\phi(\theta,\phi)$ are calcualted by using formulas as given above.

In far-field conditions, generally two different scenarios are considered. For first case, isotropic power distribution having cross polarization power ratio that is XPR = 0 dB is assumed and the diversity performance is calculated as an ideal case. For understanding the realistic behavior under outdoor scenario, gaussian power distribution for both horizontal and vertical components having $m_v = m_h = 80$, $\sigma_v = \sigma_h = 15$ with XPR = 1 dB is assumed for second case. Similarly the other parameter diversity gain(DG) related to ECC is calculated by using the following formula.

$$DG = 10\sqrt{1 - (ECC)^2} \qquad (5.3)$$

The evaluated data for ECC and DG are given in Table 5.3. Measured ECC using S-parameters for 1×2 MIMO antenna with and without the proposed FSS is shown in Figure 5.38(a). It is observed that the ECC of the MIMO antenna with FSS is less than 0.05 in operating band. TARC is defined as the ratio of the square root of the total reflected power divided by the square root of the total incident power in a multi-port antenna system. It can be computed by using S-parameters of MIMO antenna system. For two port antenna system TARC is given as,

107

$$TARC = \sqrt{\frac{|(S_{11} + S_{12}e^{j\theta})|^2 + |(S_{21} + S_{22}e^{j\theta})|^2}{2}} \quad (5.4)$$

where θ is the input feeding phase. Measured TARC using S-parameters for 1×2 MIMO antenna is shown in Figure 5.38(b). From the obtained results it indicates that the proposed decoupling structure when integrated with MIMO antenna have better diversity performance. The performance comparison of the 1×2 MIMO antenna with other referenced antennas from the literature survey are tabulated in Table 5.4.

Table 5.3: Simulated ECC and DG using far field patterns

S.No	Fre GHz	ECC Isotropic XPR = 0 dB E1-E2	ECC Outdoor XPR = 1 dB E1-E2	DG Isotropic XPR = 0 dB E1-E2	DG Outdoor XPR = 1 dB E1-E2
[1]	3.1	0.18	0.34	9.82	9.44
[2]	3.5	0.08	0.37	9.96	9.56
[3]	4.5	0.12	0.33	9.92	9.52
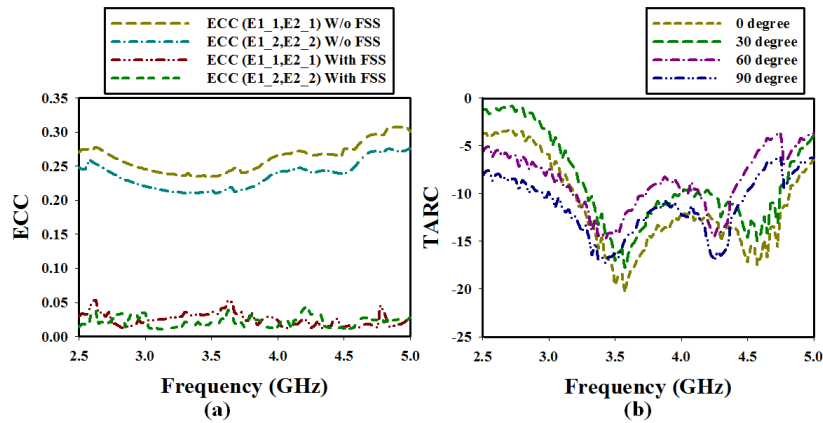
Figure 5.38: Measured (a) Envelope Correlation Coefficients(ECC), (b) Total Active Reflection Coefficient(TARC) of the proposed 1×2 MIMO antenna with and without FSS.

Table 5.4: Performance Comparison of the 1×2 MIMO antenna with Referenced Antennas

Ant.	Decoupling Technique	—S11— < -10 dB	—S12—,—S13— dB	E-E λ_0	Height λ_0
[25]	Metasurface	2.3-2.69	>25	0.27	0.285
[27]	DGS with metal vias	3.95-4.04	10.8,16.6	0.037	N/A
[28]	MDM	3.7/4.1	-28/-25	0.034	0.3
[30]	Neutralization line	2.3/3.5/5.7	18.2/32.4/24.3	0.03	N/A
[31]	Embeddable structure	3.3-4.53	>22, >20	0.56	0.21
Pro.	FSS	2.95-4.95	>25,>38	0.18	0.125

5.6   Summary

:Low profile, wideband dual polarized 1×2 MIMO antenna with frequency selective surface(FSS) decoupling technique is presented. Low profile is realized by chessboard based AMC surface designed with two different AMC cells operating at 3.5 GHz, 3.1 and 4.5 GHz. The compactness of the antenna is achieved by miniaturizing the antenna to $0.4\lambda_0$. A wide bandstop frequency selective surface(FSS) wall from 2.85 GHz to 4.75 GHz is designed to suppress near field coupling between the MIMO antenna elements. Measured results shows by inserting FSS wall vertically, coupling reduction of 27 dB is achieved. The low profile antenna with bandwidth of 57.14% (2.95 – 4.95 GHz) for a VSWR of < 2 with port isolation of more than 25 dB are obtained for entire band of operation.

CHAPTER 6

WAVE PROPAGATION MODELS AND RADIO NETWORK PLANNING FOR PRACTICAL 5G SCENARIO

6.1 Introduction

In the first section of this chapter, dual polarized MIMO antenna element with printed feed network operating under sub 6GHz band for 5G applications is presented. The designed DPA is fabricated and measured for radiation patterns with far field measurement setup. The second and third section discusses the various propagation models suitable for deployment of 5G antenna based on the selected geographical terrain like rural, sub-urban and urban areas. The proper network planning with different wireless standards supporting the 5G requirements as per 3rd Generation Partnership Project (3GPP) standards. The designs are simulated using the Altair FEKO-WinProp platform which supports the various propagation models with radio network planning for practical deployment of the 5G antennas. The signal quality and strength related parameters RSRP, RSRQ, RSSI, SNIR over the selected terrain are also discussed. The fourth section discusses the dual band microstrip patch antenna with metasurface based radome for gain enhancement along with the radome coverage for the designed antenna. The performance of the dual band antenna with and without metasurface radome are also studied and reported.

6.2   Dual Polarized MIMO Antenna Element With Printed Feed Network at Sub 6GHz

In this design, a dual polarized MIMO antenna element with printed balun feed network is implemented for sub 6GHz range to meet the 5G requirements. Dual polarized antenna element with two different polarizations address the concept of polarization and spatial diversity in MIMO antennas. The proposed dual-polarized antenna element with fully planar printed feed network makes it suitable for the large scale base stations in future 5G communication.

6.2.1   Design of Dual Polarized Bow-Tie Antenna Element:

Desirable features of a wideband antenna are low-profile and wide bandwidth in a compact size. Many existing wideband antennas are large in size and some have only circular polarization. On the other hand low-profile, dual polarized antennas frequently have limited bandwidth. The major UWB antenna design challenges include compact size while providing acceptable VSWR, bandwidth, gain, and efficiency.The ultra wide band antenna designs may be broadly divided as travelling wave structures like Vivaldi antenna, Frequency independent structures like the biconical antenna or the **bowtie Antennas**.

The well-known bow-tie antenna originally proposed by Lodge and later re-examined by Brown and Woodward exemplifies benefits like inexpensive and easily fabricated designs. Some of the various types of bow-tie antenna elements are given below in Figure 6.1.

- Triangular and Quadrate bowtie antenna
- Rounded edge/ corner bowtie antenna

• Slotted bowtie antenna
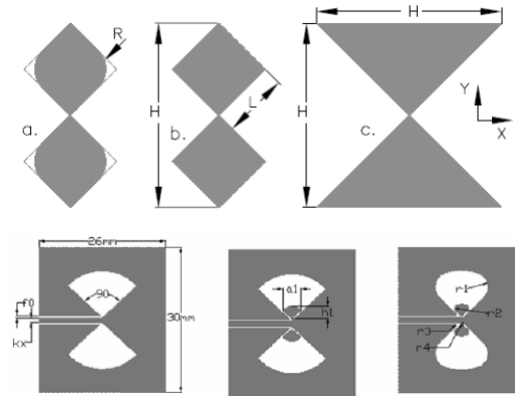
Figure 6.1: Different types of bowtie antennas with same height.

A novel dual polarized bow-tie antenna element operating at 3.5 GHz. The antenna is designed using an FR4 substrate of size 50 mm, relative permittivity of 4.4, height (h) of 1 mm and loss tangent of 0.02. The two bow-tie antenna elements are excited by the two separate printed feed network designed using FR4 substrate. The bottom ground plane is also designed by using FR4 substrate of size 100 mm, relative permittivity of 4.4, height (h) of 1.6 mm and loss tangent of 0.02.

Initially the design was started with normal patches and then introduced the L shaped slots for obtaining the better isolation and later it was modified by inserting the U-shaped notches on the radiator elements to obtain good isolation. The design obtained from different stages are shown in Figure 6.2. The geometry and isometric view of the proposed dual polarized antenna is shown in Figure 6.3.

Stage 1: Geometry of the DPA Antenna   Stage 2: Geometry of the Dual Polarized Antenna with L-Shaped Slots   Stage 3: Geometry of the Proposed Dual Polarized Antenna
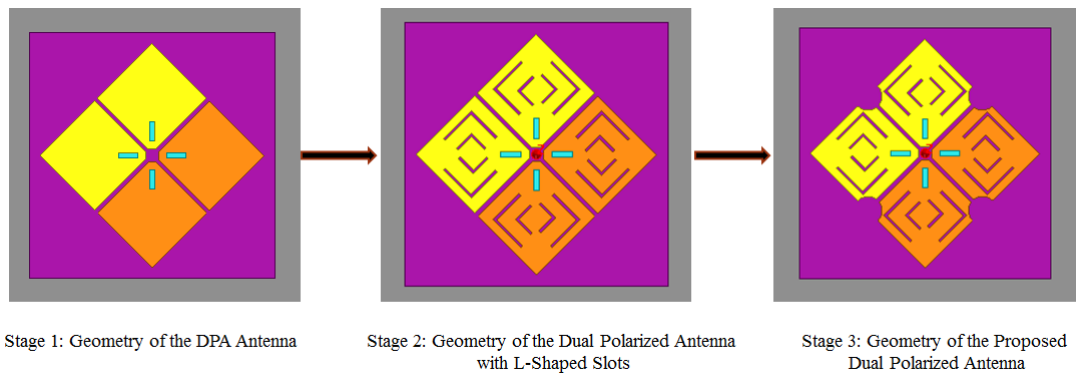
Figure 6.2: Different stages of the proposed dual polarized antenna.
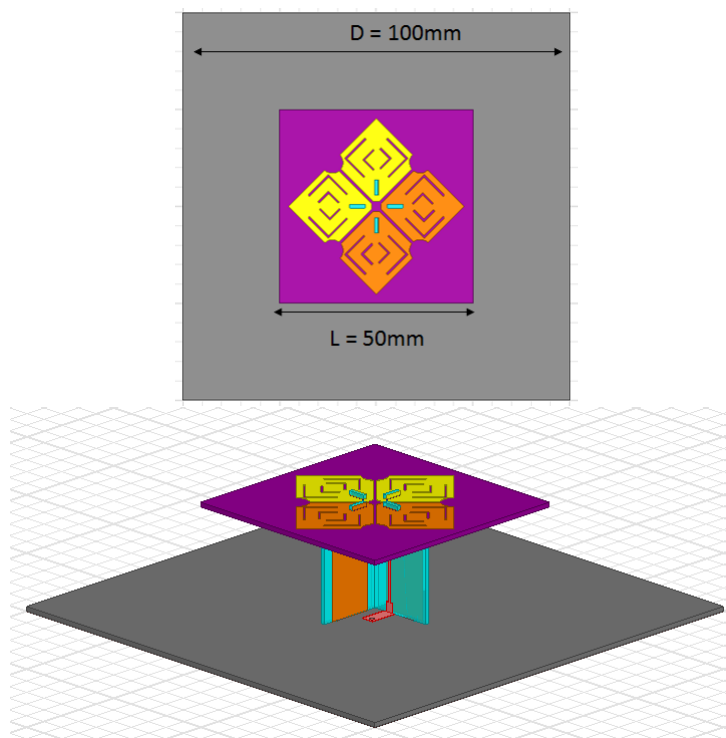
Figure 6.3: Geometry and isometric view of the proposed dual polarized antenna.

113

6.2.2 Design of Printed Feed Network:

For dual polarized antennas, port isolation is one of the most important factors that influence the sensitivity of the receiving channel and the stability of receiver. Consequently, miniaturized base station antennas with high port isolation are becoming one of the hottest issues in modern wireless communication. Due to the complexity in soldering on the top and bottom of bow-tie dipoles with coaxial cables. The alternative approach is used to design the dual polarized antenna which consists of two perpendicularly crossed bow-tie dipoles printed on FR4 substrate. Each bow-tie dipole is excited by a microstrip stub that is directly fed by coaxial line, enabling the antenna to be fully planar.

The configuration of the baluns is designed initially with single microstrip line feed on front side and two patches on the back of substrate which will be connected to the printed dipoles and ground plane at top and bottom respectively. The design is simulated in ANSYS HFSS 19.0 for desired frequency. The two printed feed networks are matched at desired frequency with 180^0 phase shift. The two feed networks are integrated with the help of slits provided in two substrates are shown in Figure 6.4 and 6.5. /the integration of the feed networks and its geometry are shown in Figure 6.6 and 6.7.
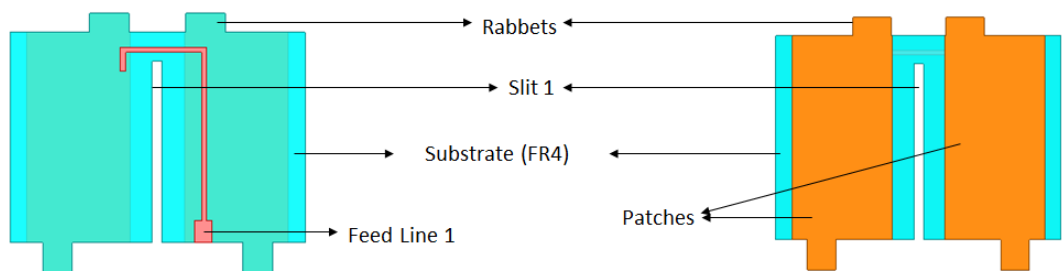
Figure 6.4: Front and Back View of Feed Network 1 .
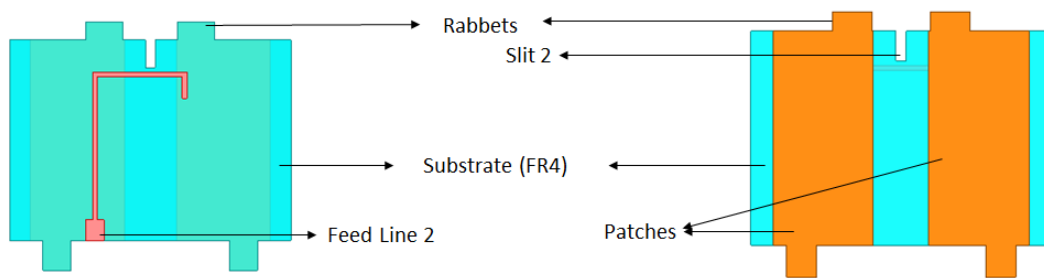
Figure 6.5: Front and Back View of Feed Network 2.
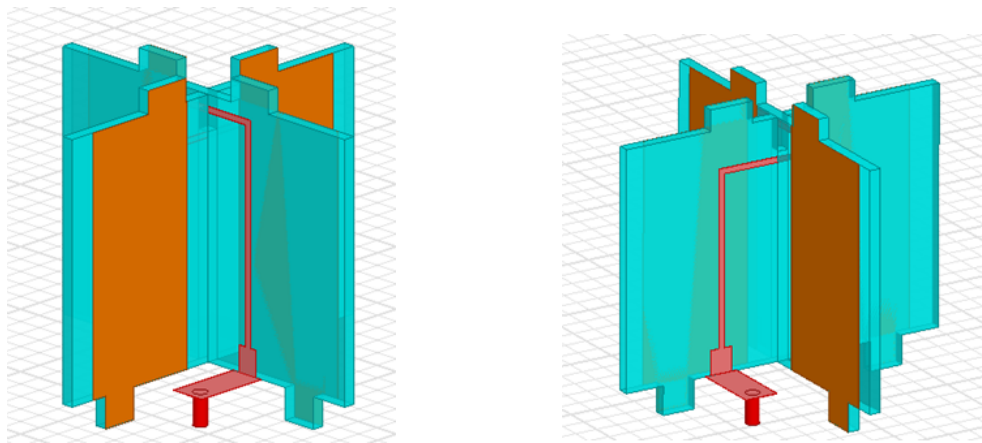
Figure 6.6: Integration of both Feed 1 and Feed 2.

The designs are simulated in ANSYS HFSS 19.0 and the observed results are shown from Figure 6.8 to 6.10. From the simulated results it is observed that the proposed dual polarized antenna covers -10 dB impedance bandwidth from 3.4 GHz to 3.6 GHz and port to port isolation is around 20 to 25 dB for entire band of operation as shown in Figure 6.8. The simulated radiation patterns are obtained for both E and H planes. The co-cross polarization levels resulted around 25 dB for both E and H planes as shown in Figure 6.9 and 6.10.

The designs are fabricated and tested. The assembly of the dual polarized
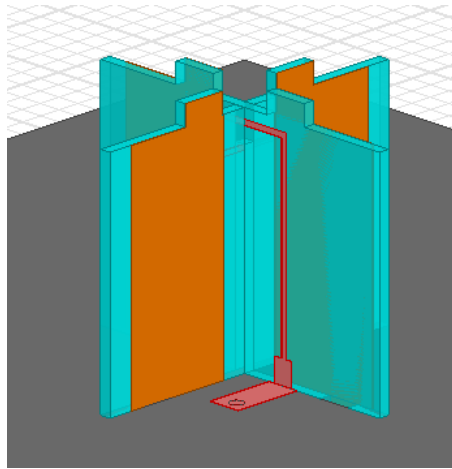
Figure 6.7: Geometry of Dual Feed Network.
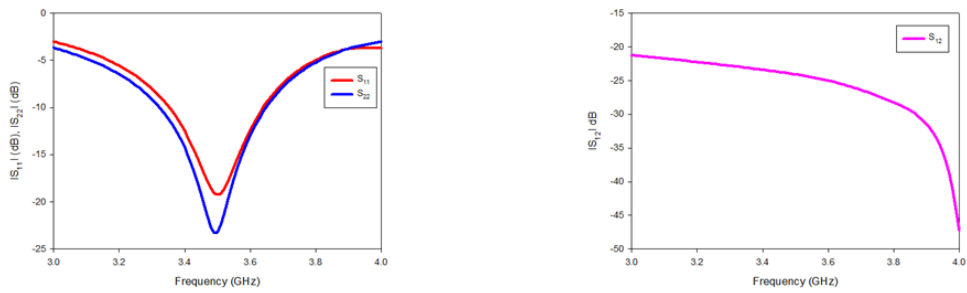
Figure 6.8: Simulated S-Parameters for Proposed DPA.

antenna is done by integrating both the printed feed networks and with the help of rabbets on top and bottom it is inserted and fixed to radiator and the ground plane which makes the entire structure to be planar. By utilizing the two different ports of two dipole elements different measurements are done. The measured results are in agreement with the simulated results. The details of the fabricated antenna are shown in Figure 6.11 and Figure 6.12.

The measured plots of the fabricated dual polarized antenna with printed feed
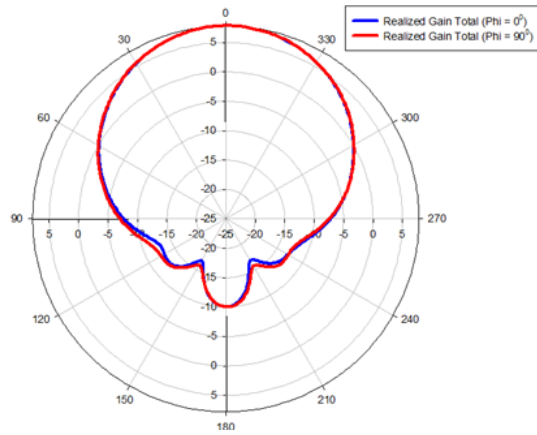
Figure 6.9: Simulated Realized Gain.
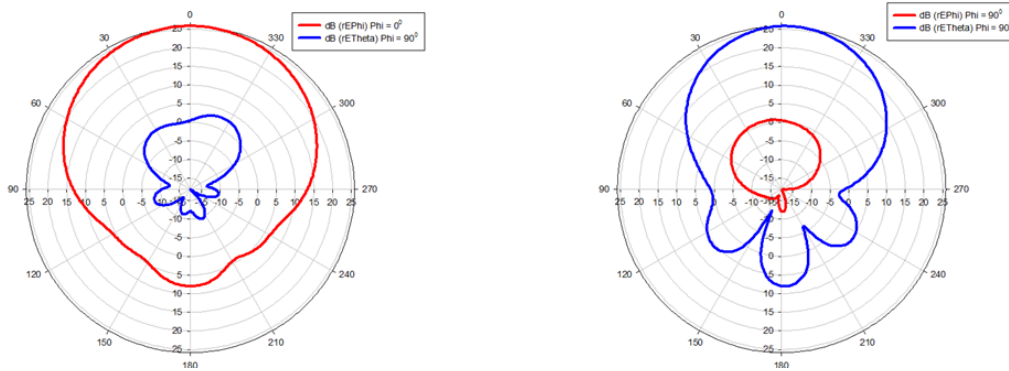
Figure 6.10: Simulated Radiation Patterns for E and H Planes.

network are shown in Figure 6.13. From the measured plots it is observed that the dual polarized antenna covers the frequency band from 3.4 GHz to 3.6 GHz which is under sub 6 GHz range for the 5G requirements. The isolation resulted to be below 24 dB for the proposed dual polarized antenna element.

The radiation pattern measurements are done separately when transmitting is placed in both horizontal and vertical polarization. The receiving dual polarized antennas are named as antenna1 and antenna2 while taking measurements. The
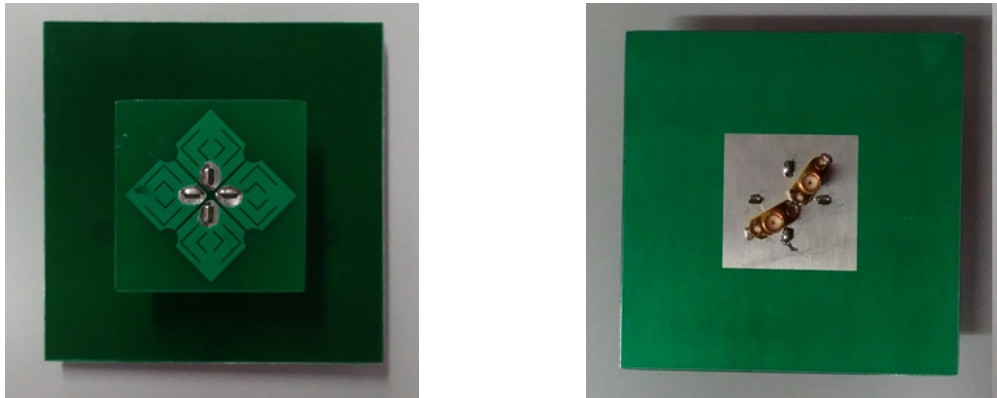
Figure 6.11: Top and Back View of the Fabricated Dual Polarized Antenna.
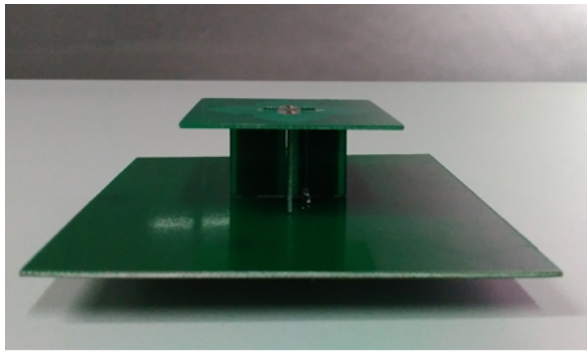
Figure 6.12: Side View of the Fabricated Dual Polarized Antenna.

far field measurement setup for the dual polarized antenna with standard horn antenna is shown in Figure 6.14.The measured radiation patterns for antenna 1 when transmitting is in both vertical and horizontal polarization are shown in Figure 6.15 and 6.16 and for antenna 2 it is shown from Figure 6.17 and 6.18.

The measured gain for the dual polarized antenna is shown in Table 6.1 and comparison of simulated and measured results are shown in Table 6.2.
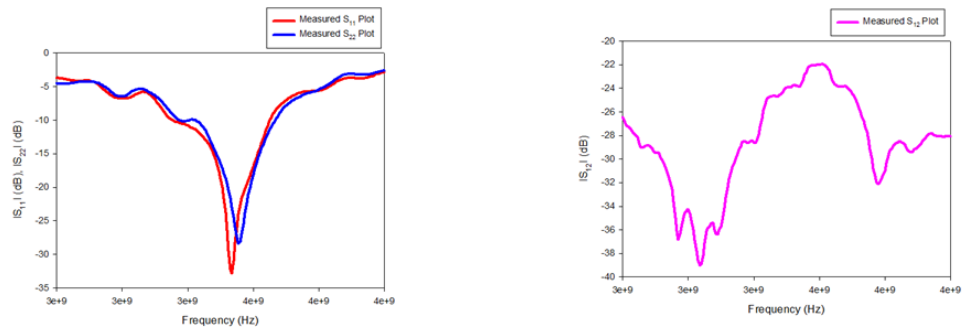
Figure 6.13: Measured Scattering Parameters.

Figure 6.14: Far Field Measurement Setup of Dual Polarized Antenna.

Table 6.1: Measured Gain for Antenna 1 and Antenna 2.

Frequency(GHz)	Antenna 1(dB)	Antenna 2(dB)
3.4	7.07	6.75
3.45	7.8	7.57
3.5	7.75	768
3.55	7.33	7.15
3.6	6.93	6.83

119

A. Transmitting Antenna in Vertical Polarization for Antenna 1

At 3.4 GHz   At 3.5 GHz   At 3.6 GHz

Co-Pol
Cross-Pol
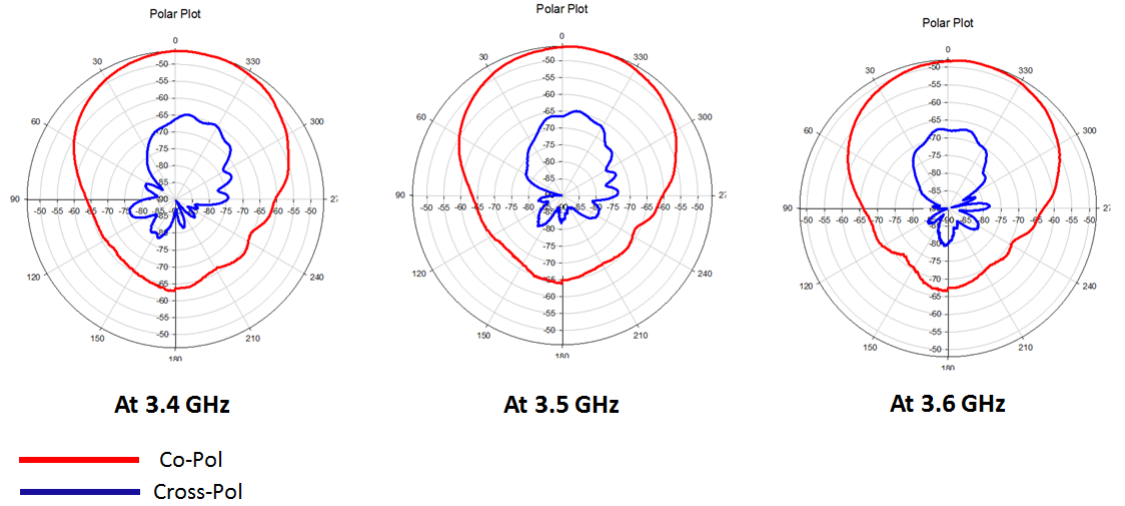
Figure 6.15: Measured Radiation Patterns for Antenna 1 with Tx. Antenna Vertically Polarized.

B. Transmitting Antenna in Horizontal Polarization for Antenna 1

At 3.4 GHz   At 3.5 GHz   At 3.6 GHz

Co-Pol
Cross-Pol
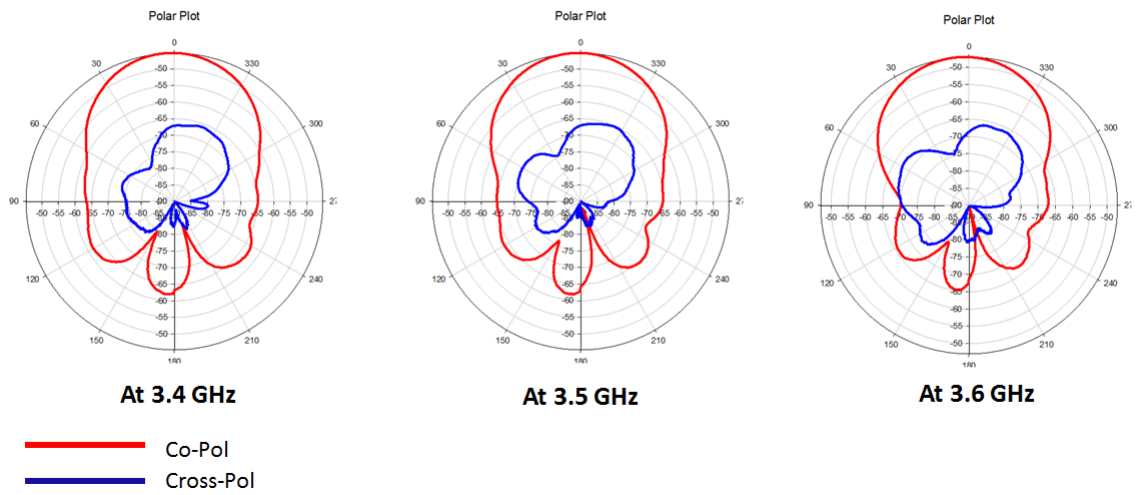
Figure 6.16: Measured Radiation Patterns for Antenna 1 with Tx. Antenna Horizontally Polarized.

A. Transmitting Antenna in Vertical Polarization for Antenna 2

| At 3.4 GHz | At 3.5 GHz | At 3.6 GHz |

Co-Pol
Cross-Pol
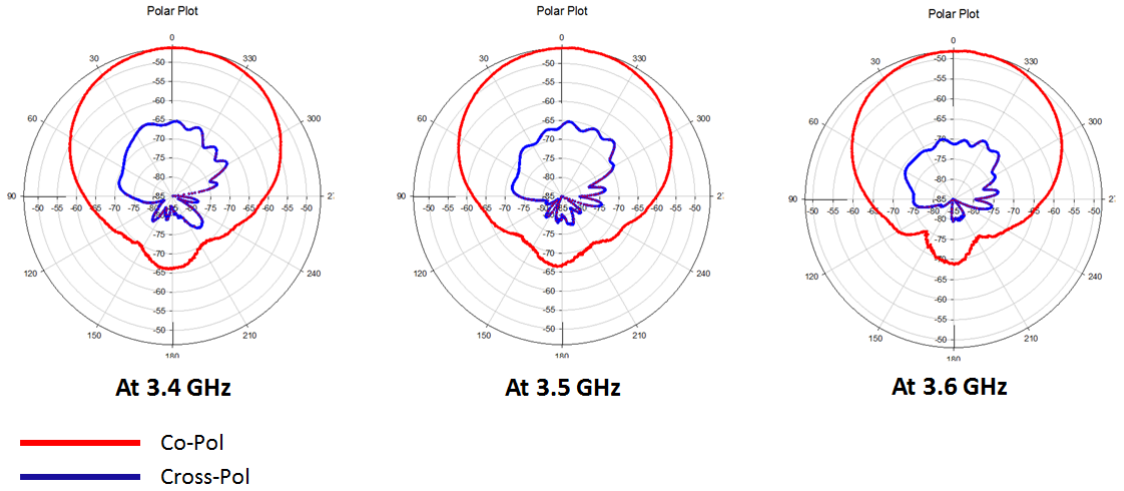
Figure 6.17: Measured Radiation Patterns for Antenna 2 with Tx. Antenna Vertically Polarized.

B. Transmitting Antenna in Horizontal Polarization for Antenna 2

| At 3.4 GHz | At 3.5 GHz | At 3.6 GHz |

Co-Pol
Cross-Pol
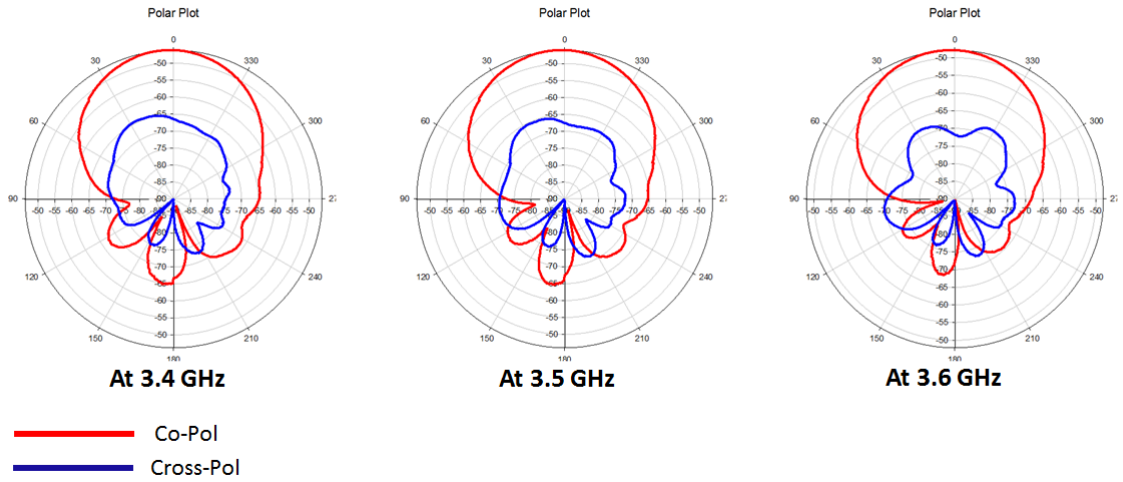
Figure 6.18: Measured Radiation Patterns for Antenna 2 with Tx. Antenna Horizontally Polarized.

Table 6.2: Comparison of simulated and measured results at 3.5 GHz.

Parameters	Simulated Results(dB)	Measured Results(dB)
Reflection Coefficient	-19 , -23	-18.4,-16.6
Isolation	-24.02	-24.2
Gain	7.97 , 7.82	7.75 , 7.68
Front to Back Ratio	17.77	20.29

6.3 Radio Network Planning for 5G MIMO Antenna

6.3.1 Deployment of 5G MIMO Antenna Element

The proposed dual polarized 5G MIMO antenna is deployed in practical scenarios with different air interface wireless standards by using FEKO-WinProp software. FEKO WinProp 3D EM software package is utilized for simulating the model as it supports ray tracing models with 3D visualization of actual deployment in campus environment. Full 3D visualization of the environment for the antenna deployment could not be implemented in MATLAB/ADS and it's not under the scope of the proposed work in the manuscript. Effect of various parameters like reflection, refraction, scattering, path loss, line of sight are taken into account with WinProp software which also supports different wireless standards as per 3GPP requirements. The effective coverage over the selected terrain and locations for proper deployment of the antennas are also shown with suitable graphs using WinProp software.

The different wave propagation models are considered for computing the radio coverage and radio channel analysis in various scenarios from large rural to dense urban cities. The step by step procedure for deploying the proposed 5G MIMO antenna is shown in Figure 6.19.The network planning modules for different air interfaces helps to compute the overall signal and interference situation by superposing the contributions from multiple deployed transmitting sites.
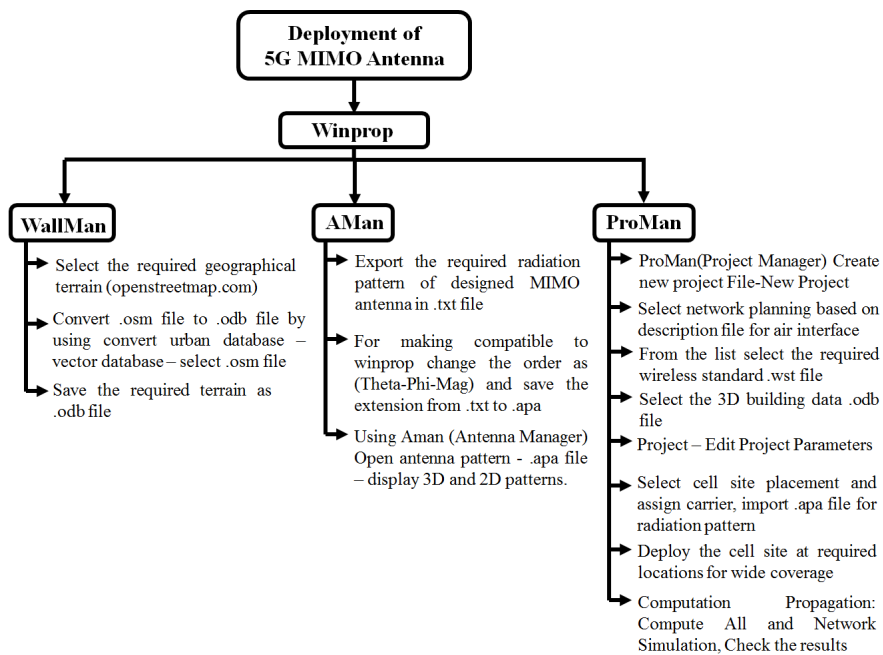
Figure 6.19: Flow chart for deployment of 5G MIMO antenna element in Win-
Prop.

The ray tracing models in WinProp considers all the dominant wave propaga-
tion characteristics (reflection, diffraction, and scattering) and support the analysis
of 3D building knowledge representing the given surroundings. The propagation
models are three dimensional by taking into account of all 3D object data. For
accurate predictions of the radio coverage the dominant path model(DPM) is ap-
plied which consists of high accuracy with short computation time. For deploying
the designed 5G MIMO antenna element a geographical terrain National Institute
of Technology Karnataka(NITK) campus is selected as shown in Figure 6.20. and
the equivalent representation of the map by using WallMan is shown in Fig. 6.21.
The designed radiation patterns for Unit cell, 2×2, 4×4 and 8×8 massive MIMO
antenna are exported from ANSYS HFSS and made compatible for WinProp by
using AMAN(Antenna Manager). The obtained 3D radiation plot for MIMO an-
tenna element is shown in Figure 6.22.

Figure 6.20: NITK campus considered locations A,B and C with respective buildings are labelled and given in map.

(a) **(b)**
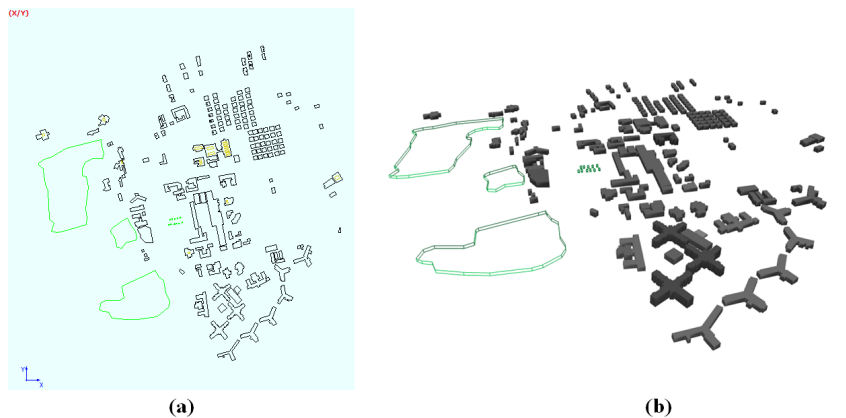
Figure 6.21: Selected geographical terrain using WallMan and ProMan (a) Layout and (b) 3D View respectively.

The radio channel predictions in terms of time, frequency and also for the spatial domain are necessary to analyze the 5G transmission modes along with various MIMO concepts. MIMO antenna arrays are developed in different configurations on both at transmitter(Tx) and receiver(Rx) side which uses spatial multiplexing or beamforming and even combination of both technologies. The signal field strength and delay with angle of depature at both Tx and Rx are considered in WinProp. This simulation tool provides several methods which are fully three

124
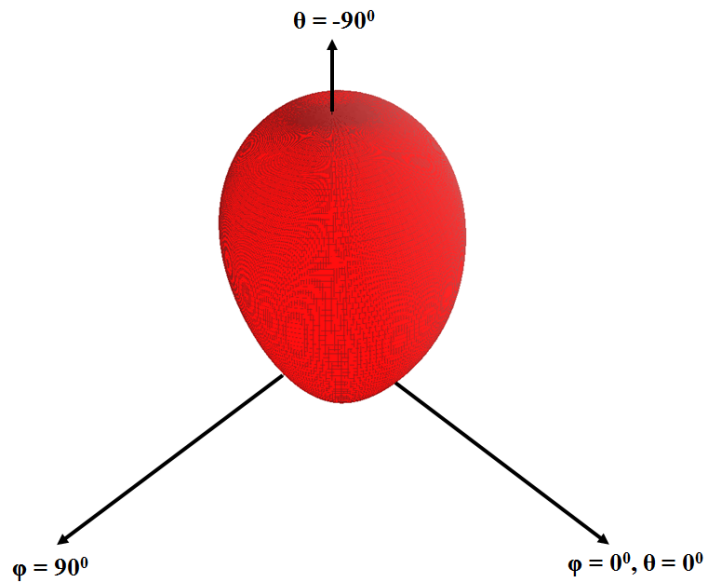
Figure 6.22: 3D Radiation pattern of Single DPA Element in AMAN.

dimensional by considering 3D objects data to compute all rays in 3D. The Pro-Man(Project Mangaer) is utilized to deploy the cell sites in selected geographical terrain and required network planning is done by using various air interfaces.

6.3.2 Measurement Locations

The measurement environment is at NITK campus and the respective deployed locations A,B and C for base station antenna are given in Figure 6.20. The deployement of the MIMO antenna with different configurations can be selected to any densely populated urban areas, for convenience the campus view itself is considered and analyzed. The measurements are taken in three locations, namely at Building A (Main Academic Building) as location-A, Building B (Lecturer Hall C) as location-B and Building C(Mega Tower) as location-C which are marked on the map. Location A and location B are on two either sides of the national highway passing in between the east and west campus which are 15m apart whereas

125

the distance between location A, location B to location C will be more than 50m. The pictorial representation of the campus with selected sites for antenna deployment are shown in Figure 6.23. The panoramic views from these locations are also shown from Figure 6.24 to Figure 6.26. These locations were selected such that the deployed MIMO antenna sees the different environment addressing the maximum number of users.

In location A, B and C the selected MIMO antenna configurations are placed at altitude of 30m from the terrace to maintain the uniform coverage. There are other bulidings in between with various departments covering the maximum number of users. The selected three locations covers the entire campus with maximum data rate and throughput with required channel modulation schemes. The various wave propagation models are studied with different MIMO antenna configurations and analyzed.
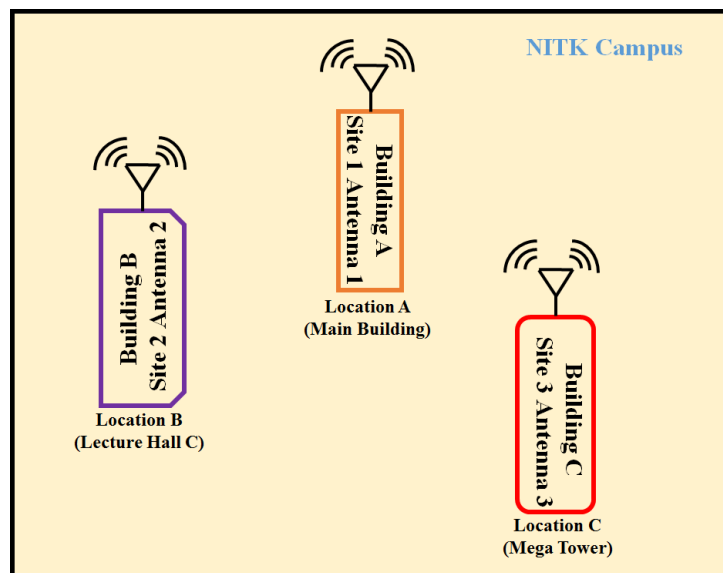
Figure 6.23: Pictorial representation of NITK campus with deployed cell site locations.

Figure 6.24: Panoramic View from Location A focusing the east side campus. This building is marked as site 1 antenna 1 in the cell site area map.

Figure 6.25: Panoramic View from Location B focusing towards building A. This building is marked as site 2 antenna 2 in the cell site area map.

Figure 6.26: Panoramic View from Location C focusing the entire hostel blocks. This building is marked as site 3 antenna 3 in the cell site area map.

6.3.3 Radio Network Planning of 5G MIMO Antenna

The performance of wireless communication networks depends on an efficient architecture of the network. Due to the wide range of available air interfaces for cellular and broadcast wireless networks with their different behavior and parameter settings, radio network planning is essential to analyze the performance of the wireless network.

For deploying 5G, ultra-dense networks consisting of base stations with low power in suburban areas are utilized to provide high data rates. Accordingly, a fast coverage prediction model is required. Here, for 5G radio planning the dominant path model is utilized as it combines high accuracy with less computation time. The dominant path model supports wide frequency range which can be used for all types of cells with Tx antennas above, below or on the rooftop. Therefore, by considering this model the radio coverage for different air interface wireless standards are tabulated in Table 6.3 and Table 6.4.

As the 5G cellular network launching gets interconnected and utilizes the already existing 4G LTE networks. To understand the LTE(Long Term Evolution) signal strength and quality few signal type terminologies and its considerable range of values are described below.

- Reference Signal Received Power(RSRP) : As per 3GPP definition of RSRP is defined as the linear mean over the power contributions for the resource elements that contain cell-specific reference signals within the desired measurement frequency bandwidth. Its typical signal quality values are $\geq$ -80 dBm (Excellent); -80 dBm to -90 dBm (Good); -90 dBm to -100 dBm (Fair to Poor); $\leq$ -100 dBm (No Signal/Disconnection).

- Received Signal Strength Indicator (RSSI) : RSSI is defined as the entire received power including the desired power from the serving cell in addition to the co-channel power and other sources of noise. RSSI typical signal quality value ranges are $>$ -65 dBm (Excellent); -65 dBm to -75 dBm

(Good); -75dBm to -85 dBm (Fair); -85 dBm to -95 dBm (Poor); $\leq$ -95 dBm (No Signal/Disconnection)

- Reference Signal Received Quality (RSRQ) : It indicates the quality of the received reference signal. RSRQ typical signal quality value ranges are $\geq$ -10 dB (Excellent); -10 dB to -15 dB (Good); -15 dB to -20 dB (Fair to Poor); $\leq$ -20 dB (No Signal/Disconnection).

- SNIR/SNR : Signal to Noise plus Interference Ratio (A minimum of 20 dB is required to detect the RSRP/RSRQ). It indicates the throughput capacity of the channel. The typical range of values are $\geq$ 20 dBm (Excellent); 13 dBm to 20 dBm (Good); 0 dBm to 13 dBm (Fair to Poor); $\leq$ 0 dBm (No Signal/Disconnection).

Table 6.3: Wave propagation model analysis for air interface with wireless standard : 5G TDD

S.No	Parameters with Units	Omnidirectional Antenna Number of Sites		
		One	Two	Three
1.	DL:Max Data Rate (MBits/s)	0.6954	1.235	1.288
2.	DL:Throughput (MBits/s)	171.4	321.2	334.9
3.	UL:Max Data Rate (MBits/s)	705.4	1.322	1.378
4.	UL:Throughput (MBits/s)	183.4	343.6	358.2
5.	Received Power (dBm)	-65	-60	-60
6.	SNIR (dB)	35	40	40
7.	RSRP (dBm)	-85	-80	-80
8.	RSRQ (dB)	0	0	0
9.	RSSI (dBm)	-68	-62	-62

WinProp platform is utilized to determine the path loss, cell coverage, signal to noise and interference ratio, throughput, maximum data rates in down link and up link, received power, individually for each transmission mode. From the tabulated data both TDD and FDD technology are utilized for 5G. However, by comparing the results and range of coverage over the selected area 5G FDD standard with Omnidirectional antenna with three number of sites is selected. The cell site areas and the best server over the selected map is shown in Figure 6.27. The calculated

Table 6.4: Wave propagation model analysis for air interface with wireless standard : 5G FDD

S.No	Parameters with Units	Omnidirectional Antenna Number of Sites		
		One	Two	Three
1.	DL:Max Data Rate (MBits/s)	1.319	2.471	2.471
2.	DL:Throughput (MBits/s)	342.9	642.4	642.4
3.	UL:Max Data Rate (MBits/s)	1.411	2.643	2.643
4.	UL:Throughput (MBits/s)	366.8	687.2	687.2
5.	Received Power (dBm)	-70	-65	-65
6.	SNIR (dB)	30	35	35
7.	RSRP (dBm)	-90	-85	-85
8.	RSRQ (dB)	-3	0	0
9.	RSSI (dBm)	-68	-64	-64

path loss, field strength, and power for the layout are shown in Figure 6.28. The line of sight(LOS) and non line of sight(NLOS) with respect to each cell sites are shown in Figure 6.29. The each cell site incorporating the designed antenna radiation pattern with an average gain of 8.26 dB is able to cover the selected geographical terrain.

6.4 Wave Propagation Models For 5G MIMO Antenna

6.4.1 Knife Edge Diffraction Model

Generally, the deterministic models utilize the physical phenomena to explain the propagation of radio waves and are based on ray optical techniques. When a radio wave is considered to propagate in straight line it gets presuaded by only the present obstacles that mostly lead to reflection, diffraction and even peneration
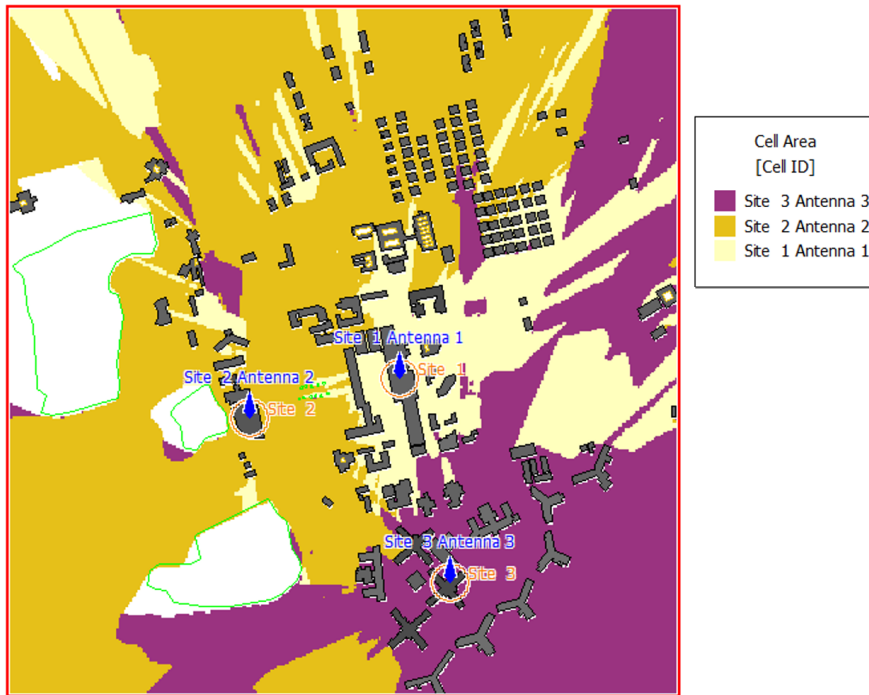
Figure 6.27: Cell site area and best server in selected map.
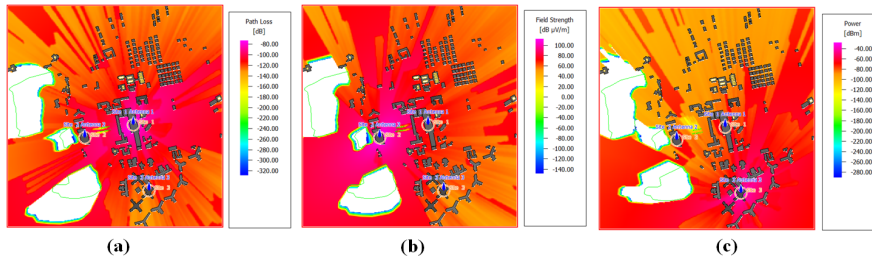
Figure 6.28: Simulation Results of (a) Path loss (b) Field strength (c) Power over the selected geographical terrain.

through these obstacles. But for scenarios where there is large distance between transmitter and receiver the computational demand is ambitious. There are also even some scenarios where there is no 3D vector data available but only the clutter height information of the located building heights in pixel format. Knife edge diffraction(KED) model is one approach where the both cases can be predicted based on either vector or pixel data. This model considers the effect of the actual

131
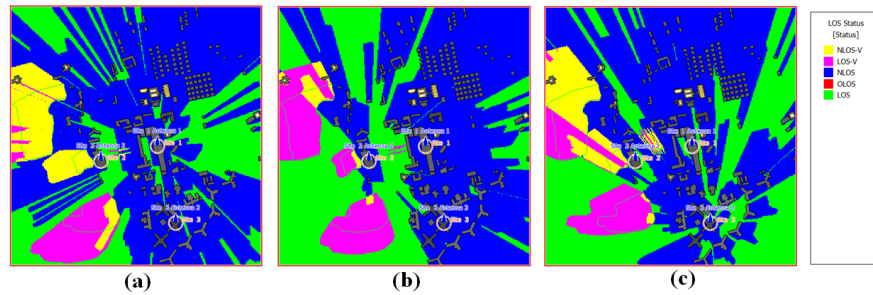
Figure 6.29: Layout of the geographical terrain with LOS and NLOS for (a) Cell site 1 (b) Cell site 2 (c) Cell site 3.

environment by utilizing the 3D vector building data along with terrain profile.

For the selected geographical terrain KED model is applied and the computation is done by using WinProp software. The number of diffractions (knife edges) can be limited to required number by editing the parameters in additional knife edge diffraction settings. The diffractions at the clutter objects including the clutter height are taken in to consideration for simulation. The general scenario how the knife edges are considered between transmitter and receiver during computation is shown below in Figure 6.30. The simulations are carried out with unit cell MIMO antenna element, 2×2, 4×4 and 8×8 massive MIMO configuration radiation patterns. The effect of single stream data rate and throughput over the area of coverage as the number of antenna elements increases are observed shown in Figure 6.31 (a) and (b).

The observed simulation results by implementing KED model are tabulated in Table 6.5. The single stream data rate and throughput of 2.576 MBits/s and 669.8 MBits/s for downlink and 2.756 MBits/s and 716.5 MBits/s for uplink are reported for the deployed cell sites at three locations A, B an C as shown in Figure 6.32. From the simulation results RSRP is -85 dBm, RSRQ is 0 dB and RSSI is -62 dBm which states that the signal strength is excellent covering the entire map with selected locations A,B and C as shown in Figure 6.33
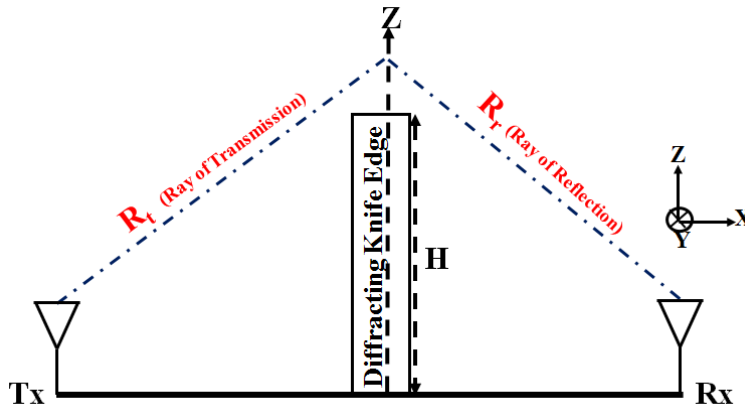
Figure 6.30: General Transmitter and Receiver Scenario in Knife Edge Diffraction Model.

6.4.2 Extended Walfisch-Ikegami Model

Extended walfisch-ikegami model(EWM) considers several parameters related to building profile in the environment for path loss prediction. It utilizes very less computation time with tolerable accuracy when compared to the deterministic ray optical models. Wave-guiding effects are not considered in this model which generally occurs in urban canyons. This model accuracy is more accurate when the transmitters are located above the rooftop levels of the bulidings as it approximates the mutliple diffractions. It considers only the characteristic values for predicting path loss. It discriminates between line-of-sight (LOS) and non-line-of-sight(NLOS) situations.

The general propagation scenario of the EWM model is shown in Figure 6.34. Where H_{Tx} is the height of the transmitter, H_{roof} is the mean value of the building heights, H_{Rx} is the height of the receiver, w is mean value of width of roads, s is mean value of building separation. The evaluation of path loss agress very well with the measurements of the base station antenna heights above the rooftop level. In this model the prediction error becomes quite larger for H_{Tx} close to H_{roof}

133
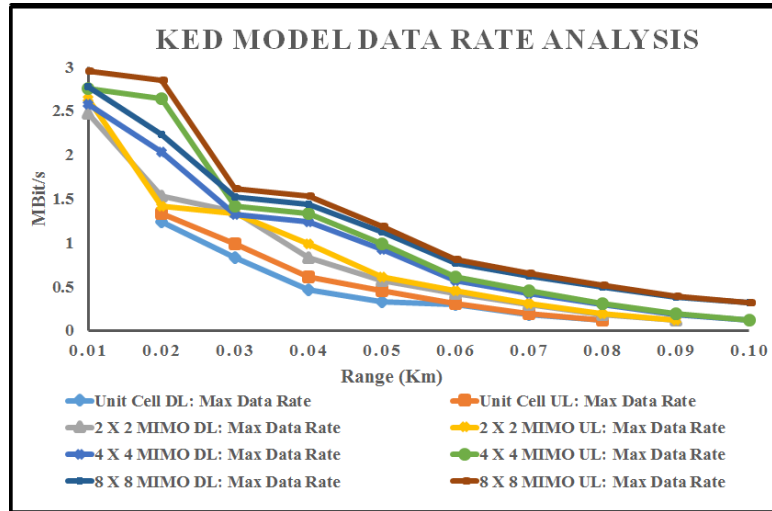
(a)
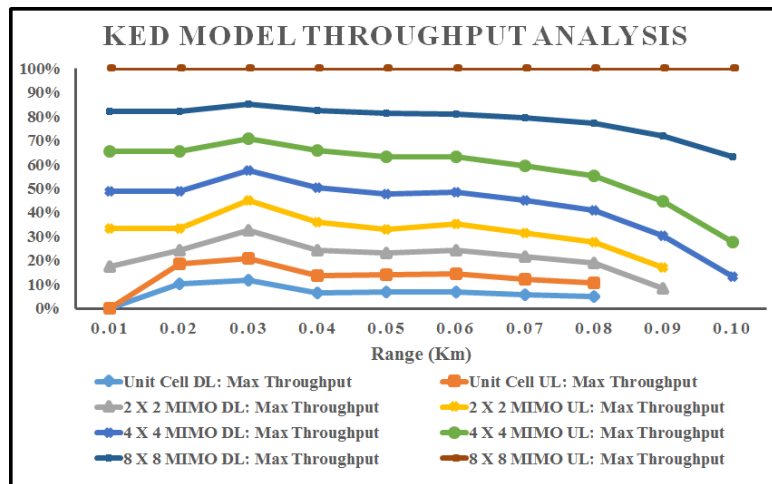
(b)

Figure 6.31: Analysis of Different MIMO Configurations with KED Model (a) Data Rate (b) Throughput.

when it is compared with the situations where $H_{Tx} >> H_{roof}$. The performance of this model is considered to be poor when $H_{Tx} << H_{roof}$.

For micro cells the prediction error is large and it does not consider the multipath propagation as a result wave guiding effects are not taken into account in computation. So, in situations where the transmitters are on over the rooftops

Table 6.5: Simulation Results of various parameters with Knife Edge Diffraction
      Model

S.No	Parameters	Sim.Res.	Exp.Val.
1.	DL:Max Data Rate (MBits/s)	2.576	—
2.	DL:Throughput (MBits/s)	669.8	—
3.	UL:Max Data Rate (MBits/s)	2.756	—
4.	UL:Throughput (MBits/s)	716.5	—
5.	SNIR (dB)	40 (E)	≥ 20
6.	RSRP (dBm)	-85 (E)	$\geq$ -80
7.	RSRQ (dB)	0 (E)	$\geq$ -10
8.	RSSI (dBm)	-62 (E)	$\geq$ -65

Note: E represents Excellent signal strength with maximum data speeds as per
3GPP.(Sim.Res.- Simulation Results; Exp.Val.-Expected Value)

Figure 6.32: Data Rate and Throughput with KED Model for (a) DownLink (b)
      UpLink.

this model provides good results. The single stream data rate and throughput for
different MIMO antenna configurations over the considered geographical terrain
with EWM are shown in Figure 6.35 (a) and (b).

135
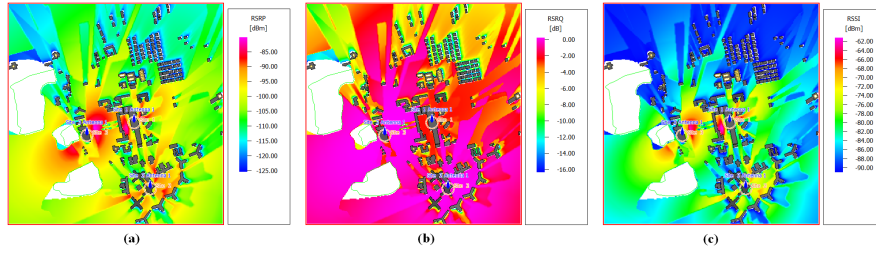
Figure 6.33: (a) RSRP (b) RSRQ (c) RSSI for the layout with KED Model.
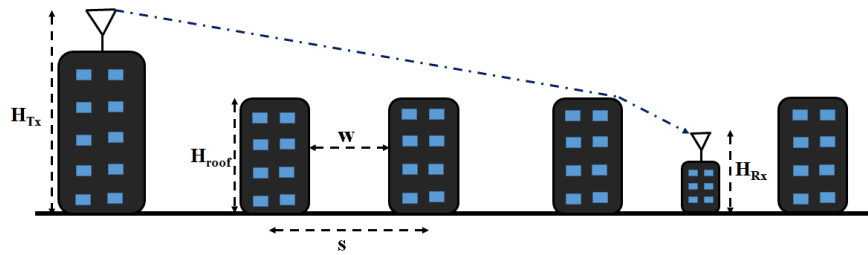
Figure 6.34: Propagation Scenario with Transmitter and Receiver in Extended walfisch-ikegami Model.

Using EWM model the simualtion results for the selected cell sites deployed for this environment are tabulated in Table 6.6. The data rate and throughput for both downlink and uplink are given in Figure 6.36 (a) and (b) respectively. The data rates and throughput of 2.576 MBits/s and 669.8 MBits/s for downlink and 2.756 MBits/s and 716.5 MBits/s for uplink are reported for the deployed cell sites. From the simulation results RSRP is -80 dBm, RSRQ is 0 dB and RSSI is -60 dBm which shows that the signal strength is good covering the entire map with deployed locations A,B and C as shown in Figure 6.37 (a), (b) and (c) respectively.

6.4.3 Dominant Path Model

Dominant path model(DPM) uses the full 3D approach in path searching and hence the results are more realistic and accurate. So far discussed wave propagation models are based on empirical approaches and they compute by direct ray
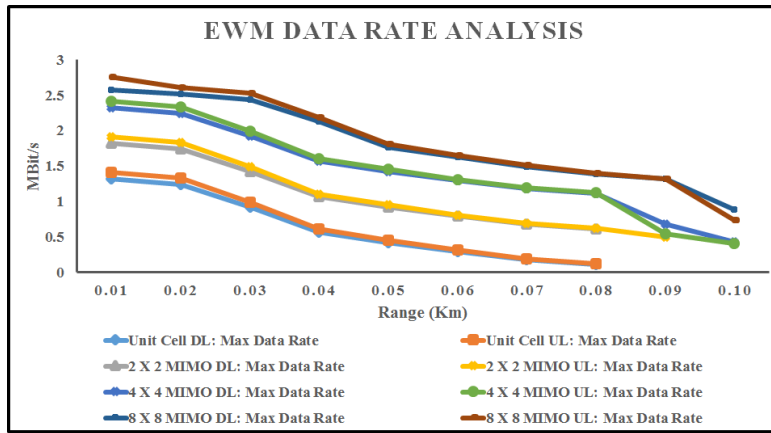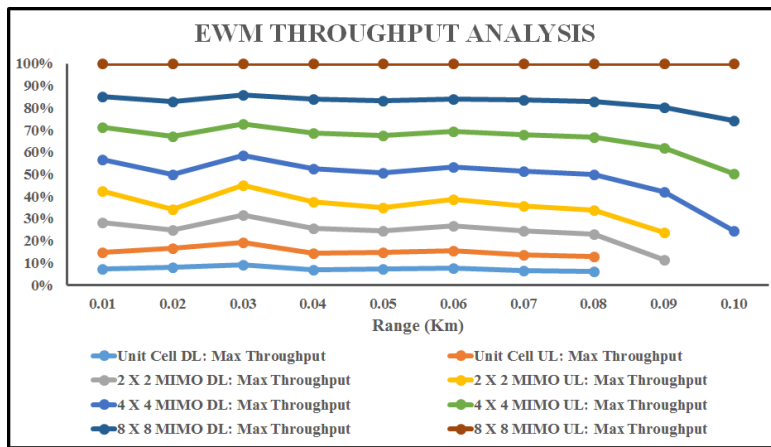
Figure 6.35: Analysis of Different MIMO Configurations with EWM (a) Data Rate (b) Throughput.

between tranmitter and receiver location which often leads to erroneous results. This model determines the one dominant path between each transmitter and receiver pixel. The computation time is very less when compared to ray-tracing models and accuracy is identical to knife edge diffraction model. As the ray tracing models are very time consuming and also they rely on vector database which indirectly influence the accuracy of prediction DPM are preferrable. DPM determines the most siginificant one propagation path between transmitter and receiver which contributes to more than 90% of the total energy. This leads to less compu-

Table 6.6: Simulation Results of various parameters with Extended Walfisch-ikegami Model

S.No	Parameters	Sim.Res.	Exp.Val.
1.	DL:Max Data Rate (MBits/s)	2.576	—
2.	DL:Throughput (MBits/s)	669.8	—
3.	UL:Max Data Rate (MBits/s)	2.756	—
4.	UL:Throughput (MBits/s)	716.5	—
5.	SNIR (dB)	40 (E)	≥ 20
6.	RSRP (dBm)	-80 (E)	$\geq$ -80
7.	RSRQ (dB)	0 (E)	$\geq$ -10
8.	RSSI (dBm)	-60 (E)	$\geq$ -65

Note: E represents Excellent signal strength with maximum data speeds as per 3GPP.(Sim.Res.- Simulation Results; Exp.Val.-Expected Value)
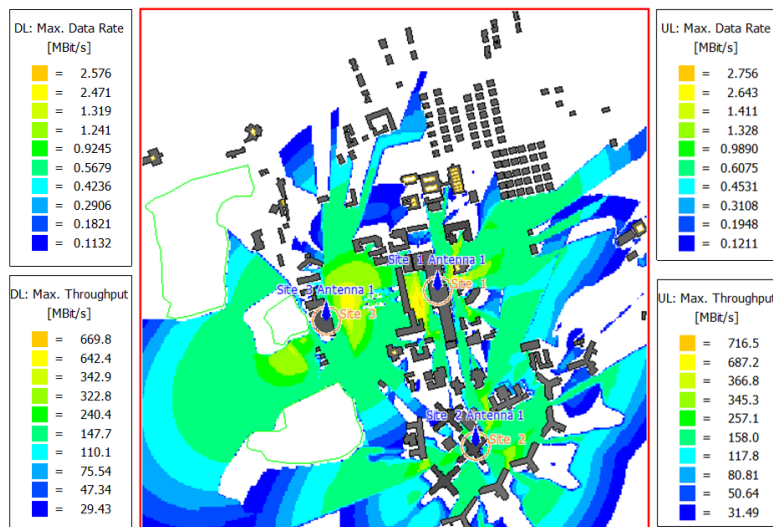

Figure 6.36: Data Rate and Throughput with EWM Model for (a) DownLink (b) UpLink.

138
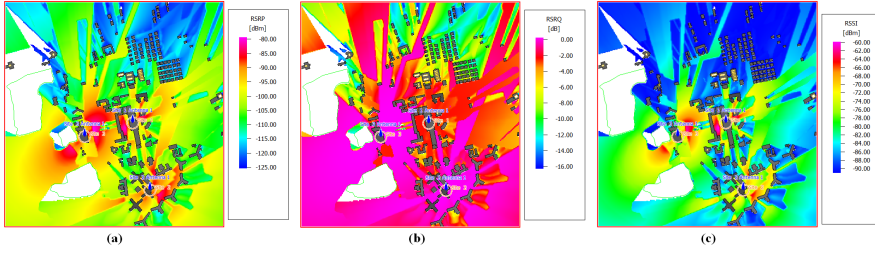
Figure 6.37: (a) RSRP (b) RSRQ (c) RSSI for the layout with EWM Model.

tation time and accuracy almost equivalent to ray-tracing models.

Ray tracing models (Knife edge diffraction) determine the numerous paths between transmitter and receiver, in empirical models (Extended Walfisch-ikegami Model) it considers the direct path but in DPM model it determines the most significant dominant path which requires less computation times. DPM model does not require preprocessing for vector database so it is ideal approach to compute coverage predictions in large urban areas. The computation path loss is given by using the following equation.

$$L = 20log(4\pi/\lambda) + 10plog(l) + \sum_{i=0}^{n} f(\phi, i) + \Omega + g_t \qquad (6.1)$$

where L is the path loss computed for the receiver location, l is the distance between tranmitter and receiver, p is path loss component, f losses due to diffraction, g_t gain of transmitting antenna. The simulations are carried out with unit cell MIMO antenna element, 2×2, 4×4 MIMO and 8×8 massive MIMO configurations. The single stream data rate and throughput for different MIMO antenna configurations over the considered geographical terrain with DPM are shown in Figure 6.38 (a) and (b).

The detailed analysis with minimum transmitting and receiving power of base station(BS), mobile station(MS) for both down link (DL) and uplink (UL) are

139
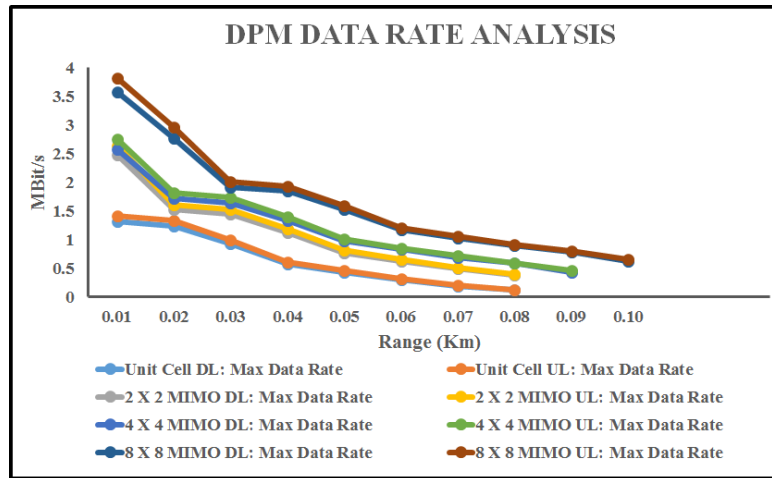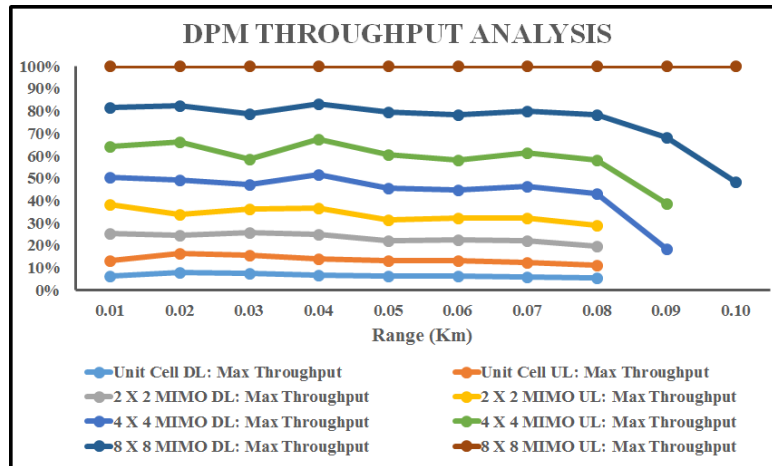
Figure 6.38: Analysis of Different MIMO Configurations with Dominant Path
Model (a) Data Rate (b) Throughput.

analysed with QPSK, 16 QAM, 64 QAM and 256 QAM modulation schemes
are shown in Figure 6.39 and 6.40. From the simulation results it is observed
with 256 QAM for deployed base station at different locations A,B and C the
maximum data rate and throughput are obtained. The comparison between the
different modulation schemes with single stream of data for dominant path model
are shown in Figure 6.41.
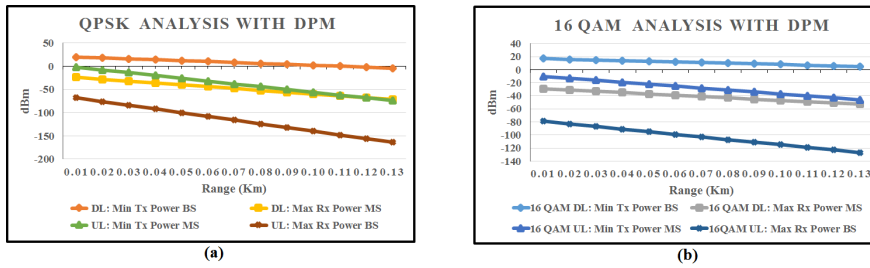
Figure 6.39: (a) QPSK (b) 16 QAM Analysis with Dominant Path Model.
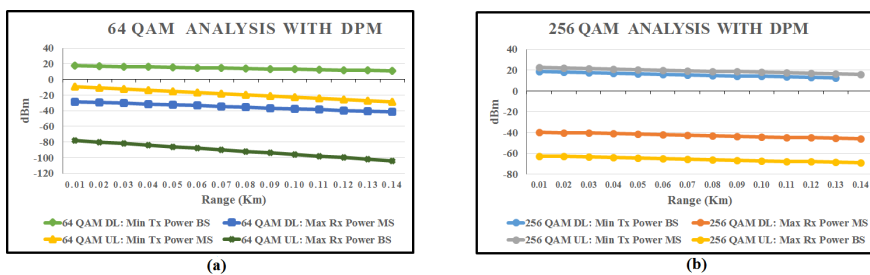
Figure 6.40: (a) 64 QAM (b) 256 QAM Analysis with Dominant Path Model.
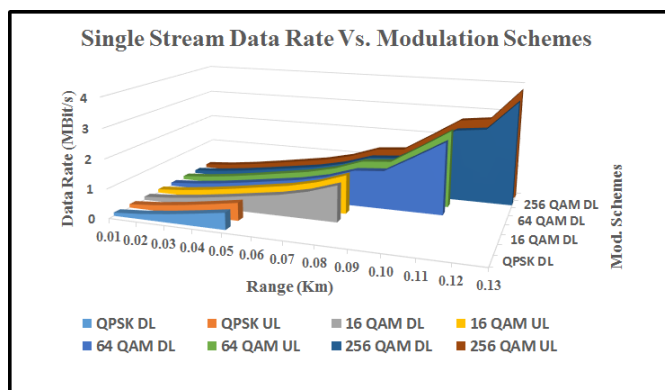
Figure 6.41: Single stream data rate for different modulation schemes with domi-
nant path model.

By considering the 5G FDD wireless standard and dominant path wave prop-
agation model the bandwidth is varied and observed the single stream of data for
both downlink and uplink as shownin Figure 6.42. From the simulation results it
is observed with rise in bandwidth the data rate also increased. The maximum data
rate of 1.37 GBit/s is reported with 20 MHz bandwidth for 8×8 massive MIMO by

utilizing 64 dual polarized antenna elements both at the transmitter and receiver when compared with other MIMO configurations as shown in Figure 6.43.
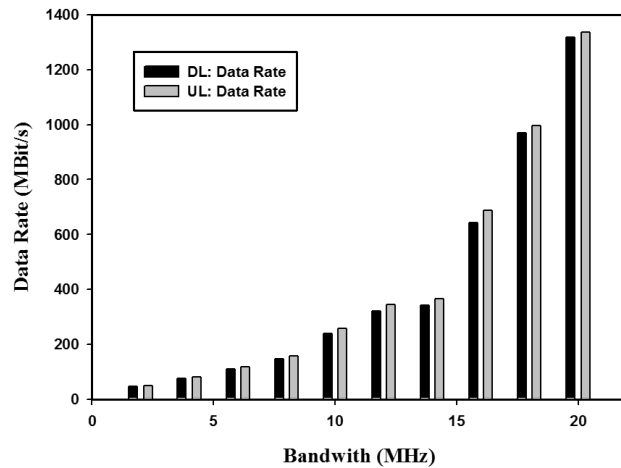
Figure 6.42: Data rate and bandwidth variation with dominant path model.
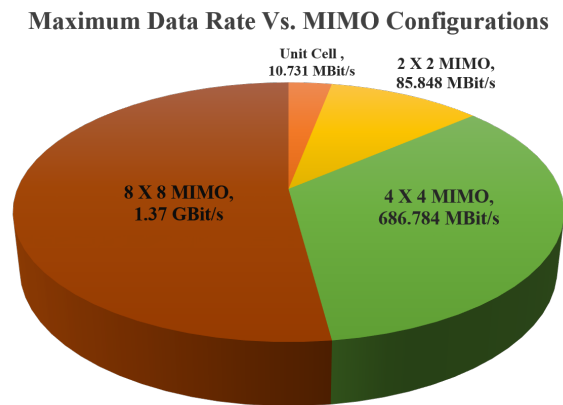
Figure 6.43: Maximum data rate with different MIMO configurations for dominant path model with same number of antennas at both transmitter and receiver.

DPM simulation results for the deployed cell sites in the selected geographical terrain are tabluated in Table 6.7. The single stream data rate and throughput for both downlink and uplink are given in Figure 6.44. The data rates and throughput

of 3.577 MBits/s and 930.1 MBits/s for downlink and 3.827 MBits/s and 995.0 MBits/s for uplink are reported for the deployed cell sites. The SNIR is simulated as 60 dB for 8×8 massive MIMO configuration and given in Figure 6.45(a). The signal strength and quality parameters RSRQ, RSRP and RSSI are shown in Figure 6.45(b), Figure 6.46(a) and 6.46(b) respectively. From the simulation results RSRP is -60 dBm, RSRQ is 0 dB and RSSI is -40 dBm which shows that the signal strength is excellent covering the entire map with selected locations of base stations at A,B and C.

Table 6.7: Simulation Results of various parameters with Dominant Path Model.

S.No	Parameters	Sim.Res.	Exp.Val.
1.	DL:Max Data Rate (MBits/s)	3.577	—
2.	DL:Throughput (MBits/s)	930.1	—
3.	UL:Max Data Rate (MBits/s)	3.827	—
4.	UL:Throughput (MBits/s)	995.0	—
5.	SNIR (dB)	60 (E)	≥ 20
6.	RSRP (dBm)	-60 (E)	$\geq$ -80
7.	RSRQ (dB)	0 (E)	$\geq$ -10
8.	RSSI (dBm)	-40 (E)	$\geq$ -65

Note: E represents Excellent signal strength with maximum data speeds as per 3GPP.(Sim.Res.- Simulation Results; Exp.Val.-Expected Value)
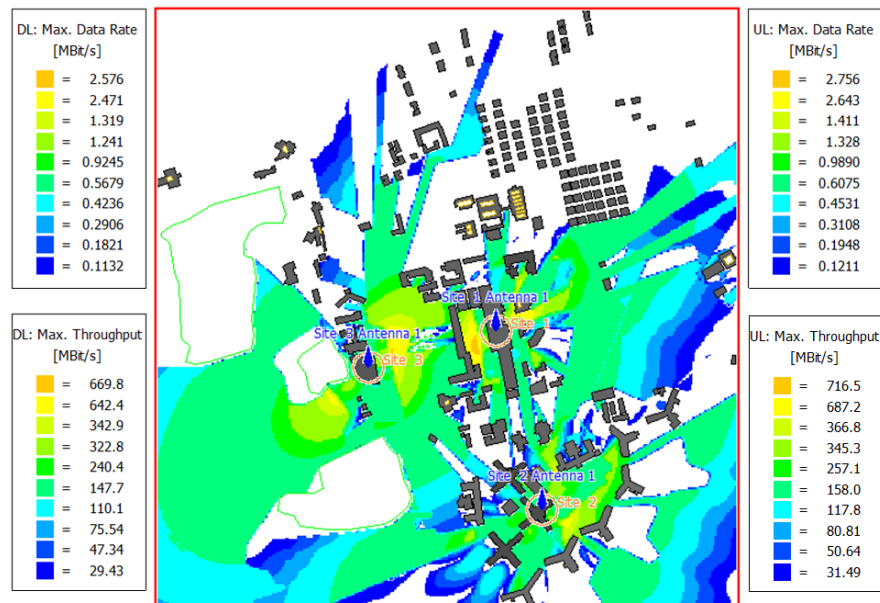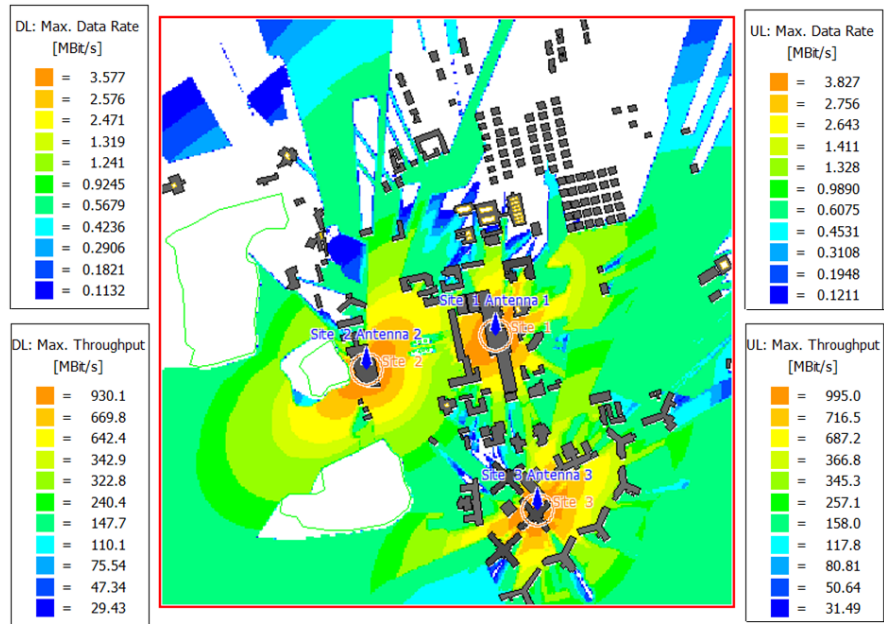
Figure 6.44: Data Rate and Throughput of Downlink and Uplink with Dominant
Path Model for 8×8 Massive MIMO.
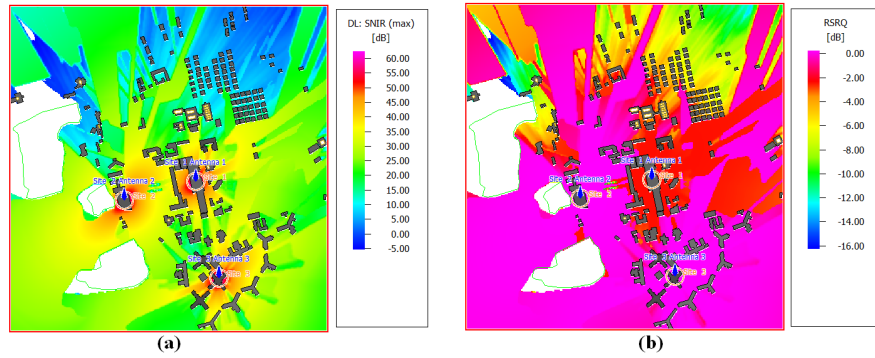
Figure 6.45: (a) Received power and SNIR (b) RSRQ for the map area with dominant path model.
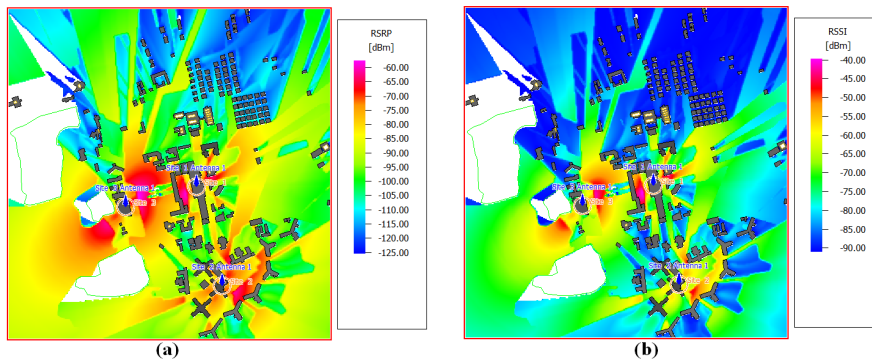
Figure 6.46: (a) RSRP (b) RSSI for the layout with dominant path model.

6.5 Metasurface Based Radome for Dual Band Patch Antenna in Sub 6GHz Range for 5G Applications

In this section, dual band microstrip patch antenna is designed in Sub 6GHz range focusing both 4G LTE and 5G applications. Dual band metamaterial is designed for same operating band and extended for 3×3 metasurface radome which also enhances the gain of patch antenna. The designs are simulated and performance is compared with and without metasurface radome.

6.5.1 Dual Band Microstrip Patch Antenna

From the various microstrip patch antennas, the most basic form of the patch antenna is selected which consists of radiating patch on one side of the dielectric substrate and ground plane on other side. Microstrip patch antenna patches have variety of shapes as rectangle, square, triangular and circular etc. The coaxial feed or probe feed is a very common technique used for feeding microstrip patch antennas. This feed method is easy to fabricate and has low spurious radiation.

The general microstrip patch antenna with coaxial feed and its fringing fields are shown in Figure 6.47.
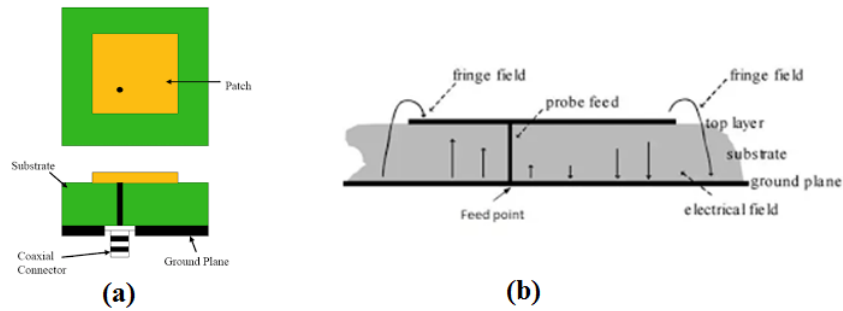
Figure 6.47: (a) General Configuration of Microstrip Antenna with Coaxial Feed (b) Fringing Effect in Microstrip Patch Antenna.

Figure 6.48(a) shows the antenna structure and it consists of the F-slot, asymmetric strips, and coaxial feed-line. The slot and asymmetric strips are printed on the top layer of the rogers substrate and the feed-line is printed on the bottom layer. FR4 substrate(ϵ_r=4.4, tanδ=0.02) is used with height of 0.8mm. Figure 6.48(b) shows the side view of the antenna with 50Ω coaxial cable feeding the F-slot patch antenna. The S-parameters obtained for the designed dual band patch antenna are shown in Figure 6.49. The realized gain at two operating frequencies 2.8 GHz and 3.5 GHz are shown in Figure 6.50 and Figure 6.51.

6.5.2   Dual Band Metamaterial Unit Cell

Metamaterials differ from regular materials in their anomalous and exotic material responses. In most naturally occurring materials both the permittivity and permeability must be greater than that of free space. Metamaterials are metal–dielectric composites structured on the microscale or nanoscale. For electromagnetic waves with relatively large wavelengths, the composite structure acts as an array of artificial atoms, giving rise to unique and exotic electromagnetic properties.

146
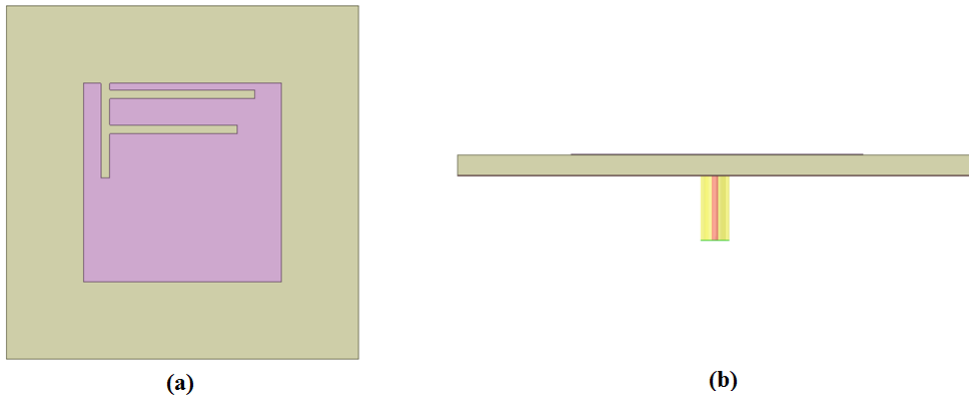
Figure 6.48: (a) Dual Band Microstrip Patch Antenna with F Slot (b) Side View of Dual Band Microstrip Patch Antenna with F Slot.
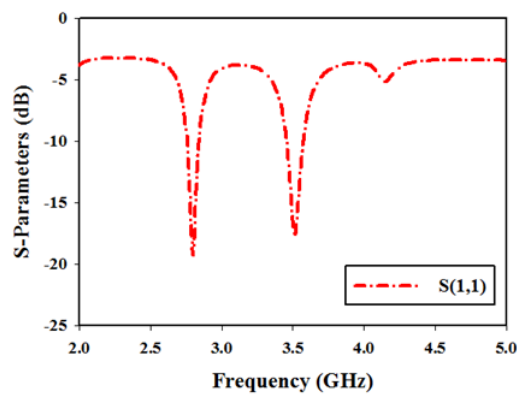
Figure 6.49: S-Parameters of Dual Band MPA with F Slot.
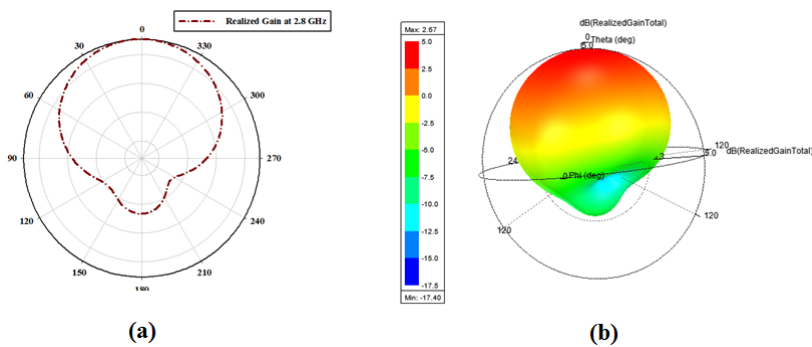
Figure 6.50: Simulated Realized Gain (a) 2D Plot (b) 3D Polar Plot at 2.8 GHz.

147
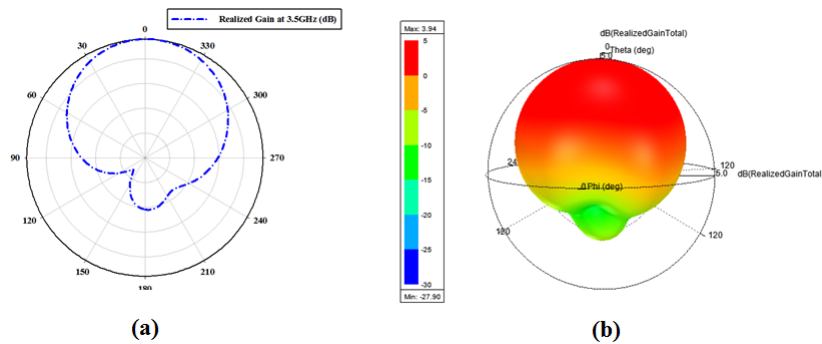
Figure 6.51: Simulated Realized Gain (a) 2D Plot (b) 3D Polar Plot at 3.5 GHz.

Dual band metamaterial unit cell operating for sub 6GHz band is designed as shown in Figure 6.52. The resulting S-parameters for the design is shown in Figure 6.53.
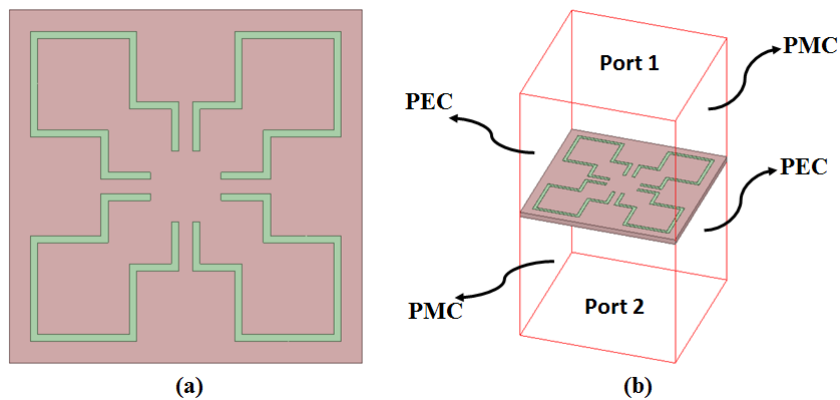
Figure 6.52: (a) Geometry of Dual Band Metamaterial Unit Cell. (b) Boundary Conditions.

6.5.3 Integration of Metasurface Radome with Dual Band MPA

A radome is an integral part of almost every antenna system, protecting antennas and antenna electronics from extreme environmental conditions (humidity, heat, cold, etc.). Metamaterials are artificial materials with a great potential for antenna design, and many studies explore applications of metamaterials to antennas but
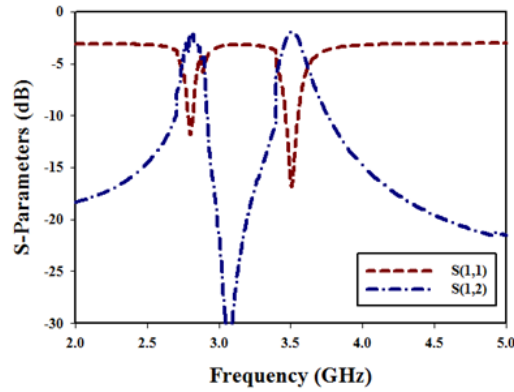
Figure 6.53: S-Parameters of Dual Band Metamaterial Unit Cell.

just a few to the design of radome. The use of metamaterials can improve or correct characteristics (gain, directivity, and bandwidth) of the enclosed antenna and add new features, like band-pass frequency behaviour, polarization transformations. The radiating element, of the antenna system, is microstrip patch antenna operating at 2.8 and 3.5 GHz. The radome is constituted by one layer of metasurface. A dual band metamaterial unit cell is designed and extended to metasurface radome on the microstrip patch antenna.

The metasurface radome is placed at a height of 3mm above the MPA and simulated for the overall performance of the antenna. The design of 3×3 array of metamaterial unit cells and the profile height above the antenna are shown in Figure 6.54. The optimizations are carried out for proper impedance matching and the resulting S-parameters are shown in Figure 6.55. The enhancement of the gain at both the operating frequencies are shown in Figure 6.56 and 6.57. The comparison of the performance with and without metsurface radome are tabulated in Table 6.8 and 6.9. There is significant increase in the gain of the antenna by around 3dB at both operating frequencies that is 2.85 GHz and 3.5 GHz for with and without metasurface radome.

149

| (a) | (b) |
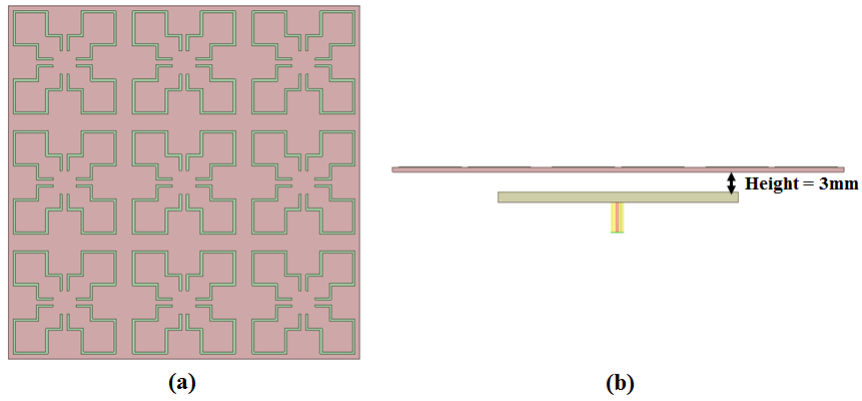
Figure 6.54: (a) Geometry and (b) Side View of Dual Band MPA with Metasurface Radome.
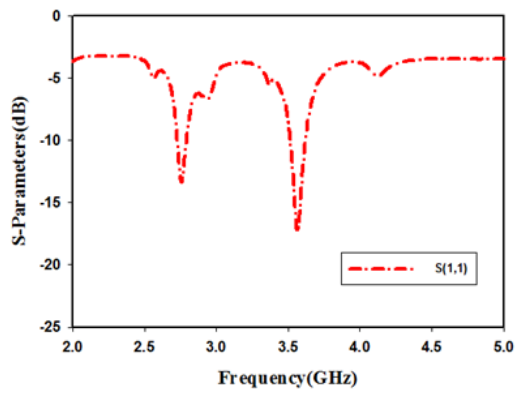
Figure 6.55: S-Parameters of Dual Band MPA with Metasurface Radome.

| (a) | (b) |
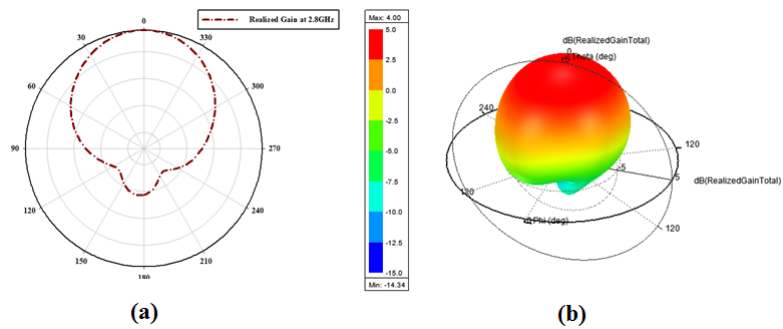
Figure 6.56: Simulated Realized Gain (a) 2D Plot (b) 3D Polar Plot at 2.8 GHz.

150
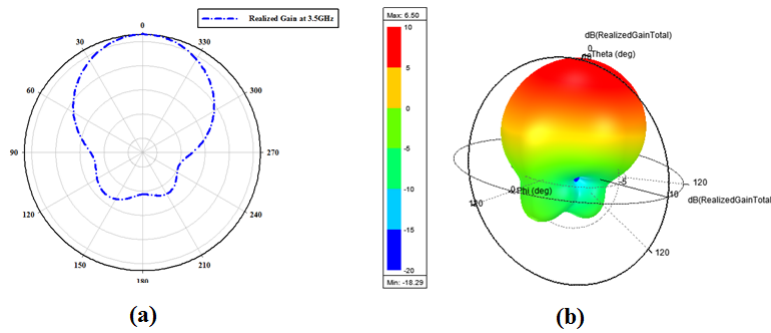
Figure 6.57: Simulated Realized Gain (a) 2D Plot (b) 3D Polar Plot at 3.5 GHz.

Table 6.8: Dual Band MPA Without and With Metasurface Radome

S.No	Parameters with Units	Without Metasurface Radome		With Metasurface Radome	
		2.8 GHz	3.5 GHz	2.8 GHz	3.5 GHz
1.	Reflection Coefficient (dB)	-19.89	-16.86	-14.52	-17.86
2.	Gain (dB)	2.67	3.94	4	6.5

6.6 Summary

In this chapter, two different topics are discussed. Dual polarized MIMO antenna element operating under sub 6 GHz for 5G applications is reported. Wave propagation models are discussed for practical deployment of the 5G antenna with different MIMO configurations. The radio network planning for the base station antenna with various modualtion schemes and wireless standards are also discussed. The proposed antenna is deployed in selected geographical terrain and analyzed the data rates, throughput for both uplink and downlink. The signal strength and quality related parameters also studied covering the entire selected map. The other topic radome analysis for the 5G antennas also studied. Dual band patch antenna is selected operating at two different bands under sub 6GHz range. Metasurface based radome is designed and loaded with dual band patch antenna which also enchances the gain of the designed antenna.

151

CHAPTER 7

CONCLUSION AND FUTURE WORK

Fifth Generation or 5G, is the contemporary new release of cellular generation, engineered to greatly increase the speed and responsiveness of wireless networks. 5G performance objectives high data rate, increased capacity, low latency and large device connectivity. 5G enables massive increase in amount of data handling capacity due to its broad spectrum allocation covering both sub 6GHz range and mm-wave frequency bands. Massive MIMO (additionally referred to as huge-Scale Antenna structures, Very large MIMO, and Hyper MIMO) is an exciting concept in wireless communications studies that promises to deal with the huge capacity requirement demanded by means of 5G systems. Massive multiple-input multiple-output (MIMO) technology, where a base station is installed with huge number of antennas serves large number of users by utilizing time-frequency resource will meet the requirements for 5G. Hence, MIMO is selected as promising candidate technology for upcoming generations of wireless systems. The selection of antenna and building the MIMO base stations which address both spatial and polarization diversity is one of the major task. Because of their large number, proximity and modes of operation, strict requirements are imposed at the antenna layout in large MIMO gadget. The presented antenna models are capable of providing both spatial and polarization diversity for large scale MIMO antenna systems.

- Dual polarization addressing the polarization and spatial diversity with compact structures by implementing 2×2 MIMO.

- A low profile, miniaturized wide band antenna is designed for micro base station applications with FSS decoupling technique by extending to 1×2 MIMO antenna.

- Wave propagation models with complete radio network planning for practical deployment in selected geographical terrain by considering dual polarized MIMO antenna are reported.

- Metasurface based radome for gain enhancement for dual band microstrip patch antenna.

7.1   Contributions

The thesis contribution can be summarized into sections based on designed antennas and their applications.

7.1.1   Compact 2×2 Dual Slant 45^0 Polarized MIMO Antenna with Low Mutual Coupling and High Isolation for 4G LTE Band 40

2×2 multiple input multiple output (MIMO) antenna system with low mutual coupling is discussed for polarization and spatial diversity. MIMO antenna operates for (2.3 – 2.4 GHz) Band 40 with a VSWR of < 2. A very good isolation of 30 dB between the two ports and gain of 7.5 dB for dual slant 45^0 polarized antenna is measured. By introducing the planar printed periodic array of SRRs loaded with transmission line on FR4 vertical substrates the mutual coupling can be significantly suppressed in both E and H planes. From the measured and simulated results it is observed mutual coupling reduction of 25 dB to 50 dB in both E and H planes. The miniaturized structure of the radiator to 0.4λ in dual slant 45^0 polarized antenna and further investigation of MIMO parameters in terms of ECC

and DG makes the entire 2×2 MIMO antenna system suitable for future wireless communication.

7.1.2 MIMO and Massive MIMO Antennas for Base Station Applications

MIMO and Massive MIMO antennas are designed with 4×4 and 8×8 configurations for base station applications. The mitigation of mutual coupling is carried out with U shaped strips placed at both azimuth and elevation planes for the designed MIMO antenna configurations. Optimizations are carried out with respect to practical deployment of the base station antennas. The designs are fabricated and tested for the functionality for both the polarizations. The radome analysis also done with proper materials for practical deployment to overcome the environmental conditions.

7.1.3 Low Profile, Wideband Dual Polarized Antenna with FSS Decoupling Technique for 5G Applications

Low profile, wideband dual polarized 1×2 MIMO antenna with frequency selective surface(FSS) decoupling technique is presented. Low profile is realized by chessboard based AMC surface designed with two different AMC cells operating at 3.5 GHz, 3.1 and 4.5 GHz. The compactness of the antenna is achieved by miniaturizing the antenna to $0.4\lambda_0$. A wide bandstop frequency selective surface(FSS) wall from 2.85 GHz to 4.75 GHz is designed to suppress near field coupling between the MIMO antenna elements. Measured results shows by inserting FSS wall vertically, coupling reduction of 27 dB is achieved. The low

profile antenna with bandwidth of 57.14% (2.95 – 4.95 GHz) for a VSWR of < 2 with port isolation of more than 25 dB are obtained for entire band of operation.

7.1.4 Wave Propagation Models and Radio Network Planning for Practical 5G Scenario

This section contributes to the design of dual polarized MIMO antenna with wave propagation models and dual band patch antenna with metasurface radome. In the first design, Dual polarized MIMO antenna element operating under sub 6 GHz for 5G applications is reported. Wave propagation models are discussed for practical deployment of the 5G antenna with different MIMO configurations. The radio network planning for the base station antenna with various modualtion schemes and wireless standards are also discussed. The proposed antenna is deployed in selected geographical terrain and analyzed the data rates, throughput for both uplink and downlink. The signal strength and quality related parameters also studied covering the entire selected map. In the second design, radome analysis for the 5G antennas also studied. Dual band patch antenna is selected operating at two different bands under sub 6GHz range. Metasurface based radome is designed and loaded with dual band patch antenna which also enchances the gain of the designed antenna. The radome analysis can further be extended to intelligent reflecting surface(IRS) for upcoming 6G communications.

7.2 Limitations

The limitations of the research work carried out are with the measurements of massive MIMO antenna configurations for the required radaition pattern measure-

ments. The selection of proper radome materials for obtaining the stable radiation patterns without affecting the S-parameters as reflects with the massive MIMO antennas. Wave propagation models and its selection to obtain the maximum data rate and throughput to meet the 5G requirements.

7.3   Future Work

In the present era, the shortage of bandwidth due to the rapid increase of mobile data and high-speed communication facing the wireless carriers needs the exploration of millimeter-wave communication. The compact and low profile antennas can be designed in millimeter-wave frequency to achieve multiple functionalities. The wideband and multi-band CP antennas can be designed with less size and low complexity. The upcoming 6G commmunications also focuses on the intelligent reflecting surface(IRS), for improve the performance of wireless data transmission system. Specially, large numbers of small reflecting unit are jointly adjusted to reconfigure the wireless signal transmitting environment.

LIST OF PUBLICATIONS BASED ON THESIS

Peer reviewed International Journals

- Anudeep B, Krishnamoorthy Kandasamy and P. H. Rao, (2020). *"Mitigation of Mutual Coupling in 2 × 2 Dual Slant Polarized MIMO Antennas using Periodic Array of SRRs Loaded with Transmission Line for LTE Band 40"* **International Journal of RF and Microwave Computer-Aided Engineering**, 2020; Vol. 30:e22454.

- Anudeep, B., Krishnamoorthy, K. and Rao P. H., (2021). *"Low-profile, wideband dual-polarized 1 × 2 MIMO antenna with FSS decoupling technique"* **International Journal of Microwave and Wireless Technologies**, pp: 1-7. $https://doi: 10.1017/S1759078721000805$

- A. Bellary, K. Kandasamy and P. H. Rao, *"Analysis of Wave Propagation Models with Radio Network Planning using Dual Polarized MIMO Antenna for 5G Base Station Applications"* **IEEE Access**, Vol. 10, pp. 29183-29193, 2022. $https://doi: 10.1109/ACCESS.2022.3158948$

International Conferences

- Anudeep B, Krishnamoorthy Kandasamy and P. H . Rao, *"A Wideband Dual Polarized Bow-Tie Antenna For 5G Applications"*, **Indian Conference on Antennas and Propagation (InCAP) 2019**, Gandhinagar, Gujarat, India, December 19-22, 2019.

CURRICULUM VITAE

Name	Anudeep B
Address	D.No: 4-405,
	Vidyaranya nagar,Kalyandurgam Road,Anantapur -515004
	Andhra Pradesh, India
E-mail	anudeepbellary@gmail.com
Qualification	• M.Tech	Commuinication Engineering	VIT University Tamil Nadu
	• B.E	Electronics and Communicatio Engineering	JNTU Anantapur
Experience	• Research Scientist	SAMEER Centre For Electromagnetics, Chennai.

REFERENCES

A. Foroozesh, M. NgMou Kehn and L. Shafai (2008), "Application of artifical ground planes in dual-band orthogonally-polarized low-profile high-gain planar antenna design." *Progress In Electromagnetics Research Letters*, 84, 407–436.

A. Habashi, J. Nourinia and C. Ghobadi (2011), "Mutual coupling reduction between very closely spaced patch antennas using low-profile folded split-ring resonators (fsrrs)." *IEEE Antennas and Wireless Propagation Letters*, 10, 862–865.

A. Jafargholi, A. Jafargholi and J. H. Choi (2019), "Mutual coupling reduction in an array of patch antennas using cll metamaterial superstrate for mimo applications." *IEEE Transactions on Antennas and Propagation*, 67, 179–189.

Arun Agarwal, Sumanshu Agarwal-Gourav Misra, Kabita Agarwal (2019), "Evolution of mobile communication technology towards 5g networks and challenges." *American Journal of Electrical and Electronic Engineering*.

Caloz, Christophe and Tatsuo Itoh (2005), *Electromagnetic Metamaterials: Transmission Line Theory and Microwave Applications*. Wiley-IEEE Press.

Costa, F. and A. Monorchio (2011), "Absorptive frequency selective radome." 1–4.

Costa, F. and A. Monorchio (2012), "A frequency selective radome with wideband absorbing properties." *IEEE Transactions on Antennas and Propagation*, 60, 2740–2747.

D. Gao, X. Quan-M. Sun S. Fu, Z. Cao and P. Chen (2020), "A low-profile decoupling slot-strip array for 2by2 microstrip antenna." *IEEE Transactions on Antennas and Propagation*, 8, 113532–113542.

Dewan, R., S. K. A. Rahim, S. F. Ausordin, and H. U. Iddi (2012), "Design of triple band artificial magnetic conductor." 253–256.

et al., Abdelheq Boukarkar (2018a), "A miniaturized extremely close-spaced four-element dual-band mimo antenna system with polarization and pattern diversity." *IEEE Transactions on Antennas and Propagation*, 17, 134–137.

et al., Huiqing Zhai (2018b), "A low-profile dual-polarized high-isolation mimo antenna arrays for wideband base-station applications." *IEEE Transactions on Antennas and Propagation*, 66, 191–202.

et al., J. G. Andrews (2014), "What will 5g be?" *IEEE JSAC*, 32, 1065–1082.

et al., M. Tang (2017), "Mutual coupling reduction using meta-structures for wideband, dual-polarized, and high-density patch arrays." *IEEE Transactions on Antennas and Propagation*, 65, 3986–3998.

et al., Naser Ojaroudiparchin (2016), "A switchable 3d coverage phased array antenna package for 5g mobile terminals." *IEEE Antennas and Wireless Propagation Letters*, 15, 1747–1750.

et al., Rifaqat Hussain (2018c), "An integrated dual mimo antenna system with dual-function gnd-plane frequency-agile antenna." *IEEE Transactions on Antennas and Propagation*, 17, 142–145.

F. Liu, L. Zhao-G. Huang Y. Li, J. Guo and Y. Yin (2020), "Dual-band metasurface-based decoupling method for two closely packed dual-band antennas." *IEEE Transactions on Antennas and Propagation*, 68, 552–557.

Ferreira, Joao Filipe Martins (2016), "Study and design of antennas for wlan mimo applications." *Thesis*.

Frenkiel, Richard (2009), "A brief history of mobile communications." *Available online*.

Hamza Ahmad, Shahid Bashir-Wajid Zaman, MuhibUr Rahman and Fauziahanim Che Seman (2020), "Miniaturized frequency selective radome operating in the x-band with wideband absorption."

Han, Y., W. Che, X. Xiu, W. Yang, and C. Christopoulos (2017), "Switchable low-profile broadband frequency-selective rasorber/absorber based on slot arrays." *IEEE Transactions on Antennas and Propagation*, 65, 6998–7008.

Huiqing Zhai, et al. (2018), "A low-profile dual-polarized high-isolation mimo antenna arrays for wideband base-station applications." *IEEE Transactions on Antennas and Propagation*, 66, 191–202.

Iqbal, O.;Bouazizi A.;Basir A, A.;A Saraereh (2018), "Metamaterial-based highly isolated mimo antenna for portable wireless applications." *Electronics*, 7, 267.

Jihoon Bang, Jaehoon Choi, Youngtaek Hong (2018), "Mm-wave phased array antenna for whole-metal-covered 5g mobile phone applications." *IEEE International Workshop on Electromagnetics:Applications and Student Innovation Competition (iWEM)*.

J.Wu, S.Yang, Y.Chen, S.Qu, and Z.Nie (2017), "A low profile dual-polarized wideband omnidirectional antenna based on amc reflector." *IEEE Transactions on Antennas and Propagation*, 65, 368–374.

K. D. Xu, S. Liao, J. Zhu and Q. Xue (2018), "A low mutual coupling mimo

antenna using periodic multi-layered electromagnetic band gap structures." *IEEE Access*, 6, 42497–42506.

K. S. Vishvaksenan, R. Kalaiarasan, K. Mithra and K. S. Raj (2017), "Mutual coupling reduction in microstrip patch antenna arrays using parallel coupled-line resonators." *IEEE Antennas and Wireless Propagation Letters*, 16, 2146–2149.

Kong, Lingyu and Xiaojian Xu (2018), "A compact dual-band dual polarized microstrip antenna array for mimo-sar applications." *IEEE Transactions on Antennas and Propagation*, 66, 2374–2381.

Kristou, N., J. Pintos, S. Bories, and K. Mahdjoubi (2017), "Design and characterization of a compact artificial magnetic conductor in the uhf band." *2017 International Workshop on Antenna Technology: Small Antennas, Innovative Structures, and Applications (iWAT)*, 68–71.

Li, H., Q. Cao, C. Yang, and Y. Wang (2016), "Design and analysis of a frequency selective radome (fsr) with wideband absorbing properties." 1–3.

Liguo Liu, Li-You-Quan (2013), "Design of an invisible radome by frequency selective surfaces loaded with lumped resistors." *Chinese Physics Letters*.

Liu, Q., H. Liu, W. He, and S. He (2020), "A low-profile dual-band dual-polarized antenna with an amc reflector for 5g communications." *IEEE Access*, 8, 24072–24080.

Liu, Y., S. Wang, X. Wang, and Y. Jia (2019), "A differentially fed dual-polarized slot antenna with high isolation and low profile for base station application." *IEEE Antennas and Wireless Propagation Letters*, 18, 303–307.

M. M. Bait Suwailam, M. S. Boybay and O. M. Ramahi (2009), "Mutual coupling reduction in mimo antennas using artificial magnetic materials." *13th Inter-*

national Symposium on Antenna Technology and Applied Electromagnetics and the Canadian Radio Science Meeting, 1–4.

Marco Salucci, Micah Gregory, Giacomo Oliveri (2014), "A frequency-tunable metamaterial-based antenna using a reconfigurable amc groundplane." *8th European Conference on Antennas and Propagation*.

Min Li, Bo. Wang C. F. Zhou, Q. L. Li and S. W. Cheun (2018), "A low-profile dual-polarized dipole antenna using wideband amc reflector." *IEEE Transactions on Antennas and Propagation*, 66, 2610–2615.

Misilmani, H. M. El and A. M. El-Hajj (2017), "Massive mimo design for 5g networks: An overview on alternative antenna configurations and channel model challenges." *2017 International Conference on High Performance Computing Simulation (HPCS)*, 288–294.

Mohammad Meraj ud in Mir, Dr. Sumit Kumar (2015), "Evolution of mobile wireless technology from 0g to 5g." *International Journal of Computer Science and Information Technologies*.

Munk, Ben A. (2000), *Frequency Selective Surfaces: Theory and Design*. John Wiley and Sons.

Nadeem, Iram and Dong-You Choi (2018), "Study on mutual coupling reduction technique for mimo antennas." *IEEE Access*, 7, 563–586.

Nagata, M., T. Hori, and M. Fujimoto (2016), "Design method of unit cell structure for realizing broadband artificial magnetic conductor." 774–775.

R. Dewan, M.R. Hamid, M.K.A. Rahim and M.F.M. Yusoff (2015), "Analysis of wideband antenna performance over dual band artificial magnetic conductor (amc) ground plane." *Applied Mechanics and Materials*, 735, 273–277.

R. Hafezifard, J. R. Mohassel, M. Naser-Moghadasi and R. A. Sadeghzadeh (2016), "Mutual coupling reduction for two closely spaced meander line antennas using metamaterial substrate." *IEEE Antennas and Wireless Propagation Letters*, 15, 40–43.

Rifaqat Hussain, Mohammad S. Sharawi and Atif Shamim (2018), "An integrated four-element slot-based mimo and a uwb sensing antenna system for cr platforms." *IEEE Transactions on Antennas and Propagation*, 66, 142–145.

Rola Saad, Kenneth Lee Ford (2012), "A dual band miniaturised artificial magnetic conductor design methodology." *Loughborough Antennas and Propagation Conference*.

S. Zhang, X. Chen and G. F. Pedersen (2019), "Mutual coupling suppression with decoupling ground for massive mimo antenna arrays." *IEEE Transactions on Vehicular Technology*, 68, 7273–7282.

S. Zuo, W.-J. Wu Z.-Y. Zhang, Y.-Z. Yin and J. Ma (2010), "Investigations of reduction of mutual coupling between two planar monopoles using two slots." *Progress In Electromagnetics Research Letters*, 19, 9–18.

Saeidi-Manesh, Hadi and Guifu Zhang (2018), "High-isolation, low cross-polarization, dual polarization, hybrid feed microstrip patch array antenna for mpar application." *IEEE Transactions on Antennas and Propagation*, 66, 2326–2332.

Shang, Y., Z. Shen, and S. Xiao (2014), "Frequency-selective rasorber based on square-loop and cross-dipole arrays." *IEEE Transactions on Antennas and Propagation*, 62, 5581–5589.

Son Xuat Ta, et al., Minh Duc Nguyen (2018), "A low-profile 45 dual-polarized

antenna based on metasurface and its arrays for base station applications." *Journal of Electromagnetic Waves and Applications*.

T. Jiang, T. Jiao and Y. Li (2018), "A low mutual coupling mimo antenna using periodic multi-layered electromagnetic band gap structures." *Applied Computational Electromagnetics Society Journal*, 33, 305–311.

Thummaluru, S. R., R. Kumar, and R. K. Chaudhary (2018), "Isolation enhancement and radar cross section reduction of mimo antenna with frequency selective surface." *IEEE Transactions on Antennas and Propagation*, 66, 1595–1600.

Tu, H., P. Liu, J. Huang, and Y. Qin (2017), "A miniaturized frequency selective rasorber with tunable passband." 1–4.

Wang, Q., c. Wang, X. Zhang, W. Wu, and N. Yuan (2014), "A his-fss radome with both wide pass band and absorbing band." 297–300.

Wei Hu, Zhao-Yang Tang, Rui-Na Lian and Ying-Zeng Yin (2016), "Wideband, low-profile, dual-polarized slot antenna with an amc surface for wireless communications." *International Journal of Antennas and Propagation*.

Weiwei Wu, Ximeng Zhang-Chenxin Li Naichang Yuan, Yuhong Ma (2018), "An ultrathin and narrow bandpass frequency selective radome with wide reflection bands." *International Journal of Electronics and Communications*, 35–40.

X. Chen, S. Zhang and Q. Li (2018), "A review of mutual coupling in mimo systems." *IEEE Access*, 6, 24706–24719.

Xianjun Sheng, Xiang Gao and Ning Liu (2019), "Design of frequency selective rasorber with high in-band transmission and wideband absorption properties." *IEICE Electronics Express*, 16, 1–6.

Xue-Yan Song, Tian-Ling Zhang Ze-Hong Yan, Chuang Yang and Rui-Na Lian (2016), "Broadband and gain enhanced bowtie antenna with amc ground." *Progress In Electromagnetics Research Letters*, 61, 25–30.

Y. Zhu, Y. Chen and S. Yang (2019), "Decoupling and low-profile design of dual-band dual-polarized base station antennas using frequency-selective surface." *IEEE Transactions on Antennas and Propagation*, 67, 5272–5281.

Yong-Wei Zhong, Guo-Min Yang and Li-Rong Zhong (2015), "Gain enhancement of bow-tie antenna using fractal wideband artificial magnetic conductor ground." *Electronics Letters*, 51, 315–317.

Z. Niu, Q. Chen, H. Zhang and T. Zhong (2019), "Isolation enhancement in closely coupled dual-band mimo patch antennas." *IEEE Antennas and Wireless Propagation Letters*, 18, 1686–1690.

Z. Qamar, S. A. Khan M. Chongcheawchamnan, U. Naeem and M. F. Shafique (2016), "Mutual coupling reduction for high-performance densely packed patch antenna arrays on finite substrate." *IEEE Transactions on Antennas and Propagation*, 64, 1653–1660.

Zhang, J., S. Yan, X. Hu, and G. A. E. Vandenbosch (2019), "Dual-band dual-polarized wearable button array with miniaturized radiator." *IEEE Transactions on Biomedical Circuits and Systems*, 13, 1583–1592.

Zhang, S. and G. F. Pedersen (2016), "Mutual coupling reduction for uwb mimo antennas with a wideband neutralization line." *IEEE Antennas and Wireless Propagation Letters*, 15, 166–169.

Zhu, H., J. Huang, N. Yuan, and B. Yi (2017), "Tunable frequency selective radome with broadband absorbing properties." 2478–2482.